# Modelling of Tumour-induced Angiogenesis

Wei Chen

A thesis submitted to the
University of Northumbria at Newcastle
for the degree of
Doctor of Philosophy

Department of computer Science and Digital Technologies,
Faculty of Engineering and Environment

December 2015

# Acknowledgements

I would firstly like to express my deepest gratitude to my supervisors, Professor Ling Shao, Dr. Li Zhang and Dr. Rosemary Bass for their unfailing support and thoughtfulness in many ways. I would also like to thank all the staff in the School of Computer Science and Digital Technologies for welcoming me into such a positive learning and research community for their support and advice. I wish to extend my thankfulness to all those who helped me at Northumbria University or elsewhere during the entire PhD period. My final thanks go to my parents and my fiancee. I thank them for their patience, understanding, encouragement, and particularly their financial support and endless love.

# Declaration

I declare that the work contained in this thesis has not been submitted for any other award and that it is all my own work. I also confirm that this work fully acknowledges opinions, ideas and contributions from the work of others.

Any ethical clearance for the research presented in this thesis has been approved. Approval has been sought and granted by the School Ethics Committee on 17 July 2013.

**I declare that the Word Count of this Thesis is 43,100 words**

Name: WEI CHEN

Signature:

Date:

# Abstract

Controlled by extracellular signals, tumour-induced angiogenesis is a crucial step in the development of tumours. Among the many cell signals already identified, the VEGF and Notch signalling pathways play a critical role in controlling endothelial cells (ECs) during angiogenesis. Although this regulatory mechanism has become a current research focus in biology, its computational modelling is still rare. We focus on developing a computational model to simulate the VEGF and Notch signalling regulatory mechanism to perceive the micro procedure of angiogenesis *in silico* and fill the gap between biology and computer engineering.

We first developed a mathematical model with nonlinear partial differential equations (PDEs) to describe the migration of endothelial tip cells during tumour-induced angiogenesis. The simulation results show that both chemotaxis and haptotaxis have impacts on the migration of ECs in velocity and density, and the impacts depend on the gradient and direction of tumour angiogenenic factor (TAF), and fibronectin, implying a possible malignant mechanism for some subgroups of tumour. We then developed the model further to simulate the regression, recurrence or clearance of tumours due to tumour cytotoxic factors, including the immune system and drugs delivered through the vessels formed during angiogenesis, providing a broader understanding of tumours. Based on the PDE model which provided parameters of continuum mathematical model, we finally developed an enzymatic catalysed regulating model in the form of ordinary differential equations (ODEs) with agent-based modelling (ABM) using Java and MATLAB languages, to visually realise the sprouting regulated by VEGF and Notch signalling during

angiogenesis. The simulation describes the process of how an endothelial stalk cell becomes an endothelial tip cell, and sprouts under the influence of VEGF and Notch signalling, revealing the relationship between sprouting and branching.

As the simulation results are consistent with reported *in vitro* and *in vivo* assays, the study bridges angiogenesis research and computer modelling from the dynamic regulatory mechanism perspective, offering a huge leap over previous studies in computationally simulating tumour-induced angiogenesis. It is hoped that the results will assist researchers in both the experimental and theoretical angiogenesis communities to improve understanding of the complexity and identify the fundamental principles of angiogenesis, whilst also using modelling approaches that will enrich knowledge for computational scientists in this field.

**Key words:** angiogenesis, mathematical model, agent-based model, endothelial cells, VEGF and Notch signalling, regulatory mechanism

# Contents

## Contents

# List of Figures

# List of Abbreviations

| | |
|---|---|
| **ABM** | Agent-based modelling |
| **αFGF** | Acidic fibroblast growth factor |
| **bFGF** | Basic fibroblast growth factor |
| **CAF** | Cancer-associated fibroblasts |
| **CRC** | Colorectal cancer |
| **CIMP** | CpG island methylator phenotype |
| **Dll4** | Delta-like ligand 4 |
| **EC** | Endothelial cell |
| **ECM** | Extra cellular matrix |
| **EPC** | Endothelial progenitor cell |
| **GBC** | Gallbladder cancer |
| **MDE** | Matrix degradatory enzymes |
| **NICD** | Notch intracellular domain |
| **ODE** | Ordinary differential equation |
| **PDE** | Partial differential equation |
| **PDGF** | Platelet-derived growth factor |
| **SCLC** | Small Cell Lung Cancer |
| **TGF** | Transforming growth factor |
| **TAF** | Tumour angiogenic factor |
| **TNF** | Tumour necrosis factor |
| **VEGF** | Vascular endothelial growth factor |

| | |
|---|---|
| **VEGFR** | Vascular endothelial growth factor receptor |
| **Flt-1** | Vascular endothelial growth factor receptor 1 |
| **sFlt-1** | soluble Flt-1 |

# List of Publications

**Conference Paper**

Wei Chen, Alamgir Hossain, Li Zhang (2012) Review on Cellular Automaton Modelling Techniques in Cancer. *Proceedings of the 6th Conference on Software, Knowledge, Information Management and Applications*, SKIMA 2012.

Wei Chen, Li Zhang, Ling Shao, Rosemary Bass, Chenyu Liu, Alamgir Hossain (2015). Modelling of tumour-induced angiogenesis with regress by immune factor. *9th International Conference on Software, Knowledge, Information Management & Applications,* SKIMA 2015.

**Journal Paper**

(Submitted) Wei Chen, Li Zhang, Chengyu Liu, Ling Shao, Rosemary Bass (2015) Modelling of tumour-induced angiogenesis influenced by haptotaxis. *Journal of Biomedical Informatics*.

# Chapter 1. Introduction

Computational models of complex biological phenomena, such as tumour development and tumour-induced angiogenesis, have become an important part of building our understanding of tumour biology and developing new methods of tumour therapy. In biology or biomedicine, biological experiments, such as *in vivo* and *in vitro* assays, are crucial in the exploration of the complex field of tumour biology. Computational models may be developed from the discoveries of biological experiments. When a computational model's simulation results are consistent with the experiments, it will be a successful model in predicting experimental results and can be used to significantly improve biological and biomedical research throughput by allowing virtual *in silico* modelling. Therefore, we aimed to develop computational models to simulate the tumour-induced angiogenesis in the thesis. This chapter discusses the motivation for the research, proposes the research aim and objectives, points out the contributions of the research, outlines the organisation of the thesis, and finally provides a conclusion to the chapter.

## 1.1 Introduction

This chapter provides an introduction to the thesis, outlining the focus and main areas of inquiry relevant to the research. It concludes with the structure of the thesis.

## 1.2 Motivation

Angiogenesis is the process of new blood vessel formation from pre-existing ones, which plays a key role in various physiological and pathological conditions [1]. Angiogenesis involves the vascular endothelial growth factor (VEGF) directory regulation which leads to the formation of vessels in an appropriate pattern, including the process of nascent sprouting and branching [2]. Tumour-induced angiogenesis is a crucial step in the development of tumours [3] and many researchers have investigated this area, leading to a large number of discoveries related to angiogenesis which includes the selection of tip and stalk phenotypes from endothelial cells (ECs) by VEGF-Notch regulation [4].

Computational modelling simulation is another way to explore this field. Since the development and achievements in bioscience have provided many useful clues for explaining angiogenesis and a great number of hypotheses about mechanisms have appeared, modellers are directed to simulate and verify these hypotheses from the computational aspect. Through simulation *in silico*, researchers can invest these hypotheses.

Many models have already been developed in the last few decades which simulate angiogenesis [5-15]. The majority of models merely simulate the morphology of

angiogenesis, and are rarely related to the simulation of dynamic regulation mechanisms during angiogenesis; this is, therefore, a current research focus in both the experimental and theoretical angiogenesis communities [4]. There is a wide gap between the *in vitro, in vivo* assay and *in silico* simulation of angiogenesis, and computational modelling has been left well behind in the present achievements in angiogenesis research.

Based on the bio-discoveries in the last decade, especially in the area of regulatory mechanisms, many signalling pathways have been proposed in the regulation of angiogenesis. Among the most important ones are vascular endothelial growth factor (VEGF) and Notch signalling pathways, which determine the specification of tip and stalk phenotypes [4]. This will influence the behaviour of endothelial cells (ECs), such as migration, proliferation etc. [4, 16-23]. Hence, if we can develop a model to obtain simulation results consistent with the results from *in vivo* and *in vitro* assays, we will verify the hypotheses from bioscience to a certain extent. It will robustly promote the development of computational modelling, and in turn assist researchers in both the experimental and theoretical angiogenesis communities to understand better the complexity of the regulation mechanism in angiogenesis, and identify its fundamental principles.

## 1.3 Aim and Objectives

We aimed to develop a model including VEGF and Notch signalling pathways to regulate sprouting in tumour-induced angiogenesis. We established an enzymatic catalysed autonomous regulatory model to simulate tumour-induced angiogenesis with the help of

Agent-Based Modelling (ABM) and advanced mathematical tools, including Partial Differential Equations (PDEs) and Ordinary Differential Equations (ODEs). The simulation was to elucidate EC differentiation, migration, proliferation, tip/stalk specification, sprouting, and branching behaviours. In this way, we aimed to decipher the secrets of angiogenesis based on the VEGF/Notch regulatory mechanism, which is an advance on simulating morphology visually as seen in previous studies. This involved:

(1) Developing a mathematical model using PDEs to simulate the continuum field of biological phenomena which change in space and time. These biological phenomena included the VEGF gradient, matrix degradatory enzymes (MDE), extracellular matrix (ECM), and EC migration, proliferation, and branching, both spatially and temporally. The simulation result was used as local parameters for ABM.

(2) Developing an enzymatic catalysed competitive kinetic reaction model to simulate the VEGF and Notch signalling regulatory mechanism governing the specification of tip and stalk from ECs, the proliferation of ECs, and their sprouting and branching. This model is in ODEs.

(3) Developing an ABM model using Java language to accelerate the calculation speed, by combining Matlab language with Java language to realise clear results to solve the ODEs, and to iteratively integrate with the Euler Method to realise the VEGF and Notch signalling feedback loop competitive regulatory control of cell differentiation and activation, etc.

(4) Simulating sprouting and branching through using ABM method. Representing ECs, agents are endowed with the functions of calculation, memory, comparison, judgment, taking information, sending signals, and reacting.

## 1.4 Contributions

This work makes original contributions in the following ways:

- The innovative model we developed was based on VEGF and Notch signalling regulation, which depends on an enzymatic catalysed competitive reaction. This reaction generates VEGF and Notch regulatory signals in the form of ODEs. The simulation results revealed the pivotal role of VEGF and Notch signalling in the specification of tip and stalk which is a vital activity in sprouting. Our results are similar to published biological reports. Thus, to a certain extent, our simulation results support the VEGF and Notch signalling theory [4, 22-31] from the computational point of view (see Chapter 6).

- We have integrated the ABM method with the Euler method to solve the ODEs, and realised the simulation of regulated angiogenesis. The agents are dynamically endowed with more functions compared with cellular automate (CA) in similar research. In our model, the VEGF and Notch signalling regulatory mechanism is at the core. The successful simulation shows that our model enriches the methods in the computational modelling of angiogenesis. Hence, we recommend that the ABM

method is a desired approach in the modelling of cancer related to a regulatory mechanism (see Chapter 6).

- We used the ABM technique by dynamically endowing the agents with different functions, including calculation, memory, comparison, judgment, and update, by taking data from outside and sending signals to the adjacent agents. In this way, we have successfully simulated the regulated ODEs, and thus the study provides a new perspective for computer scientists (see Chapter 6).

- We improved Anderson and Chaplain's [8] two-dimensional hybrid continuum-discrete model by introducing and simulating the degradation of ECM proteolysed by enzymes generated by ECs in tumour-induced angiogenesis. This is necessary for the development of the capillary network when ECs migrate and proliferate, approaching tumours. Our work extends previous studies in simulating angiogenesis, by helping to reveal the fundamental principles of angiogenesis. It enriches knowledge of modelling in this field and provides a good example of the use of Matlab, which is a more current software development tool for computational modellers (see Chapter 4).

- We innovatively linked the relationship of tumour-invasion and tumour-induced angiogenesis through simulating the migration of ECs accelerated by enhanced haptotaxis. In our continuum model, the simulation results show that invasive tumours may enhance haptotaxis by producing fibronectin. According to the consensus theory, in which angiogenesis supplies nutrients and promotes tumour development, turning it from harmless to fatal, we propose a possible mechanism in which both

tumour-invasion and tumour-induced angiogenesis promote each other to make the tumour develop faster and become more harmful for some subgroups of tumours. The possible mechanism for this has not yet been noticed. Our proposal would point out a possible direction for researchers working in the field of cancer (see Chapter 4).

## 1.5 Thesis Outline

The remainder of the thesis is organised as follows:

Chapter 2 gives a critical literature review of the key research published from a biological background and from the perspective of computational modelling of tumour-induced angiogenesis. Particular attention is paid to work concerned with regulatory mechanisms.

Chapter 3 presents the methods involved in the thesis. These methods include mathematical tools such as PDEs and ODEs, and discrete methods such as CA and ABM.

Chapter 4 introduces Anderson and his colleague's continuum model in PDEs which describes the ECs migration during angiogenesis. Based on the PDE model, we develop our PDE model which simulates EC migration influenced by both chemotaxis and haptotaxis at different conditions, and simulates how ECM is degraded by enzymes which are secreted by the ECs in a two-dimensional domain between a tumour and a parent vessel. In the model, the variables include TAF, fibronectin, ECs, enzymes, and ECM. Finally through simulation results, we proposed a possible mechanism that invasive tumour and angiogenesis promote each other in this chapter.

Chapter 5 describes in details how the PDEs model simulates tumour-induced

angiogenesis with regress by cell cytotoxic factor in a two-dimensional domain, in the model the variables include ECs, TAF, tumour load, blood vessel density, immune factor and drug.

In Chapter 6, we develop an innovative model. The model described the VEGF and Notch signalling regulatory mechanism during tumour-induced angiogenesis which is based on an enzymatic catalysed competitive kinetic reaction. The kinetic reaction rate is presented in ODEs hybrid with ABM. The model governs the specification of tip and stalk, and sprouting and branching. The mechanism of VEGF and Notch signalling feedback loop is simulated in this chapter.

Chapter 7 is a summary of the relevant conclusions and possible extensions that can be drawn from the work presented in this thesis.

## 1.6 Conclusion

This chapter presents the research objectives and the rationale for the research. In the following chapter, Chapter Two, the literature review presents the biological background relevant to the research undertaken for this thesis.

# Chapter 2. Biological Review

Tumour-induced angiogenesis is a very complex biological and pathological phenomenon. The achievements of research in biology and discoveries in cancer field in recent decades are very important and crucial for computational modelling. Therefore, we should have possession of the cancer related knowledge, especially the tumour-induced angiogenesis and the fundamental biological theory about it. This chapter provides biological background and reviews relevant concepts and theories of tumour-induced angiogenesis related to the research, placing VEGF and Notch signalling pathways as a key strand in the regulation of angiogenesis. Finally, a conclusion to the review is provided.

## 2.1 Introduction

Angiogenesis is the process of forming new blood vessels from existing parent vessels, and is a crucial requirement for the growth, progression and metastatic spread of a tumour [32-34]. Tumour-induced angiogenesis is the phenomenon that in a hypoxia or low oxygen microenvironment the tumour secretes vascular endothelial growth factor (VEGF) and triggers angiogenetic processes [4]. In this study, the research aims to develop models of tumour-induced angiogenesis based on VEGF and Notch signalling regulatory mechanisms, and to reveal the implications for research on angiogenesis. The purpose of this chapter is to outline the main areas of biological research which have informed, and are relevant to, the present study.

## 2.2 Biological background

### 2.2.1 The development of tumours

Cancer is a collection of different diseases. It is "a neoplasm resulting from a continuous proliferation of abnormal cells that have the ability to invade and destroy other tissues" [35]. Another term for cancer is "tumour," which is a swelling, neoplasm, or mass. Tumours do not have a blood supply and their size is limited. Several years may have passed before a tumour grows to about *2mm* in diameter [8]. Within the mass of the tumour, cell replication is balanced by programmed cell death, which is the avascular period for the tumour, during which it has a sufficient supply of oxygen and nutrients [36].

However, a tumour does not tend to stay in this state forever, as it begins to progress to the

surrounding tissues in a feature of acceleration. With the development of the tumour, the tumour runs out of oxygen and nutrients. Inside the tumour towards the centre, cells are deprived of an adequate supply of oxygen, situation known as hypoxia. The hypoxic cells activate the hypoxia stress response. These changes in the cells lead to the release of soluble proteins, which are called tumour angiogenic factors (TAF), from the tumour or its immediate vicinity [6, 8]. These TAFs diffuse and spread into the surrounding tissues, binding to receptors on the surface of the endothelial cells (EC) of nearby blood vessels [8]. The combination triggers a series of complicated reactions, initiating a cascade of processes leading to the formation of blood vessel sprouts which develop towards the tumour, and which consequently promote the development of the tumour [8].

Early in 1975, Folkman and Klagsbrun [37] first reported the event of tumour-induced angiogenesis by a solid tumour secreting a number of chemicals, collectively called tumour angiogenic factors (TAF). These chemical factors diffuse through the tissue creating a chemical concentration gradient between the tumour and existing vessels. Since then, the term TAF is generally used in modelling tumour induced angiogenesis. TAF represents several angiogenic factors, for example, vascular endothelial growth factor (VEGF), acidic and basic fibroblast growth factor (αFGF, bFGF), angiogenin, and others [37]. In this thesis, we have used the term TAF to establish the tumour-induced angiogenesis, where TAF mainly refers to VEGF ligands which are secreted by the tumour cells in hypoxia and diffuse from the tumour into the adjacent microenvironment.

VEGF binds to its receptors on the surface of ECs in the interior of blood vessels. VEGF causes ECs to break through existing blood vessels and migrate towards the signal, thus causing the growth and replication of new blood vessels. Through angiogenesis, tumours

induce the host's blood vessel system to supply them with the nutrients the tumour needs to grow and develop, in a process known as tumour-induced angiogenesis.

### 2.2.2 Angiogenesis

Angiogenesis is the procedure of creating new blood vessels from the parent vasculature [38]. It has become the focus of a great number of experimental and theoretical studies on tumours, in that it is a pivotal requirement for the growth, progression, and metastatic spread of a tumour [32-34]. Hence, it is vital to model computationally the micro procedure of angiogenesis for research purposes. Among the many models in the literature attempting to address different features of the angiogenic process, the beginning of tumour-induced angiogenesis marks the new phase of tumours which turn from harmless to fatal for the patient [6, 8]. The concept that tumour growth is dependent on tumour-induced angiogenesis was firstly proposed by Judah Folkman in 1971 [39]. Since then, a huge amount of research in the field related to tumour-induced angiogenesis has been developed.

After several decades, significant progress has been made. The phenomena of angiogenesis occurs in many situations, such as the growth of the embryo and the process of wound healing [36]. The tumour releases proteins which stimulate cellular growth, proliferation, and differentiation, and these are classified as growth factors, such as VEGF, bFGF, transforming growth factors (TGF- and platelet-derived growth factor (PDGF), interleukin-8 (Il-8), and tumour necrosis factor alpha (TNF-alpha) [40]. Section 2.3.3 will discuss the growth factors related to the present study in detail.

### 2.2.3 Cell signalling

Cell signalling is an important concept in biology which is discussed here to provide a general understanding of tumour-induced angiogenesis. Organisms have the ability to constantly adjust and dynamically coordinate their own activities with environmental changes. An essential requirement for this process is a communication function between cells and their environment inside organisms. The function of communicating with the environment, between cells and within a cell, is called signal transduction. The signal transduction is realised through a series of pathways by which signals are received and processed, amplified, and/or terminated [41]. Signal transduction occurs when an extracellular signalling molecule, the ligand called primary messenger, binds to the receptor on the cell surface. The receptor activates and generates a cascade of signals through the cell embrane. This receptor triggers intracellular molecules creating a response, called second messagers, inside the cell, through the nuclear membrane into the nucleus, enabling gene transcription and protein synthesis. The second messengers can influence gene expression after they diffuse to the nucleus, and can also be amplified significantly. Thus, a low concentration of signalling molecule in the environment can yield a large intracellular signal and response [42]. The signalling transduction mechanism can be simply illustrated with the following schematic diagram.

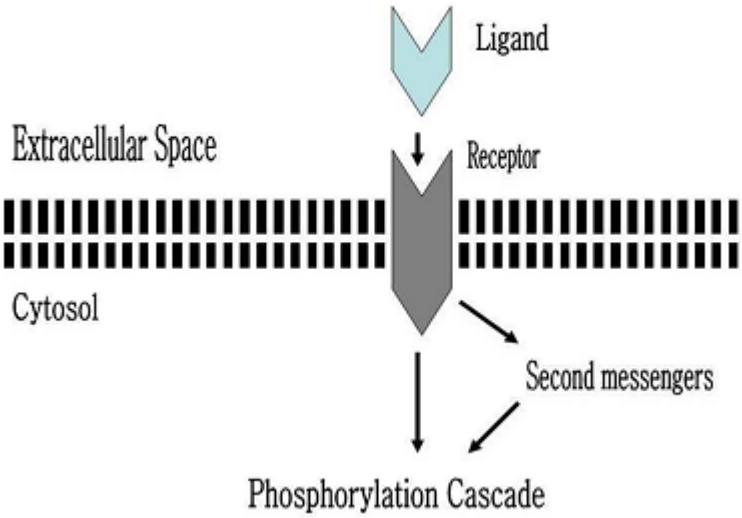


Figure 2.1. A schematic diagram of a simplified transduction signal pathway

Cells communicate with each other in order to combine into networks that achieve higher levels of organisation, such as tissues and organs. The cell-cell communication in all organisms is mediated through complicated networks. The networks integrate intracellular processes and extracellular signals to generate cellular responses [43].

Signal transduction occurs when an extracellular signalling molecule binds to the cell surface, where receptors activate as a sequence of the passive diffusion of the ligand through the plasma membrane [42]. In turn, these receptors trigger intracellular molecules, creating a response inside the cell when the ligands pass through the nuclear membrane into the nucleus, enabling gene transcription and protein synthesis [42].

Intracellular signals are mainly caused by protein kinases and phosphatases in the cellular structure. Cytokines and tyrosine kinases surrounding the nucleus are phosphorylated and translocate from the cytoplasm to the nucleus to act as transcription activators [42].

Extracellular signals are caused by many different chemical signals from their surroundings. The basic cell-cell communication depends on cell membrane receptors and is triggered by the extracellular signals generated by cells [44]. During the process of

signal transduction, information is transmitted from extracellular signals to intracellular signals. An external signal stimulates a receptor at the cell membrane and the stimulus can be altered between physical forms through intracellular biochemical reactions [45, 46]. In this way, the relay of information can be promoted. The receptors are usually transmembrane proteins on the target cell surface. When they bind with specific signalling molecules (ligands), they become activated and produce the signal through a series of intracellular reactions that culminate in changes to the rate of gene expression or enzyme activity [47]. Through ligand binding, signalling often modifies intracellular enzymes or activation factor activity.

In addition, a signalling feedback loop plays an important role in the biological process. The phenomenon of signalling regulation between cells has been reported [4, 48, 49]. For example, Freeman [50] observed that up- and down-regulatory feedback loops are important in dynamic regulation in the intercellular communication. He analysed the temporal and spatial control of signalling by feedback and pointed out that while up-regulatory feedback generates distinct signals, down- regulatory feedback can restrict the ligand range to contribute to stability [50]. Signalling regulation occurs in angiogenesis, and thus should be considered in research on tumour-induced angiogenesis. In section 2.3.4, particular signalling pathways related to our study will be discussed in detail.

### 2.2.4 Cell communication in nascent sprouting

Every cell must have the ability to sense their surroundings for changes in conditions (for example, through the detection of extracellular molecules), and must be able to generate a

range of responses to these changes [51]. The situation is the same during angiogenesis. The ECs in the tip phenotype sense the soluble protein molecule VEGF-A by developing filopodia to probe into the ECM. A range of responses is generated, such as to migrate, bind the ligand with receptors, and trigger a cascade of reactions inside, leading to generate VEGF signals [4]. These sense and response systems need to be tightly regulated and there are a number of signalling pathways that cells may signal to each other, which mainly depend on the concentration of the interactions involved [52]. If cells are adjacent, they may signal through surface ligands and membrane receptors, or through the membrane-bound ligands of one cell identified and combined by a membrane receptor on a neighbouring cell [51]. If the cells are further apart, they may communicate through the release of signalling molecules, such as hormones, cytokines and growth factors [53]. In angiogenesis, these may include soluble VEGFR-1 (sFlt-1), tumour necrosis factors (TNF), and the members of VEGF family. Examples of growth factors include platelet derived growth factor (PDGF), epidermal growth factor, and fibroblast growth factor.

## 2.3 Tumour-induced angiogenesis

### 2.3.1 A complicated procedure involved in angiogenesis

Tumour-induced angiogenesis is a complicated procedure, including the activation and migration of ECs, the specification of tip and stalk phenotypes of ECs, and the proliferation and formation of a pathogenic capillary network [4]. The formation of the network is mainly carried out by spearhead sprouting capillary vessels and emerging new branches [4].

These vessels and branches are connected and subsequently remodelled into a functional capillary network [34].

Angiogenesis initiates from the sprouting of tips from existing parent vessels. In tumour-induced angiogenesis, the produced vessels appear tortuous, are uniquely formed, and are also notoriously leaky and mosaic in their cellular composition [54, 55]. The structure of the abnormal vessels affects the delivery of drugs in chemotherapy, and also affects the opportunity for tumour cells to spread along the vessels to distant parts of the body to form new metastases [35]. Thus, there are many reviews on the interaction between tumour and vessels, and between vessels and extracellular matrix (ECM), and the different phenomena and functions between normal vasculature and that produced by tumour-induced angiogenesis [56].

A huge and complicated variety of cells, bio-chemicals and processes have been found to be involved in tumour-induced angiogenesis, including both proangiogenic and antiangiogenic factors, the specification of cell phenotypes, the signalling pathways and their regulation. The discussion here is not meant to be exhaustive, but rather to cover a selection of the fundamental topics in the biology of tumour-induced angiogenesis which have informed and are relevant to the present study. Thus, focus in this thesis is given to ECs, VEGF, the relationship between EC specification and blood vessel formation, and sprouting and branching, in which VEGF and Notch signalling pathways are highlighted.

### 2.3.2 Endothelial cells (ECs)

ECs are the most important cells involved in the process of angiogenesis, and sprouting is

the fundamental process of angiogenesis [4]. Those ECs that form the vessel at a nascent sprouting differentiate into tip and stalk phenotypes. The choice of tip and stalk depends on the position of the ECs and the VEGF condition. This is because during sprouting ECs in the nascent sprout are specified into two distinct cellular phenotypes, tip cells and stalk cells, both of which are endowed with specialized functions [4].

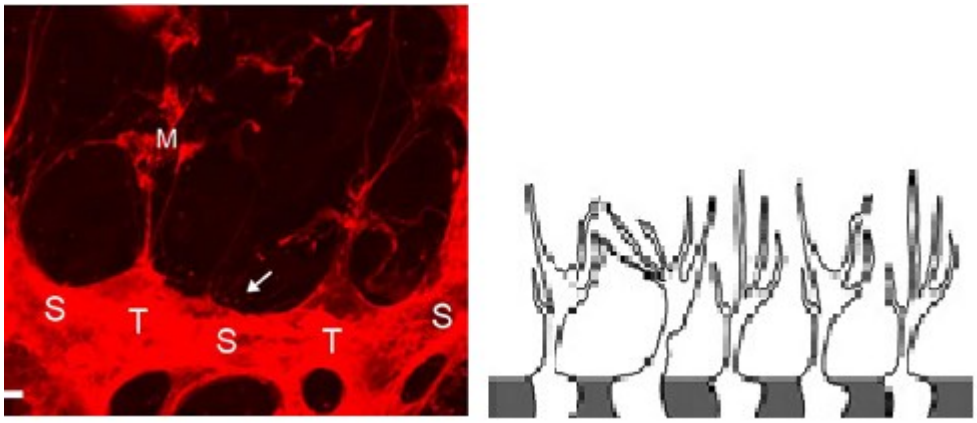


(a) (b)

Figure 2.2 Illustrations of endothelial cells.

(a) A limited number of endothelial cells which correspond to either tip cells (T) or stalk cells (S) and macrophage (M); (b) The tip and stalk cell specification under the influence of VEGF and Notch signalling, forming a consistent pattern of pairing tip and stalk cells [31].

The cells which guide new vessels at nascent sprouts are specialised as endothelial tip cells [4]. The function of tip cells is to lead the movement of nascent blood vessels into an avascular tissue [7]. The tip cell at the spearhead of the vasculature consists of a single EC which extends multiple, long filopodia which probe into the ECM [16, 27, 57]. It determines the route of sprouting to form an organized vessel network [16], and is capable of migrating and invading but is unable to proliferate [16]. It also does not take part in the

generation of the lumen of a vasculature [58].

Following tip cells are stalk cells. These ECs are referred to as endothelial stalk cells with different characteristics from tip cells. They are also the ECs that produce fewer filopodia but are proliferative [16, 30, 57]. Stalk cells proliferate more frequently, and are linked to each other to maintain the stability of the vessels and keep the vessels growing in length and diameter [4]. In addition, stalk cells undergo positional rearrangements within a vessel to form the lumen [4] and to make the vessels bigger in diameter. Endothelial tip and stalk cells are also different in their gene expression profile.

The phenotype selection of ECs is determined by VEGF and Notch signalling, because the VEGF and Notch signalling regulatory mechanism engage in a complicated crosstalk to balance tip and stalk cell differentiation and to regulate directed tip cell migration and stalk cell proliferation [4, 31]. In this way, sprouting occurs and finally makes angiogenesis develop. The VEGF and Notch signalling regulatory mechanism is crucial in angiogenesis [4].

EC migration is also influenced by VEGF and other factors. Recently, a number of studies have shown that sequestering the VEGF-A by the injection of antibodies leads to the inhibition of EC migration and delays the plexus formation [59]. The result is the same as that of the removal of the VEGF gradient in the retina by increased expression of VEGF-A in transgenic mouse models [16, 60]. This proves that the VEGF gradient plays an essential and sufficient role in the formation of the vasculature. During angiogenesis, the migration of ECs in the ECM is very important. The interactions between the ECs and the ECM are mainly influenced by fibronectin, which has been shown to enhance cell adhesion to the matrix. Fibronectin, a matrix macromolecule, is a major component and an insoluble

constituent of the ECM and basement membranes of cells [61]. The insolubility of the cell adhesion function is known as haptotactic influence. Haptotactic influence in the migration of ECs is well known, and is mainly expressed by the existence of fibronectin gradient [7]. ECs use fibronectin for attachment in the matrix through integrins, a family of cell-surface receptors [62], and migrate up a concentration gradient of fibronectin [63]. The migration of ECs is promoted by fibronectin. The response of the ECs to a gradient of adhesiveness of bound fibronectin is termed haptotaxis [64, 65]. In addition to chemotaxis by VEGF, there is a complementary haptotactic response of endothelial tip cells to the fibronectin present within the extracellular matrix [66]. Astrocytes, a type of cell which can express VEGF-A in central nervous system angiogenesis, is another haptotactic factor which prevents the migration ability of ECs by the inhibition of ECs binding to fibronectin [59]. Tip cells may use its filopodia to attach to the astrocytes to migrate. The astrocyte-derived matrix may involve transient fibronectin deposition on astrocytes, which have been observed together with fibronectin-type integrin receptors localized at the tips of the endothelial filopodia [16]. Both chemotaxis and haptotaxis play an important role in ECs migration during angiogenesis; thus, in Chapter 4 we will demonstrate the modelling of the influence of VEGF and fibronetin. The function of VEGF will be discussed in detail in section 2.3.3.

### 2.3.3 Vascular endothelial growth factor (VEGF)

VEGF is a kind of glycoprotein found in the form of homodimers, with a mass in the range of 34-45 kDa. It is able to stimulate the generation of new blood vessels [67]. VEGF-A is

one of the important members in the VEGF family which induces angiogenesis; other members are VEGF-B, VEGF-C, VEGF-D and placental growth factor (PLGF) [68]. VEGF-A has multiple isoforms. At least seven different VEGF-A isoforms are found in humans, including VEGF-$A_{121}$, -$A_{145}$, -$A_{148}$, -$A_{165}$, -$A_{183}$, -$A_{189}$ and -$A_{206}$ [67], and among them, three major secreted forms of isoforms are VEGF-$A_{121}$, VEGF-$A_{165}$, and VEGF-$A_{189}$ [69]. The number in these names refers to the number of amino acids in the mature protein. The most frequently secreted isoform is VEGF-$A_{165}$ [70]. In mice, VEGF isoforms all have fewer amino acids, and so the corresponding major isoforms are VEGF-$A_{120}$, VEGF-$A_{164}$ and VEGF-$A_{188}$ [67].

Isoforms of VEGF-A are the same in the receptor binding region and the carboxyl terminal section [2, 4]. There are two regions of the protein, which appear different in different isoforms. In an area known as the heparin binding domain, sequences may be coded by both exon 6 and exon 7 of the gene such as in VEGF-$A_{189}$, or be coded just by exon 7 such as in VEGF-$A_{165}$, or there are no sequences such as in VEGF-$A_{121}$[71, 72]. The sequences encoded by exon 6 and exon 7 are for binding to the cell surface and ECM, especially for binding heparin and heparin-sulphate proteoglycans (HSPGs), which are abundant in both the cell surface and ECM [73]. The VEGF-$A_{189}$ with both exon 6 and exon 7 binds strongly to the ECM and cell surface, VEGF-$A_{165}$ with exon 7 binds moderately, and VEGF-$A_{121}$ without exon is known to diffuse freely [74]. The sequences encoded by exon 7 enable it to bind to neuropilin, so VEGF-$A_{189}$ and VEGF-$A_{165}$, both with exon 7, can bind to neuropilins, the cell-surface glycoproteins, which were discovered as other co-receptors. The neuropilin1 (Nrp1) and neuropilin-2 (Nrp2) enhance the binding activity of VEGF to VEGFR1 and VEGFR2 and the effectiveness of the VEGF stimulation of their

receptors [48, 70, 75].

Although a number of different variants of VEGF-A have been identified in recent research, VEGF-$A_{165}$ and VEGF-$A_{164}$ are the most widely expressed variants of human and murine homologue splice variants, respectively [76]. Both of the variants can bind to ECM and diffuse in the extracellular microenvironment. VEGF-$A_{164}$ is the major isoform for the formation of the vasculature in retinas of mice [16, 76]. It is assumed that the isoforms have different angiogenic effects as a result of the differences in binding ability.

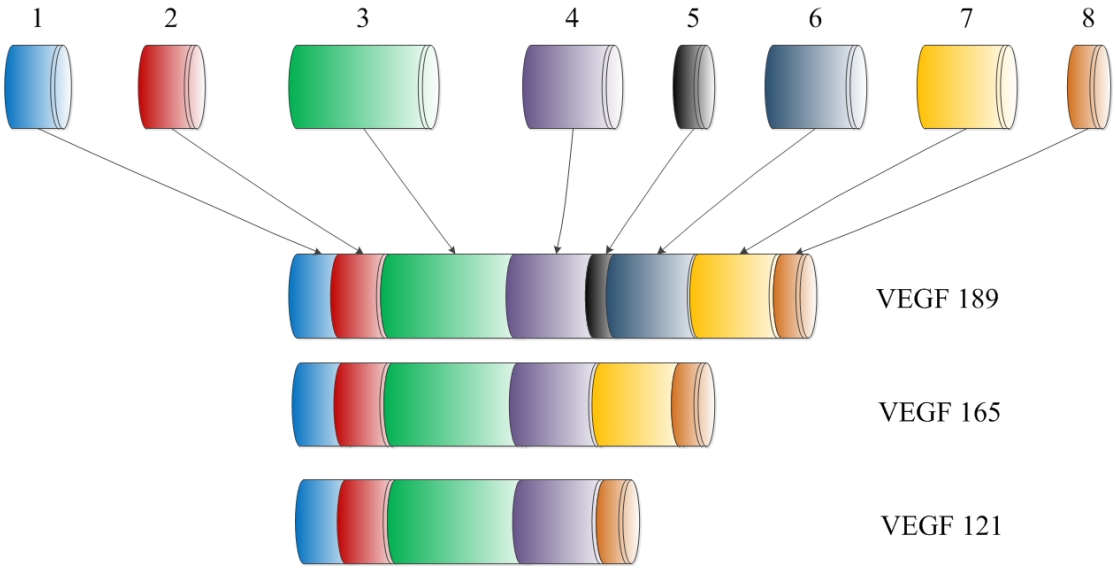


Figure 2.3 Illustration of three major VEGF-A isoforms which are different in molecular weight and in binding ability.

Three major VEGF-A isoforms (ignore minor isoforms) VEGF-$A_{121}$, VEGF-$A_{165}$ and VEGF-$A_{189}$ (in mice, VEGF-$A_{120}$, VEGF-$A_{164}$ and VEGF-$A_{188}$) Exons 6 and 7 have heparin-binding domains, and each major isoform has a different capacity for matrix interactions [2].

Actions of VEGF-A include at least two aspects:

1. VEGF-A gradient is necessary for the migration of ECs. It can be secreted by tumours or by astrocytes, a kind of cell which can generate VEGF in hypoxia. Astrocytes contact the filopodia of the tip cells and can guide the direction of sprouting. In the development of the retina, astrocytes are found as a source of VEGF-A secreted in hypoxic regions [16]. Once the tissue is in hypoxia, VEGF-A is generated by astrocytes. The highest VEGF-A concentration is found in the avascular region of a retina, and the lowest is found in the vascularised centre [16]. Disturbed VEGF-A gradient inhibits endothelial tip cell migration and results in defective tip cell filopodia formation [16]. Endothelial tip cells respond to a VEGF-A gradient but not to the local concentration of VEGF-A, whereas endothelial stalk cells do not respond to a VEGF-A gradient but to the local concentration of VEGF-A [16]. Since the local concentration of VEGF-A affecting the stalk cell proliferation leads to the increase of ECs per vessel length, the diameter of vessels is increased. Thus, the balance of guided tip cell migration and stalk cell proliferation determines the vessel patterns [16].

2. VEGF-A is the factor which increases the permeability of vessels, and the action is very effective. The effect of VEGF-A is 50,000 times more than that of histamine [77], with an effective concentration of below 1nmol/L [77]. VEGF-A is also known as vascular permeability factor due to its effect on increasing the permeability of blood vessels. In experiments where VEGF-A was injected *in vivo*, the promoted permeability was within one minute [77]. When the vessels become more permeable, blood plasma leaks out and the clotting system is activated; this will finally result in deposition of fibrin [77].

Here in the thesis, the model established focuses on the first action of VEGF-A, whereas the second action of VEGF-A used as the factor to increase vessel permeability will not be discussed. The reason for this is that our focus is to establish the model to describe the development of the vascular network and the regulatory mechanism of VEGF and Notch signalling pathways, and if too many variables and parameters are involved in a model it becomes too complex and the results will be confused. Thus, keeping the model free of excessive elements is a trend known as simple focus but extendable modelling [78].

The expression and functions of VEGF-A are crucially important for angiogenesis. VEGF-A is required for chemotaxis of ECs migration, differentiation and vascular remodelling [4]. The presence of VEGF-A promotes the migration and differentiation of ECs. In vascular development, VEGF-A increases the differentiation of ECs and the expression of genes related to these processes, such as matrix metalloproteases (MMP) activation and specification of tip and stalk from ECs [4]. It may also promote the expression of receptors, such as VEGFR1 and VEGFR2. VEGF-A also acts on some other cell types, for example it has been found accumulated in EC membrane (see, for instance, [79]).

VEGF-A is described as a survival factor for ECs [80-82], particularly for the cells of immature vessels or those vessels that have not acquired mural cell coverage. For instance, inactivation of VEGF-A allele in mice can cause deficient development of ECs and the inhibition of vessel development, and thereby results in early embryonic fatality [83, 84]. More recent research [85, 86] has found that interactions between VEGF-A, VEGFR2 and TGF-1 can lead to uncontrolled apoptosis in ECs, pointing to a more complex role of VEGF-A in EC survival.

The functions of VEGF are determined by the specificity of their receptors. There are two VEGF receptors (VEGFR), VEGFR-Flt-1 (VEGFR-1) and VEGFR-Flk-1/KDR (VEGFR-2), which are members of the tyrosine-kinase family and conserved in ECs. These VEGF receptors are located in ECs and tumour cells, among others [87, 88]. The expression of these receptors is up-regulated during the development of those pathological states when angiogenesis occurs [89].

### 2.3.4 EC specification and blood vessel formation

Normal blood vessels are tubular shaped [90, 91]. Blood flows through the cavity of the tube which is called a lumen [90, 91]. The coverage on the tube is the vascular basement membrane which acts to maintain the vessel's stability [90, 91]. In the microvasculature, pericytes sparsely distributed on the exterior of the vascular basement membrane are known as the mural cells, but in larger vessels more layers and cell types may be presented [90, 91].

After the contact with angiogenic growth factors such as VEGF-A in particular, the existing parent vessels begin to swell and become more permeable. The ECs begin to secrete enzymes, the proteases, especially matrix metalloproteases (MMPs), which perform a number of functions, including facilitating the ability of ECs to remove the physical barrier in ECM in order to form pathways for the growth of new vessels [92, 93]. When VEGF-A presents, ECs begin to migrate up the gradient of the VEGF toward the tumour. The influence of VEGF leading to ECs migrating up the gradient is called chemotaxis [92, 93]. The proliferation of ECs also takes place simultaneously.

Since signalling pathways always branch and a signalling network may be comprised of multiple pathways, researchers often simply describe signalling pathways diagrammatically as linear sequences of events [94]. There are two possible ways to mediate the branching and generation of networks. One is to combine different signals into a pathway through activating a given signalling component which can receive a signal from different upstream components; the other is to branch into more than one downstream pathway through forming different signals by a given signalling component [94]. Cells receive signals associated with multiple signalling pathways, so their integration of these multiple stimuli can be promoted through a combination of multiple upstream and downstream pathways [47]. Hence, the term crosstalk is used to describe the interdependence of signalling, such that the activity of components in one pathway may impact on signalling in other pathways; crosstalk also enables cells to coordinate multiple inputs at the level of signal transduction [47].

Tumour-induced angiogenesis is a system involving many types of elements, such as ECs, fibronectin, fibroblast and many soluble proteins like VEGF-A, -B, -C, etc. The regulatory signalling system is also very complex, in which the elements can be divided into at least three groups: soluble molecules that transmit signals between cells (e.g. VEGF-A); receptors (e.g. VEGFR1, VEGFR2, sFlt-1); and intracellular signalling components (e.g. Notch receptor) that transmit the stimulation of cell surface receptors through one cell to activate another cell response [4]. The activity of cells is regulated by a series of signalling pathways, with many regulatory molecules, soluble and insoluble molecules to be distributed across the various cell types [4]. Hence, exploring signalling pathways is a

way to understand tumour-induced angiogenesis.

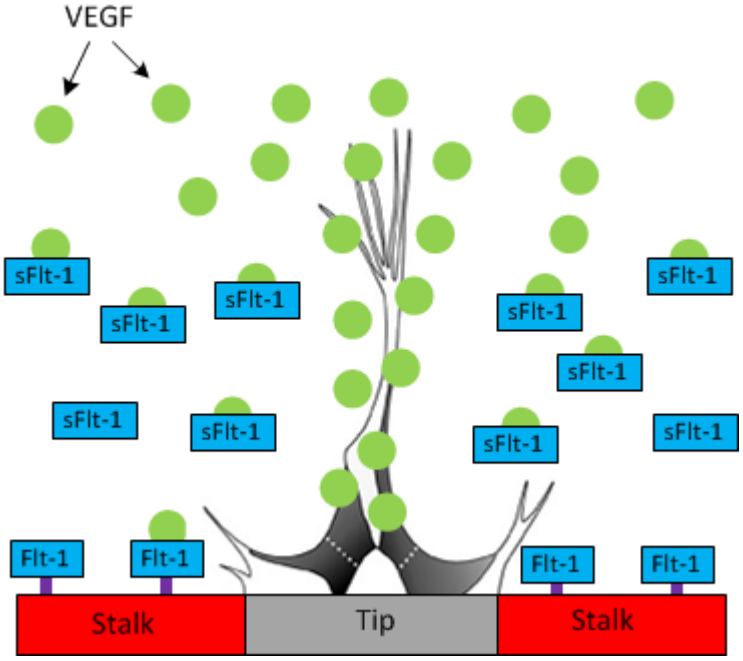


Figure 2.4 Illustration of VEGF-A signalling components.

VEGF-A is secreted and released from a tumour source (top of figure), and forms a gradient from the source to the target vessel. Some endothelial cells respond to this signal. These cells represent the characteristics of tip cell (grey). Its adjacent lateral base cells (red) up-regulate Flt-1 (VEGFR-1) and secrete sFlt-1, which inactivates VEGF-A in the lateral areas, providing a corridor of ligand for effective outward migration of the sprout [2].

#### 2.3.4.1 VEGF signalling pathway

VEGF is known as a key factor of angiogenesis, as mentioned above in section 2.3.3. Mostly, receptors on the target cell surface are activated following the binding of specific ligands. Receptors which are on the surface of cells or the transmembrane are specialised

proteins, and they are utilised for the sensing of signals from the exterior. The signal is sensed externally through binding and activating the cell membrane receptor, or it crosses the cell membrane and activates a receptor. The proangiogenic VEGF signal reaches and reactivates the quiescent ECs to initiate angiogenesis [16].

VEGFR-1 is a member of the VEGFR family, and binds VEGF-A. The binding-affinity of VEGFR-1 for VEGF-A is of a magnitude 10-fold higher than that of VEGFR-2, whereas the kinase activity of VEGFR-1 is only about one tenth that of VEGFR-2 [88]. VEGFR-1 expresses two types of mRNA: one for a full-length receptor known as (Flt-1) and another for a soluble short protein known as soluble VEGFR-1 (sFlt-1). Therefore, VEGFR-1 plays a negative role in angiogenesis because of its high affinity with VEGF-A, but cannot strengthen tyrosine kinase activity, which is vital in VEGFR-2 and crucial in the expression of the VEGF signalling pathway [95]. VEGFR-1 suppresses angiogenesis by trapping VEGF-A and suppressing the local concentration of VEGF-A near VEGFR-2 on the surface of ECs [95]. Thus, VEGFR-1 can act as a competitive inhibitor in the expression of VEGF signalling.

Flt-1 isoforms bind VEGF-A with high affinity and function as competitive inhibitors of the VEGF pathway by ligand binding. Through negatively regulating VEGF expression, the Flt-1 isoforms potentially dominate the mechanism of developmental angiogenesis. Flt-1 isoforms affect vessel proliferation versus sprouting. Secreted from ECs, it potentially inactivates VEGF at a distance from producing ECs. Flt-1 can form a gradient into the matrix from its source. The expression of sFlt-1 by ECs adjacent to an emerging sprout is proposed to inactivate local VEGF [2].

The family of VEGF ligands reacts with tyrosine kinase receptors (VEGF receptor) at the

corridor of tyrosine kinase to form an active complex [4]. In the VEGF signalling pathway, VEGF-A reacts with the tyrosine kinase receptor to form the dimerization of the VEGF receptor (VEGF-VEGFR complex), then releases the VEGF signal. This is VEGF signalling pathway expression. The signal stimulates the ECs to become tip cells. At the same time, during the tip cell formation, the VEGF signalling stimulates Delta-like4 (Dll4) expression which is up-regulated in the tip cells. The mechanism of the VEGF signalling pathway formation is much more complex, but to model the VEGF signalling pathway a simple schematic is used as shown in Figure 2.5.

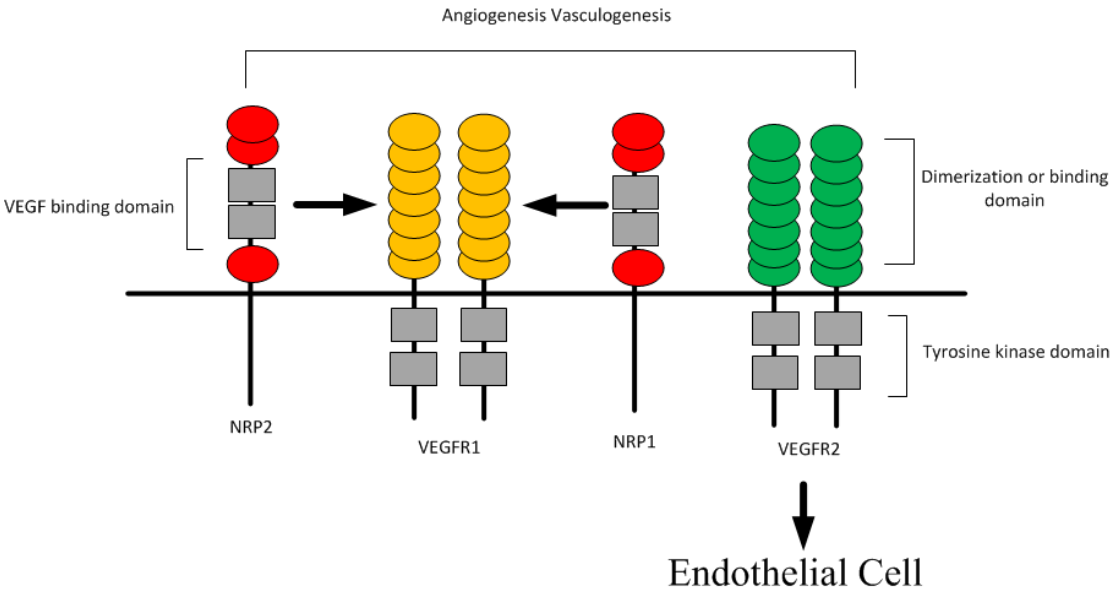


Figure 2.5 Illustration of VEGF-A, VEGF receptors, and co-receptors.

VEGF-A binds the tyrosine kinase receptors, VEGFR2, VEGFR1 and Nrp1; VEGFRs interact with the co-receptors Nrp1; VEGFR2 is the principal mediator of VEGF-A signalling; VEGFR2 regulates angiogenesis during sprouting angiogenesis; VEGFR1 or soluble VEGFR1 (sVEGFR1) acting as a decoy receptor and limits the VEGF activity [4]. Activation of VEGFR1 and VEGFR2 regulates vasculogenesis and angiogenesis.

Once activated, the receptors propagate the signals by triggering a cascade of intracellular

biochemical reactions that change the rate of gene expression or enzyme activity [47]. This situation occurs at the process of the nascent sprouting of angiogenesis: the VEGF-A is the ligand binding with the receptor VEGFR2 on the surface of target ECs, and the receptor propagates the VEGF signals and triggers a cascade of biochemical reactions inside ECs, which consequently generates the ligand Dll4 on its surface [31]. In most cases the consequence of signalling generation through the receptor binding ligand is a modification of the activity of intracellular enzymes [24, 30, 31, 47], such as tyrosine kinase and phosphatase.

#### 2.3.4.2 Notch signalling pathway

Among all the signalling pathways involved in tumour angiogenesis, the Notch signalling pathway is the most crucial, as it regulates the angiogenesis by forming a pattern of pairing tip and stalk cells [31]. It is an intercellular contact-dependent signalling mechanism involved in multiple cell fate decisions and patterning processes during angiogenesis [18, 31, 96]. The core components of the Notch pathway are constituted by Notch receptors and Notch transmembrane ligands, including Delta-like ligands, Jaggeds, among which Dll4 and Jagged1 are the most important [31].

Dll4 acts as a negative regulator of angiogenesis and is up-regulated in tumour vasculature by VEGF signalling [31, 97-100]. After binding with Dll4, the transmembrane Notch receptor is cleaved sequentially, first by an extracellular matrix metalloprotease and then by secretase which releases the Notch intracellular domain (NICD) [31]. After being liberated, NICD translocates to the nucleus where it interacts with the DNA-binding

protein CSL [31]. The Notch signalling pathway is critical in regulating the formation of an appropriate ratio of tip and stalk cells by suppressing tip cell formation in adjacent cells [31]. The molecular mechanism is responsible for the fact that not all ECs stimulated by VEGF become tip cells due to the activity of Dll4-Notch signalling [31]. Thus, the activation of Notch signalling cooperates to promote a suitable pattern of tip cell formation.

Since overexpression of Notch signalling inhibits the tip cell characteristic, the activation level of Notch signalling expression quantitatively determines the ability of individual EC differentiation to the tip or stalk cell during the sprouting [16, 27, 30, 57]. The activation of Notch signalling using a synthetic Jagged1 ligand peptide to reduces the formation of filopodia [22]. The reduction of filopodia means the tip characteristic is weakened, and accordingly the emergence of branching is inhibited [22]. This phenomenon suggests a decrease in the number of ECs acquiring tip cell behaviour [22]. Notch signalling in ECs is more active in the absence of Jagged1, and thereby Jagged1 negatively regulates Notch activity.

Jagged1 enhances differential Notch activity by competitively interfering with the ability of Dll4 [16]. The different ability of Jagged1 and Dll4 ligands to activate Notch is dependent on the glycosyltransferase Fringe, which is strongly activated by Dll4 but inhibited by Jagged1 [16]. The Notch signalling pathway, which appears to function as a central regulator of vascular branching, can be modulated not only by the quantity of individual ligands, but also by their activity profile when Dll4 or Jagged1 interacts with the Notch receptor [4].

Notch signalling, acting as a negative regulator of VEGF-induced angiogenesis, is

essential for proper vascular morphogenesis [18, 24, 30, 31]. The blocking of Notch signalling significantly increases vessel branching and density of the tumour vasculature [18, 24, 30, 31], while over-activation of Notch signalling leads to an unbranched and less dense tumour vasculature devoid of sprouts and filopodia [17, 101]. In the absence of functional Notch signalling, tumour-induced angiogenesis is reduced, despite there being extensively abundant and dense vessel networks [17, 97, 102, 103].

#### 2.3.4.3 Summary

VEGF-A and Notch signalling pathways are key players governing tip and stalk cell behaviour. VEGF-A is crucial in inducing endothelial tip cells, and its role in the procedure is both necessary and sufficient [4]. If tip cells are formed, they are not formed by adjacent ECs but at characteristic intervals to enable adequately spaced branching and sprouting. When VEGF-A is blocked, the tip cell filopodia is completely retracted in the sprouting retinal front [57]. As a result, the blocking of VEGF-A prevents tip cell migration and progression of vascular sprouting [16].

Accordingly, endothelial Notch activation regulates the expression of the different VEGFRs (VEGFR1, VEGFR2 and VEGFR3) as well as their co-receptor Nrp1. Soker et al. [104] reported that the activation of Notch leads to VEGFR1 mRNA induction. In contrast, the reduction of Notch activation in human umbilical vein endothelial cells (HUVECs) marks an increase in VEGFR2 and Nrp1 mRNA, indicating that Notch signalling is able to regulate the ECs responding to VEGF signalling. In fact, it has been suggested that the reduction of VEGFR2 and Nrp1 expression may be responsible for the low proliferative

and migratory response observed in Dll4 overexpressing ECs [21, 26, 104, 105].

VEGF and Notch signalling pathways have, in addition to their role in the development of physiological angiogenesis, also been implied in tip and stalk specification during pathological angiogenesis, such as cancer [17, 23]. We believe that modelling of tumour-induced angiogenesis based on VEGF and Notch signalling pathways is an innovative and promising direction.

### 2.3.5 Sprouting and branching

Sprouting in tumour-induced angiogenesis is a dynamic procedure, including EC migration, establishing connections with vessels encountered, shaping lumen, and finally forming a hierarchically branched and functionally perfused vascular net [4]. In the nascent sprout, ECs are specified into two distinct cellular phenotypes, tip and stalk cells, which are endowed with specialized functions and gene expression patterns [4]. The specification is due to VEGF and Notch signalling as discussed above in section 2.3.4. VEGF-VGEFR-2 and Dll4-Notch signalling engage in an intricate collaboration to balance tip and stalk cell selection and to regulate tip cell migration and stalk cell proliferation during angiogenesis, in which the sprouts and branches emerge and finally create the capillary network [4]. It is thought that during sprouting, specialized with distinct phenotypes and functions, individual ECs cooperate with each other in behaviour which might be described as teamwork [106].

The ECs at the spearheading positions of the vascular sprouts are known as the endothelial tip cell, which has its own characteristic, such as being migratory with long and dynamic

filopodia [16]. Through filopodia, the tip cells sense the directional cues presented by the environment, and thereby define the route in which the new sprout grows [16]. Gerhardt [16] concluded that the extension and maintenance of tip cell filopodia depends on an appropriate VEGF-A concentration distribution, such as its concentration gradient is necessary for the correct guidance of tip cell filopodia. The tip cells create new connections between different sprouts to form an interconnected and circulated functional vascular network [107]. Behind the tip are the cells in stalk phenotype. Producing less filopodia, the stalk cells are highly proliferative [108, 109]. They establish adherent and tight junctions for the new sprout, and form the nascent vascular lumen [108, 109].

As angiogenesis with regard to the formation of a capillary network is too complex to be described clearly, we concentrated on two phenomena, sprouting and branching. To determine angiogenesis, sprouting predominates as the major function and process during the formation of capillary networks, while branching is a special state of sprouting. Thus, we focussed our attention on the mechanism of sprouting, regrade branching as a special type of sprouting.

#### 2.3.5.1 VEGF-Notch signalling pathway crosstalk

First, we must consider how ECs become either tip or stalk cell phenotypes. Previous research shows that the VEGF and Notch signalling pathways are fundamental in the process of ECs becoming either tip or stalk during the angiogenesis sprouting process in tumour angiogenesis [16, 17, 22, 57].

It is necessary for the cells to communicate during angiogenesis. Communication in all

organisms is mediated through complex networks that integrate extracellular signals and intracellular processes for the generation of appropriate cellular responses [43]. The process of angiogenesis is the same, in that the signalling pathway is generated inside and between cells [43]. The fundamental elements for this intercellular communication are the receptors in the cell membrane or on the surface of cells, and the extracellular signals released by adjacent cells [45, 46]. After the receptors sense the extracellular signalling, the transmission of signals to genes and the gene-regulatory mechanism occur through a cascade of reactions known as signal transduction [45, 46]. Here, the stimulus from external signals is received by the receptors on the surface of the cell or at the cell membrane, and are transmitted using intracellular biochemical reactions. This promotes the relay of information [45, 46].

The cells in different phenotypes show their distinct gene expression profiles, including cell surface receptors such as VEGFR1, VEGFR2, VEGFR3, Dll4, and Nidogen-2 [110]. The different expression behaviours and the mechanism of tip and stalk cells in the nascent sprout are still not clear, so recent efforts have been aimed at deciphering the functional relevance of sprouting [4].

The VEGF and Notch signal pathways are both key regulators of the angiogenic process involved in the specification of the tip and stalk cell phenotype. These two pathways work together to achieve functional patterning during sprouting angiogenesis. Several lines of evidence indicate that VEGF signalling acts upstream of the Notch signalling pathway during physiological and pathological angiogenesis, controlling the expression of different Notch components [21, 23, 98].

The cell immediately adjacent to the vascular and hypoxic retina expresses high levels of

VEGF-A, in which high Dll4 expression is found at the vascular sprouting front [23, 57]. An intravitreal injection of VEGF-A increases Dll4 expression, showing that VEGF-A signalling in ECs *in vitro* and *in vivo* quantitatively regulates Dll4 expression [23, 57].

In addition to VEGF-A acting upstream of Dll4, it has become clear that Notch, in turn, controls VEGF signalling. In general, all observations support the concept that Notch signalling via Dll4 principally acts as a negative feedback regulator to control VEGF-induced angiogenesis [4].

Signalling pathways are often branches, and indeed multiple pathways may be integrated into a signalling network, much like the metabolic pathways network noted by Nicholson [94]. The signalling in one pathway may influence the activity of the components of other signalling pathways. This interdependence of signalling is termed crosstalk [47], and enables the cell to coordinate multiple inputs at the level of signal transduction. For example, the VEGF signalling pathway has crosstalk with the Notch signalling pathway in regulating the specification of tip and stalk phenotype from ECs during sprouting. Both the VEGF signalling pathway and the Notch signalling pathway are interdependent. The crosstalk occurs between two adjacent cell membrane receptors.

As described above, we can see the important role of VEGF-VEGFR and Dll4-Notch signalling pathways in angiogenesis. Many studies have investigated the regulatory mechanism involved *in vivo* and *in vitro*. Even if there are many models in tumour-induced angiogenesis *in silico*, it is rare in the modelling of the VEGF-VEGFR and Dll4-Notch signal pathway regulation in angiogenesis. Modelling the regulatory mechanism is a very challenging task, and our goal is to explore the field innovatively by establishing a model based on enzymatic catalysed kinetics.

## 2.3.6 Fibronectin

Fibronectin is a major component of the ECM. The ECM macromolecule occurs in two distinctly different forms. One is soluble a glycoprotein molecular form found in various body fluids (including blood) known as plasma fibronectin, and the other is on insoluble constituent of the ECM and basement membranes of cells, known as cellular fibronectin [111]. Fibronectin plays a very important role in the migration of ECs during angiogenesis. The interactions between fibronectin and ECs directly affect cell migration. These specific interactions between ECs and fibronectin have been verified in Boyden-chamber assays by Greenberg at al. The verification showed that fibronectin stimulates ECs and a number of other cell types' migration directionally [112-114]. Fibronectin has been shown to enhance cell adhesion to the matrix [7, 8]. For both cellular fibronectin and plasma fibronectin, ECs use fibronectin as a major ligand for attachment to the ECM through integrins, a family of cell-surface receptors [51, 62]. The ECs directional migration stimulated by fibronectin have demonstrated that fibronectin promotes cells to migrate up its concentration gradient [63, 115, 116]. The response of ECs to a concentration gradient of fibronectin via adhesiveness of bound was termed haptotaxis [64, 65]. Therefore, in addition to the chemotactic response of ECs to the TAF known as chemotaxis, there is a complementary haptotactic response to the fibronectin presented within ECM known as haptotaxis [66].

## 2.3.7 Retinal models

Mouse retinas are the biological materials mostly used to establish angiogenesis models *in*

*vitro and in vivo* experiments, because retinas are of an ideal structure to visualize the development of angiogenesis and make it observable during vasculature, including sprouting, branching fusion and network formation [16]. Researchers set or disrupt VEGF-A concentration gradient on retinas to study different aspects of vessel formation, including the proliferation, survival and migration of endothelial cells. Retinal models are also used to investigate functions of VEGF-A, the crucial regulator, which regulates the differentiation of tip and stalk phenotypes during blood vessel formation. In retinal models, it can be observed that VEGF-A controls angiogenic sprouting by guiding filopodia extension from specialized endothelial cells situated at the tips of the vascular sprouts. It also can be observed that the tip cells respond to VEGF-A only by guided migration; the stalk cells respond to VEGF-A, occurring in the proliferation. Both of the two cellular responses are triggered by the mediation of VEGF-A on VEGF receptor2 on the surface of ECs. In retinal models, experiment results show that tip cell migration depends on a gradient of VEGF-A, while stalk cell proliferation is regulated by VEGF-A concentration. Thus, in retinal models, it is demonstrated that vessel patterning depends on the balance between two different qualities of the extracellular VEGF-A distribution, which regulates distinct cellular responses during angiogenesis [16]. Dll4 and Notch receptor also play an important role in regulating pattern of vessels [31]. Therefore, the experiment results and conclusions mentioned above come out from retinal models, and are vital and fundamental for researchers in the modelling of angiogenesis. In our thesis, we use the conclusions of retinal models *in vivo* and *in vitro* to establish the models of tumour-induced angiogenesis *in silico*, such as modelling the VEGF-Notch regulatory mechanism of angiogenesis in Chapter 6.

## 2.4 Conclusion

The chapter has reviewed the biological literature which is relevant to the research focus for this thesis. The chapter has performed a comprehensive analysis of research on tumour-induced angiogenesis from the biological perspective, which identified that tumour-induced angiogenesis is a central step in the development of the tumour and regulatory mechanism of VEGF and Notch signalling pathways, which play a crucial role in the selection of tip and stalk during the angiogenesis process. Although a vast amount of biological research has been completed in the field, computational research attached to this aspect is still rare, especially the modelling of angiogenesis based on the VEGF-Notch feedback theories; thus there is a gap between biology and computer engineering. Our focus on the signalling by feedback control mechanism makes an original contribution to the modelling of tumour-induced angiogenesis, and the VEGF and Notch signalling regulatory mechanism is the most important point for us to begin with. The next chapter, Chapter Three, discusses the computational models and modelling methods which helped us to determine the selected technique routes.

# Chapter 3. Modelling and Methods

Modelling of tumour-induced angiogenesis needs advanced mathematical methods, including ordinary differential equations (ODEs), partial differential equations (PDEs) and computer engineering methods such as cellular autometa (CA) and agent-based modelling (ABM). On the other hand, the model to be developed should be in front of the field, so it is necessary to review the models of tumour-induced angiogenesis developed in the past decades to provide an overview of the field. In this chapter we present a review of the modelling of angiogenesis and the methodologies developed so far, providing the basis for the choise of technique approach for the research aim.

## 3.1 Introduction

The development of tumour research has led to a massive and rapidly evolving area covering biological, physiological, chemical, and physical processes to medical investigation. Later on, computational simulation is also involved. Computational modelling is a promising strategy to reveal the mechanism of tumour-induced angiogenesis and provides clues to develop therapy for patients suffering from a tumour. The use of computational modelling and simulation has been adopted by a growing number of researchers [117]. For instance, models based on mathematical equations and based agents have been used to generate hypotheses and decipher secretes of tumour [117].

To model tumour-induced angiogenesis, it is necessary to apply advanced mathematical tools. We used ordinary differential equations (ODEs), one useful advanced mathematical tool, to solve the regulation control problems for tumour-induced angiogenesis, involving the VEGF/Notch signalling feedback loop. We also used partial differential equations (PDEs), another advanced mathematical tool, to establish a two-dimensional continuum model to simulate the continuum of the biological phenomena, such as VEGF gradient, ECM, enzymes secreted by ECs and EC migration. These different substances as variables are in continuum distribution, and we used discrete agent-based modelling (ABM) to realise the simulation of angiogenesis. Hence, in this chapter we will discuss modelling methods which could give us insights into the modelling field related to our research.

## 3.2 Mathematical Modelling Techniques

### 3.2.1 ODE Models

ODEs are an advanced mathematical tool used to solve problems including reaction rate kinetics, enzymatic catalysed reactions, and feedback control systems [9, 118]. It has been used to model cancer for many years. The early work was described by Greenspan in modelling solid tumour growth [9, 118]. ODE models are generally simpler to analyse and can provide early, useful results, where spatial considerations can be ignored. ODE models can obtain and send control parameters dynamically [118]. By establishing an enzymatic catalytic reaction kinetic model which represents the VEGF and Notch signalling feedback loop, we can use ODEs to generate control signals to control the sprouting which is key to tumour-induced angiogenesis (Chapter Two).

Perhaps Goodwin [119] may have been the first to model intracellular regulatory mechanisms. He studied the essential control features of enzymatic regulatory processes, through which he proposed a regulatory model. The model considered the intracellular interactions between enzymes and their mRNA in a negative feedback loop which lead to a set of ODEs describing the dynamics of this system. This showed oscillatory behaviour in relation to the organization of cellular processes in time [119]. Goodwin [119] reported that the majority of enzymes were synthesised in a cell and their activities were regulated by negative feedback control processes.

Many aspects of signalling pathways have been modelled, and the models are mainly based on ODEs. Some of the models have involved very complex equations, with many variables, coefficients, and a series of complicated reactions. For example, a representative model in

ODEs in describing NF-κB signalling pathway is the model of Hoffmann et al. [120]. They developed an ODE-based computational model using Gepasi software. This mathematical model is comprised of 24 ODEs describing kinetic reactions and the change of variables' concentrations. In these equations, they were particularly interested in the temporal control of NF-κB activation by the coordinated degradation and synthesis of IκB proteins. This kind of model succeeds in modelling the signalling pathway, but is too complex to be verified in wet-lab because too many coefficients should be determined and explained, which limits its usefulness.

The models mentioned may represent the major components of the NF-κB signalling pathway, both mathematically and computationally. Although these models are successful in describing a series of complicated reactions, they are still questionable because the complex nature of these models makes them computationally expensive to run, and also complicated analysis techniques are required to make inferences from simulation results. As such, the term minimal models have been proposed and developed as simply as possible, by establishing a minimum number of equations of models to replicate the majority of the more complex computational models [121]. These reductionist models can also be investigated *in vitro*.

After Carlotti and colleagues' work, Krishna et al. [122] developed the first minimal model in NF-κB signalling pathway [123] and focused on a small core network of the pathway that drove oscillatory behaviour. By reducing the model of Hoffmann et al. to a core feedback loop of three coupled ODEs, they were able to ascertain the minimal model which was required to generate oscillations in modelling the signalling pathway. They focused on describing the crucial reaction generating oscillation behaviour, and set an

upper limit within the system for the degradation rate; they then conjectured that this effectively introduced a time delay into the negative feedback loop, which is known to generate oscillations. Thus, minimal models represent another trend of modelling in signalling pathways.

Based on the recent experimental evidence, Stamper et al. [9] developed a model considering both angiogenesis and vasculogenesis, both of which contribute to vessel formation, by using a nonlinear ODEs-based continuum approach. This model is composed of seven variables, such as the vessel within the tumour, activation of ECs by TAF (e.g. VEGF), and levels of endothelial progenitor cells (EPCs) which contribute to the construction of new blood vessels by vasculogenesis [9]. In their model, angiogenesis was referred to as the migration and proliferation of ECs from pre-existing vessels, while vasculogenesis referred to the mobilisation of bone marrow-derived EPCs. The EPCs homed in on the tumour, where subsequently they might differentiate into ECs and form vascular structures. In this model, vessels were created by angiogenesis and vasculogenesis, and tumours were shown to exhibit similar growth dynamics. The model reveals three possible results: the tumour had unlimited vascular growth; the tumour evolved to a vascular equilibrium; or the tumour remained in an avascular steady state [9]. Neither the immune system response to the tumour nor chemotherapeutic drugs were involved in the model. The aim of the modelling was to reduce vasculogenesis and inhibit tumour growth, but a detailed discussion was given on using the model dependent parameter values to predict the effects of these treatments.

In our study, the use of ODEs was to describe reaction kinetic-based interactions between different variables, and to present the rate of change in system variables over time.

Applying the mathematical tool ODEs in our model, we established a VEGF and Notch signalling regulation minimal model based on enzymatic catalysed kinetic reactions.

### 3.2.2 PDE Models

ODE models are very useful in the field of signalling feedback control, but their limitations are very clear. They are not able to describe reactions in which reactions occur spatially and temporally. Particularly, they ignore the spatial aspects of biological phenomena that are of critical importance, such as tumours' inhomogeneous nutrient delivery, heterogeneous tissue structure, and angiogenesis [117].

In the modelling of tumour-induced angiogenesis, there are many different types of reactions, such as EC migration and proliferation, enzymes secreted by ECs, degradation of ECM through secretion of MMPs, and the diffusion of VEGF from the tumour to its environment. The simulation to describe those reactions that occur at different locations and times depends on Fick's diffusion law [117].

These are all implemented at space and time dimensions. Hence, all these biological phenomena should be solved by the use of PDEs allowing for additional independent variables, such as space and time [117]. For example, a PDE model can spatially represent the change in concentration of ECs in time and space to represent their movement.

Early in 1985, Balding and McElwain [124] established a one-dimensional, mathematical model to describe published angiogenesis experiment results. In these experiments, TAF was placed in the avascular cornea of a host animal [124]. TAF diffuses and forms

concentration gradient chemotactically. This triggered angiogenesis, which caused sprouting and growth from nearby pre-existing vessels. The sprouts or tips move toward the source of TAF, form loops by anastomosis and leave new capillary vessels in their trails [8]. Disruption of the concentration gradient of TAF results in a gradual regress of the new vessel [124]. To model these experiment results, Balding and McElwain [124] developed conservation equations for the TAF or angiogenic factor ($c$) and for the blood vessels. In their model, the new vessel was composed of two variables, motile tips ($n$) and capillary vessel lengths ($\rho$). This concept elegantly distinguished the different behaviours and spatial distribution in angiogenesis.

One of the most influential mathematical models of tumour-induced angiogenesis using PDEs is the work of Anderson and Chaplain et al. [6-8, 36]. In their models, the variables are ECs, fibronectin, VEGF, ECM, and enzymes secreted by ECs. The application of PDEs to simulate angiogenesis exhibits the migration of ECs from the side of an existing vessel towards the side of tumour, during which the concentration of ECs changes at different locations and time. During angiogenesis, ECs move by random motion, chemotaxis generated by the VEGF gradient, or haptotaxis. But their model does not contain any consideration of EC proliferation, even though the equations reveal angiogenesis dynamics, such as diffusion of TAF, fibronectin, and angiostatin [125].

In fact, during angiogenesis when the capillary network approaches the tumour, the density of the capillary network also increases, which means the density of the ECs should increase first [125]. To supply enough cells to form the capillary network, proliferation is essential for the formation of the capillary network [126-128]. During the procedure, ECM is

degraded to make way for the development of the capillary network. As a result, the degradation dynamics of the ECM is catalysed by protease enzymes.

Mantzaris, Webb and Othmer [125] point out that EC proliferation influences the protease enzyme dynamics in the tissue. Hence, the protease enzyme concentration should be above a certain threshold value so that cells can proliferate. Moreover, high values of the protease enzyme also stimulate migration through the degradation of fibronectin [125]. Thus, Mantzaris, Webb and Othmer [125] argue that the tight relationship between proliferation and migration in this model contradicts some experimental observations; they point out that localisation of proliferation behind the leading tip of the vasculature is multiplying the proliferation term with an arbitrary function depending on tip curvature. Since ECs have a long half-life [129], Mantzaris, Webb and Othmer [125] further propose that Anderson and Chaplain's continuous model does not include EC proliferation. We agree with Mantzaris's opinion and so we improved in this aspect by involving the EC proliferation in our model. Anderson and Chaplain assumed the highest concentration of fibronectin is at the side of the parent vessel and the lowest concentration is at the side of the tumour line source, which is opposite to that of TAF in the concentration gradient. Based on this assumption, they established a model and simulated the migration of ECs influenced by the concentration gradient of fibronectin. The simulation results show that the velocity of ECs migration is slowed by the concentration gradient of fibronectin [7, 8]. However, we noticed that in recent studies, some bio-clues imply that for some subgroups of tumours, the highest concentration of fibronectin may be at the side of the tumour line source and the lowest concentration at the side of the parent vessel. For this reason, we may improve their work by establishing a model to simulate tumour-induced angiogenesis influenced by

haptotaxis. The bio-clues are dip50, scussed as follows.

The fibroblasts have high expression of fibronectin at the tumour side according to Lundberg [130]. Their results indicate that fibroblasts induce the CpG island methylator phenotype (CIMP)-negative tumour cells to produce more fibronectin. Because cancer is always associated with fibroblasts, the term CAF is known as cancer associated fibroblasts. It implies that for some cancers the fibronectin density in the ECM near the tumour may be higher than that in the ECM far away from the tumour. The tumour stroma is enriched in fibrillar proteins, including collagen I and fibronectin [130]. According to Kumar, Das and Sen [131], “Cancer progression is marked by increased deposition and cross linking of fibrillar ECM proteins, including collagen and fibronectin, which lead to an increase in ECM density and enhance the progression.” This means that the invasive tumour increases the density of fibronectin by deposition at the ECM near the tumour. In turn, this implies that the concentration of fibronectin may be higher near the tumour. For example, in breast cancer, there is a nearly 10-20 fold increase in bulk stiffness in the tumour microenvironment [131].

According to a recent study, fibronectin also plays a critical role in the invasion of cancer progression. Cao et al. [132] report that fibronectin protein expression in human gallbladder cancer (GBC) tissue samples is primarily overexpressed. The overexpression of fibronectin promoted cancer progression and was associated with a worse prognosis in GBC patients. Their experimental results indicate that exogenous fibronectin significantly enhances and promotes the proliferation and metastasis of GBC cells not only *in vitro* but also *in vivo*. The overexpression of fibronectin near tumours has also been reported [130]. From these clues, we assume that it may be possible that in some subgroups of tumours,

especially the invasive tumour, the density of fibronectin is higher near the tumour than far away from the tumour. For other types of tumour, including Small Cell Lung Cancer (SCLC), an aggressive form of lung cancer, the ECM surrounding SCLC cells contains a great amount of fibronectin [130, 133-141].

In some cases, fibronectin density is increased near tumours which would enhance the haptotactic influence. The increased fibronectin density might enhance the haptotactic influence by increasing the cells express receptors to bind to the matrix. We aimed to improve the continuous model of Anderson and Chaplain's work [6-8] from perspectives considering EC proliferation, enzyme catalyzed ECM degradation, and the impact of fibronectin on EC migration. As there are many biological phenomena which occur in space and time during angiogenesis, by establishing a two dimensional model in PDEs and simulating the model, we can obtain a better insight into tumour-induced angiogenesis and achieve parameters of PDEs for the agent-based model which is used to simulate angiogenesis regulated by a VEGF/Notch signalling pathway.

## 3.3 Agent-Based Models

For the modelling of complicated biological systems, the advanced mathematical tools were traditionally used to approach the dynamics of the systems. Through establishing and solving ODEs, the modeller can obtain time-series dynamics at the system level; through establishing and solving PDEs, the modeller can obtain dynamic spatial and temporal information of biological phenomena in the domain simulated. Both of the two advanced mathematical tools are unsuitable for describing individual behaviour. Recently, a number

of computational approaches taken from the field of computer engineering have been used to model individual components. For example, agent-based modelling (ABM) is the one emerging in the computer field.

ABM is an innovative computational methodology using computational objects that focus on the rules and interactions between the individual agents of system [142]. ABM is based on rule setting, agent discrete, and time discrete methods [142-144]. The goal of ABM simulation is to generate the populations of the system agents, to simulate the interactions in a 'virtual world', and to create an experimental model *in silico* [142]. ABM starts with mechanisms or rules for behaviour, and seeks to reconstruct through the computational instantiation of those mechanisms [142]. Thus, ABM can be extremely useful if the goal is to test the veracity of a set of identified or presumed mechanisms in a system.

ABM has been widely applied in the modelling of geographical system and financial marketing research. It rarely enters into the area of biological field. A large amount of significant *in vitro* and *in vivo* data already exists, but it is still difficult to develop a complex modelling technique based on these data. One initial study in using ABM of filopodia is provided by Bentley et al. [30]. They developed an agent-based model to analyse the role of Notch-mediated selection of cells in the early stage of angiogenesis. This model only involves the VEGF-A gradients and simulates filopodia extension during the stalk cell activation procedure, but does not actually refer to the VEGF-Notch regulatory mechanism.

## 3.4 Hybrid Models

De Pillis et al. [145] developed a mathematical model of tumour-immune system/cell interactions, which discussed tumour-immune system/cell dynamics. The model focused on the role of natural killer (NK) and CD8+ T cells. The tumour-immune cell interactions described in the model were in the form of ordinary differential equations (ODEs), including several variables such as the (CD8+ T)-tumour kill term, the immune recruitment term, and the cell-cell kill term. They considered that in previous work tumour cells were assumed to grow logistically in the absence of an immune response, but in fact both CD8+ T cells and NK cells could kill tumour cells. In the presence of tumour cells, the CD8+ T cells were recruited as part of specific immunity. They developed the model associated with variables including tumour immune growth, interaction rates and immune response. The solution of the model was realised by using a numerical differential equations solver and a least-squares method. The simulation results showed that in the immune system the dynamics of CD8+ T cells were different from that of NK cells. Simulations of tumour growth in the developed model can give predictive data by using different levels of immune ligands, effector cells, and tumour resistance.

A number of recent papers used a hybrid continuum mathematical/cellular automata approach to model the interactions between tumours and the immune system. For example, Mallet and de Pillis [146] used a hybrid approach to model the interactions between tumour and immune system on a two-dimensional domain, but angiogenesis was not involved in this model. Byrne et al. [147] developed a hybrid continuous mathematical model, which focused on the response of a vascularised tumour to chemotherapeutic drugs which

targeted proliferating cells. The proliferation and death of tumour cells can be influenced by nutrient diffusion. Tumour cells and the surrounding stromal cells were modelled using a cellular automata approach, while a number of variables such as oxygen and an angiogenic factor were modelled using a continuum approach. The chemoattractant is generated by the tumour cells under hypoxic conditions. The blood vessels in this model were represented by a hexagonal network superimposed on the cellular automata grid. The tumour volume was a mixture composed of macrophages, tumour cells, and extracellular material. The volume of tumour spheroid was assumed to be constant. Simulation results show that changes induced in the vasculature by TAF can lead to oscillations in a tumour's composition. Macrophages infiltrate solid tumours, in which macrophages cause fatal damage to the proliferating tumour cells. This occurs either by delivering cytotoxic factors directly or by releasing enzymes that activate an external pro-drug, thus making the tumour more sensitive to chemotherapeutic drugs that target proliferating cells [148].

Eikenberry et al. [149] presented a model of melanoma invasion into healthy tissue with an immune response. They established a two-dimensional mathematical model, with seven variables such as the growth and metastasis of malignant melanomas. These variables include ECs and angiogenic factors. In this model, the immune system was introduced to simulate its effect on tumour suppression. The immune system includes two variables, cytotoxic cells of the immune system and their attractant. The authors thought that small metastatic satellite lesions could be held to a minimal size through the immune system's interaction with the larger primary tumour, because the existing tumour can trigger and maintain the host's immune activity. So metastatic satellite lesions were optimally suppressed by immune activation when the primary tumour was moderately rather than

minimally or surgically removed. The model illustrates that disruption of the host's immune response after surgical incision of a tumour could lead to increased metastasis which encourages the total cancer mass to increase more quickly. These simulation results are consistent with many clinical case investigations involving surgical resection of a primary melanoma followed by recurrence in local metastases. ECs did not undergo chemotaxis in this model, though TAF affects the rate of EC mitosis and apoptosis. As the immune system cells are assumed to undergo both diffusion and chemotaxis, from the model of Eikenberry et al. we might think that the tumour-immune system dynamics is critically important in determining the likelihood and the extent of tumour regrowth following surgical resection. Thus, their work implies that in the modelling of tumour-induced angiogenesis it would better to include the immune system.

Rejniak and McCawley [150] provided an excellent mini review on approaches to the computational modelling of a variety of interactions between a tumour and its surrounding microenvironment. These computational models mathematically include continuum, cellular automata, particle based, IB cell, and cellular Potts methods. The microenvironment of tumour is very complex, including tumour stromal cells, the dense network of various ECM fibres, and the immune cells (e.g. cytotoxic T-lymphocytes). A tumour was modelled at different scales of complexity, such as chemical interactions, biochemical pathways, cellular functions, and tumour-induced angiogenesis. In the article, the advantages and disadvantages of modelling approaches in the area have been analysed. The authors assume that computational models of cancer are invaluable for researchers by providing them with powerful tools to integrate the complexity into organising principles as well as suggesting testable hypotheses in the future.

## 3.5 Modelling of tumour-induced angiogenesis

For the modelling of tumour-induced angiogenesis, the most representative ones are from the work of Anderson et al. between the 1990s to 2010s. Byrne and Chaplain [148, 151] proposed a snail-trail model for the scenario in which the formation of the vascular network was stimulated by the production of VEGF by a tumour. Anderson et al. [6-8, 152] proposed two dimensional models by using nonlinear partial differential equations (PDEs) to describe the migration of ECs, which are considered as tips from a parent vessel moving towards a solid tumour [7, 11, 153]. In the models, fibronectin and TAF are characterised by the presence of haptotaxis and chemotaxis terms, respectively. Chemotaxis is influenced by the soluble angiogenic isoforms gradient in concentration, which is secreted and diffused from tumours such as TAF. Haptotaxis is formed by insoluble ECM molecules such as fibronectin gradient density. The continuum models successfully simulate the migration distances, moving the velocity and local density of ECs.

As the continuum models could not retain the exact features of capillary networks, since 1998 they have integrated the continuum models with a discrete method to model the spatial and temporal progression of tip cells and capillary network formation [6, 154]. This involves the influence of perfused blood in the development of vessels induced by the tumour [15, 155, 156]. The inclusion of blood perfusion in growing capillary networks implies that the modelling of angiogenesis is going to involve more factors which can influence the forming of vessels [5-7, 157, 158]. With the discrete method, ECs follow a random path in a square lattice towards the tumour. The stochastic version of continuum

models captures the cell-scale structures, which could be called a hybrid discrete-continuum model. The macroscopic clusters of cells in the continuum are described into microscopic as entities in discrete forms, according to laws obtained by a discretization of suitable continuum models, moving towards the tumour under the influence of PDEs and substrata [10]. In this way, Anderson and Chaplain have developed the hybrid discrete-continuum models, and their achievement represents a breakthrough in modelling realistic vascular structures [6-8, 152].

Their idea is to use the coefficients from the five-point stencil of the standard central finite-difference scheme to generate the probabilities of movement for an individual cell, which is influenced by TAF and fibronectin gradients, to superimpose to an isotropic random walk. Branching might take place when sprouts are older than a threshold branching age, and branching occurs stochastically, which means the possibility of branching is based on the concentration of TAF. This is under the assumption that new sprouts must be mature enough before being able to branch [10]. Branching might take place when sprouts are older than a threshold branching age; branching occurs stochastically, and the possibility of branching is based on the concentration of VEGF [10].

The two-dimensional hybrid partial differential equation-discrete model was further developed by Watson and McDougall [36]. The model was derived to track the migration of endothelial tip cells and individual astrocyte in response to the appropriate biochemical cues, such as chemotactic gradient of PDGF-A, including blood perfusion in retinal vascular plexus (RVP), which successfully simulates a wild-type *in silico* RVP structures [36]. They thought that the implementation of the retinal vascular process is an excellent tactic for mathematical modelling, by which modellers can compare the results of retinal

vascular experiments with the results of simulation by computer. This gives a rigorous test for studies *in silico*, especially for the mathematical modelling of tumour-induced angiogenesis, which often results in highly heterogeneous capillary networks which are more straightforward to reproduce numerically by simulation [36]. In their models, the biological regulatory mechanism is still not included.

Many models have appeared in the last decades but few have described the fascinating developmental process of the differentiation of cells during vessel formation. Regulated by VEGF and Notch, the differentiation of cells mainly includes tip and stalk phenotypes specified from ECs. Maggelakis et al. have developed a model approaching to study the interaction between VEGF, oxygen and capillary density in angiogenesis by employing continuum PDEs [12, 159], whereas Liu et al. [13] used a small digitised network taken from the human retina to predict distributions of flow and oxygen partial pressure. Briefly, the exploration of VEGF and Notch signalling regulatory mechanism in the tumour-induced angiogenesis is crucial.

## 3.6 Conclusion

The computational modelling in the field of tumour-induced angiogenesis has developed rapidly in the last few decades. For instance, tip cell density, vessel density, vessel pattern, vessel morphology, developing velocity, etc. have been simulated. Moreover, a variety of methodologies have been developed, including mathematical methods such as PDEs and ODEs, the stochastics method, and the CA and ABM discrete method. Even though effort has been made in the field, the progress of computational modelling is still far behind

compared with the progress in biology, which has recently achieved significant discoveries. Most models focus on simulating the blood vessel morphology, but rarely explore the angiogenesis regulatory mechanism.

This chapter has performed a comprehensive analysis of research on tumour-induced angiogenesis from the computational modelling perspective. The PDEs, ODEs are the powerful mathematical tools which are used to deal with continuum models. ABM and CA are the appropriate methodologies which are used to deal with discrete models. With the help of these methodologies and by integrating these tools, we may model the very complicated tumour-induced angiogenesis in which both the continuum and discrete models are involved. Based on the review in this chapter which has helped to determine our technique routes towards our goal, we decided to model the tumour-induced angiogenesis by using ODEs to model the regulatory signalling kinetically, by using PDEs to model the variables such as ECs, blood vessels, and VEGF etc. spatially and temporally. In this way, we aimed to model the VEGF and Notch signalling regulatory mechanism in the process of angiogenesis to decipher its secret. In the next chapter, Chapter Four, we present and discuss our mathematical models of tumour-induced angiogenesis by chemotaxis, haptotaxis, aiming to provide parameters of PDEs and a broader understanding of the tumour.

# Chapter 4. Modelling of Tumour-Induced Angiogenesis by chemotaxis and haptotaxis

Mathematical modelling of tumour-induced angiogenesis has itself been developed and expanded over years. In general, the angiogenesis occurs temporally and spatially. To incorporate the temporal and spatial scales, PDE is a powerful mathematical method to be used to describe the migration of ECs. The main aim of this chapter is to understand the influence of chemotaxis and haptotaxis in tumour-induced angiogenesis using two mathematical approaches: a continuum approach and an individual cell-based approach. For the continuum approach, first we started from a model of tumour-induced angiogenesis developed by Anderson and Chaplain [2], where the locomotion of ECs is governed by random motility, directional migration towards gradients of soluble chemoattractant TAF or chemotaxis, and directional movement up gradients of insoluble ECM components fibronectin or haptotaxis. We used this model as a basic model for tumour-induced angiogenesis, extended the model by incorporating cell proliferation and proposed a possible mechanism in which invasive tumours enhance haptotaxis and promote angiogenesis. In this chapter we present the continuum approach and discretised approach respectively.

## 4.1 Introduction

This chapter presents and discusses the proposed mathematical models of angiogenesis by tumour-induced chemotaxis and haptotaxis, providing parameters of PDEs and a broader understanding of tumour-induced angiogenesis.

Angiogenesis is the process of forming new blood vessels from the existing ones, and is a crucial requirement for the growth, progression and metastasis of a tumour [32-34]. Tumour-induced angiogenesis is the phenomenon that in hypoxic microenvironment, the tumour triggers angiogenesic processes by secreting the tumour angiogenic factor (TAF), such as vascular endothelial growth factor (VEGF) [4]. The concept that tumour growth is dependent on the tumour-induced angiogenesis was first proposed by Judah Folkman in 1971 [39]. Since then, lots of studies on the tumour-induced angiogenesis have been developed.

Endothelial cells (ECs) are the most important cells involved in the angiogenesis process. Endothelial tip cells are some ECs spearheading at the nascent sprouts and guiding the newly formed vessel there (see section 2.3.2). The procedure of angiogenesis is the migration of the endothelial tip cells and the proliferation of the stalk cells following the endothelial tip cells. Modelling of the migration of the endothelial tip cells is a pivotal aspect for studying the angiogenesis process.

Previously, the most commonly used models of tumour-induced angiogenesis were mainly based on the partial differential equations (PDEs). One of the most influential PDEs model in two dimensions was firstly proposed by Anderson and Chaplain [5-8, 152]. The variables of ECs, fibronectin, TAF and the matrix degrading enzyme (MDE) secreted by

ECs were included in this model. The migration process of ECs from vessel side towards tumour side could be observed from the PDEs, giving the details about ECs concentrations at different locations and times. During angiogenesis, concentrations of TAF (or VEGF) and fibronectin varied over time, inducing the changes of concentration gradients of TAF (or VEGF) and fibronectin. These changes were related to two important features in angiogenesis process, named as chemotaxis and haptotaxis respectively. According to the previous works [160-162], Anderson and Chaplain assumed that the largest concentration for fibronectin locates at the parent vessel side, while the lowest concentration locates at the side of tumour line source. However, other different points of view appeared in some recent studies. Cao *et al* [132] reported that fibronectin protein from the human gallbladder cancer (GBC) tissue samples is primarily overexpressed. The overexpression of fibronectin protein will accelerate the cancer progress and is associated with a worse prognosis in GBC patients. The overexpression of fibronectin at the tumour side has also been reported by Cervantes-Arias *et al* [130, 131, 137, 163, 164]. Thus, we argue that, at least in some cases, fibronectin plays a critical role in the invasion of cancer progression and the fibronectin density is higher at the side of the tumour, which would enhance the influence of haptotaxis.

In addition, the most important aspects for modelling the migration of endothelial tip cells are density and velocity. There are two factors influencing the migration of endothelial tip cells: chemotactic and haptotactic factors. The chemotactic factor is the soluble bio-compound which is secreted by a tumour, such as VEGF, and is diffused to the surrounding microenvironment, forming a concentration gradient. The soluble bio-compound is generally called TAF in the computational modelling field. The

phenomenon of the tip cell migration by introducing TAF concentration gradient and moving up the gradient towards the tumour is called chemotaxis. The haptotactic factor is the insoluble bio-molecular compound concentration gradient in an extra cellular matrix (ECM) such as fibronectin. The phenomenon of the tip cells migrating by introducing insoluble bio-molecular compound concentration gradient and moving up the gradient is called haptotaxis. Therefore, chemotaxis and haptotaxis have vital influences on the migration of endothelial tip cells, and can play important roles in the development of angiogenesis.

Therefore, we aimed to model the relationship between tumour-invasion and tumour-induced angiogenesis, which until now has rarely been considered. In this study, we proposed an improved tumour-induced angiogenesis model based on Anderson and Chaplain's work and the improvements included three new characteristics: 1) Involving endothelial tip cell proliferation the angiogenesis process; 2) Modelling the degradation of ECM by enzymes secreted by endothelial tip cells; 3) Modelling the different influences of haptotaxis according to the fibronectin concentration gradient direction. For simplicity, the endothelial tip cells are called ECs in this chapter.

## 4.2 Anderson and Chaplain's model

### 4.2.1 Model construction

We started from Anderson and Chaplain's mathematical model [5-8, 152]. In this model, the EC density (at or near a capillary sprout tip) per unit area is denoted by $n$, which is

influenced by random motility, chemotaxis, and haptotaxis. The TAF concentration and the fibronectin concentration are represented by $c$ and $f$, accordingly. Chemotaxis is in response to TAF gradients and haptotaxis is in response to fibronectin gradients [115, 116, 165]. To derive the nonlinear partial differential equation (PDE) governing the ECs motion, the total cell flux balance was considered as follows. The conservation equation for cell density was used. The three contributions to the ECs flux $J_n$, are given by,

$$J_n = J_{random} + J_{chemo} + J_{hapto} \tag{4.1}$$

where $J_{random}$ represents the ECs flux generated by random motility, $J_{chemo}$ indicates the ECs flux by chemotaxis, and $J_{hapto}$ refers to the ECs flux by haptotaxis respectively. To describe the random motility of the ECs at or near the sprout tips, the flux of the ECs is assumed to be proportional to the concentration gradient of ECs $\nabla n$. Thus, the first term of Eq. (4.1), $J_{random} = -D_n \nabla n$ , where $D_n$ is the cell diffusion coefficient, a positive constant, and the minus represents that the diffusion direction is opposite to the concentration of the ECs.

The flux of tip migration is assumed as being proportional to the gradient of TAF. Considering the second term of Eq. (4.1), $J_{chemo}$, the chemotactic flux is assumed proportional to the concentration of ECs *n* and to the concentration gradient of TAF $\nabla c$; the chemotactic flux can be described as $J_{chemo} = \chi(c) n \nabla c$, where the chemotactic migration is characterized by the function $\chi(c) = \frac{\chi}{1+\delta c}$, which reflects the decrease in chemotactic sensitivity with increased TAF concentration, where $\chi$ , the chemotactic coefficient, and $\delta$ are positive constants.

The symbol $\frac{\partial n}{\partial t}$ represents the change rate of ECs. The migration of tips, *n*, can also be

influenced by haptotactic factor. For the third term of Eq. (4.1), $J_{hapto}$, the haptotactic flux is assumed proportional to the concentration of ECs $n$ and to the concentration gradient of fibronectin $\nabla f$, so the influence of fibronectin on the ECs is modelled by the haptotactic flux, $J_{hapto} = \rho \nabla f$, where ρ is a positive constant which is the haptotactic coefficient. The conservation equation for the ECs density $n$ is given as:

$$\frac{\partial n}{\partial t} + \nabla \cdot J_n = 0 \tag{4.2}$$

and hence the PDE governing ECs motion is,

$$\frac{\partial n}{\partial t} = D_n \nabla^2 n - \nabla \cdot (\chi(c) n \nabla c) - \nabla \cdot (\rho n \nabla f) \tag{4.3}$$

where $n$ denotes the ECs density (at or near a capillary sprout tip) per unit area, $c$ denotes the TAF concentration, $f$ denotes the fibronectin concentration. To derive the equation governing TAF, the procedure of tumour-induced angiogenesis should be considered. This procedure is starting from the secretion of TAF by the tumour cells. Then, TAF is diffused into the surrounding tissue and ECM. Thus, the concentration gradient between tumour and nearby vessels is set up and finally establishes a steady state. As the ECs migrate through the ECM in response to this steady state gradient, there is some uptake and binding of TAF by the cells [166, 167]. According to Ausprunk and Folkman's report, when the ECs migrate in the microenvironment towards the tumour, there is some uptake and binding of TAF molecular by the ECs [168]. Anderson and Chaplain [2] proposed a simple TAF uptake function. The function describing the change rate of TAF concentration is as follows:

$$\frac{\partial c}{\partial t} = -\eta n c \tag{4.4}$$

where $\eta$ is a positive constant coefficient, it represents the consumption rate of TAF, n is the density of ECs, and c is the concentration of TAF.

Fibronectin is a component of ECM, and can be produced and secreted by ECs [169-171]. Then, it becomes bound to the ECM and does not diffuse [169, 172]. The equation for fibronectin contains no diffusion term. The production rate of fibronectin by ECs is proportional to the density of ECs $n$ and the coefficient $\beta$ is a positive constant.

The degradation of fibronectin $f$ is proportional to the matrix degrading enzyme (MDE) density m and to the density of fibronectin, the coefficient is a positive constant $\gamma$. The MDE is produced by each individual EC $n$ at rate $\alpha$. The MDE is induced by the growth factor from the tumour. These production and degradation processes are modelled by the following equation:

$$\frac{\partial f}{\partial t} = \beta n - \gamma m f \tag{4.5}$$

Where $\gamma$ is a positive constant coefficient, it represents the degradation rate of fibronectin, *m* represents the matrix degradatory enzymes (MDE) activity, and $\beta$ is a positive constant coefficient, it represents the generation rate of fibronectin secrated by ECs.

Once the MDE is produced, it diffuses locally with diffusion coefficient ε and is degraded at rate ν. These production, diffusion and degradation processes are modelled by the following equation:

$$\frac{\partial m}{\partial t} = \alpha n + \varepsilon \nabla^2 m - \nu m \tag{4.6}$$

Hence, by putting Eq. (4.3), Eq. (4.4), Eq. (4.5) and Eq. (4.6) together, the complete continuous model of Anderson and colleagues' [6-8] is shown as follows,

$$\frac{\partial n}{\partial t} = D_n \nabla^2 n - \nabla \cdot (\chi(c) n \nabla c) - \nabla \cdot (\rho n \nabla f) \tag{4.7}$$

$$\frac{\partial c}{\partial t} = -\eta n c \tag{4.8}$$

$$\frac{\partial f}{\partial t} = \beta n - \gamma m f \tag{4.9}$$

$$\frac{\partial m}{\partial t} = \alpha n + \varepsilon \nabla^2 m - \nu m \tag{4.10}$$

### 4.2.2 Initial conditions and parameter settings

*1) TAF concentration distribution*

An assumption that a large initial concentration of TAF locates at the side of the tumour line source and a low concentration locates at the parent vessel was considered in the original Anderson and Chaplain's model [8]. The initial conditions of TAF concentration in a two dimension domain $\Omega(x, y)$ were described as follows:

$$c(x, y, 0) = e^{-\frac{(1-x)^2}{\varepsilon_2}}, \quad (x, y) \in [0, 1] \times [0, 1] \tag{4.11}$$

where $\varepsilon$ are positive constants.

*2) Fibronectin concentration distribution*

To establish an equation describing the concentration of fibronectin, Anderson and Chaplain [8] considered the following points. First, the TAF activates ECs, which damage the parent vessel basement membrane, resulting in an increased vessel permeability [163]; second, the plasma fibronectin leaking from the parent vessel is diffused into the corneal tissue and becomes bound to the ECM of the corneal tissue [160-162]; third, a high initial concentration of fibronectin is formed in and around the parent vessel [161, 173-175]. According to Anderson and Chaplain's consideration, they assume the highest concentration of fibronectin is at the side of parent vessel and the lowest concentration is at the side of the tumour line source. They set an exponential function to describe the initial condition of fibronectin concentration as:

$$f(x,y,0) = ke^{-\frac{x^2}{\varepsilon_2}}, \qquad (x,y) \in [0,1] \times [0,1] \tag{4.12}$$

where $f$ represents the concentration of fibtronectin, Anderson took the parameters $\varepsilon_2$ to be 0.45 and the coefficient $k$ to be 0.75 [8]. Eq. (4.12) describes the fibronectin concentration distribution where the concentration of fibronectin is lowest at the side of $x$=1 which represents the side of tumour. The highest concentration of fibronectin is at the side of $x$=0 which represents the parent vessel

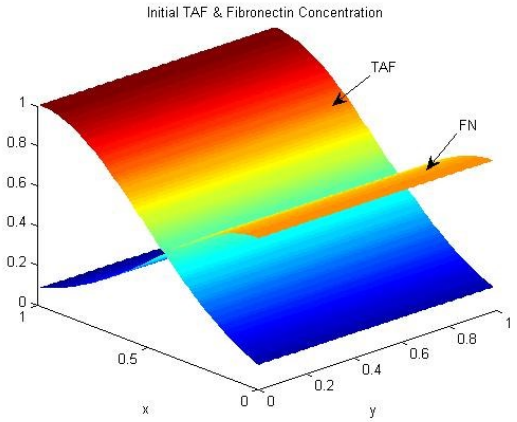


Figure 4.1. Concentrations of the TAF and fibronectin presented in Eq. (4.11) and Eq. (4.12)

From Figure 4.1, we can observe that the gradient of TAF and the gradient of fibronectin is in opposite direction.

## 4.3 Improved model in this work

Based on the Anderson and Chaplain's model, we modified and improved their model in three aspects: i.e., involving ECs proliferation, ECM degradation and fibronectin concentration gradient.

### 4.3.1 Improved model with the new assumptions

In Anderson and Chaplain's model, there are no birth and death terms, which means the total number of cells does not change. In fact, during the progress of angiogenesis, the density of the capillary network increases. This means that ECs density should increase in magnitude. So the proliferation of ECs occurs during the approach. In addition, the fact that ECM is degraded by enzymes should be also taken into account.

We have created a proliferation term $\mu Mn\left(1-\frac{n}{n_0}\right)$, which means that proliferation is proportional to the density of ECs, $n$, and is also limited by the density of itself autonomously, as described in $\left(1-\frac{n}{n_0}\right)$. Here $n_0$ should be at the same scale of the non-dimensionlized initial ECs concentration $n$ so we set $n_0 = 0.9$. We assume that the proliferation rate is also proportional to ECM because the proliferation of cells requires growth factors which rely on ECM. The ECM is a vast source of potent growth factors which can promote EC proliferation and subsequent invasion through a degraded ECM [125]. $\mu$ is the constant proliferation coefficient. By including the proliferation term into Eq. (4.7) we obtained Eq. (4.13).

$$\frac{\partial n}{\partial t} = D_n\nabla^2 n - \nabla\cdot(\chi(c)n\nabla c) - \nabla\cdot(\rho n\nabla f) + \mu Mn\left(1-\frac{n}{n_0}\right) \qquad (4.13)$$

*1) TAF concentration distribution*

Under hypoxia condition, the tumour secretes TAF to induce angiogenesis. The TAF is produced by the tumour and diffuses into the two dimensions surrounding tissue and ECM toward the vessels based on Ficks' diffusion law with diffusion constant $D_c$. At the same time, the decay of TAF occurs. Thus, the TAF concentration c satisfies Eq. (4.14). Once

TAF is secreted and diffused, a steady state concentration gradient between the tumour and vasculature can be set up. Therefore, the steady state concentration gradient of TAF concentration $c$ can be used as the initial condition for inducing angiogenesis:

$$\frac{\partial c}{\partial t} = D_c \nabla^2 c - \theta_c c \tag{4.14}$$

where $D_c$ is the TAF diffusion coefficient and $\theta_c$ is the decay rate, both are positive constant.

*2) Degradation of ECM*

ECM degradation as Mantzaris *et al* point out [125], it is necessary to account for the fact that the ECM should be degraded during the approach. In order to make way for the capillary network process, we assume that the ECM degradation rate follows the first order dynamic reaction and is proportional to the MDE concentration. Thus, we modelled ECM degradation using Eqs. (4.15) - (4.17):

$$\frac{\partial f}{\partial t} = \beta n - \gamma m f \tag{4.15}$$

$$\frac{\partial m}{\partial t} = \alpha n + \varepsilon \nabla^2 m - \nu m \tag{4.16}$$

$$\frac{\partial M}{\partial t} = -\omega M m \tag{4.17}$$

where *M* and *m* represent the concentration of ECM and MDE respectively, $\omega$ is a positive degradation constant, and the minus represents the opposite direction of the ECM concentration change [176]:

Consequently, we obtained the mathematical model, including Eqs. (4.13) - (4.17) to describe the migration and proliferation of ECs, the concentration diffusion of TAF, the change of MDE and ECM. These equations combine together to form a mathematical model of tumour-induced angiogenesis.

### 4.3.2 Parameter settings and non-dimensionalisation

To simplify the simulation, the first step was the non-dimensionalisation for the model and parameters. The procedure can be shown as follows. First, we should consider the length of the two dimensional domain at an appropriate range. From the experiments of Gimbrone, an average distance from a tumour implant to the parent vessels in the cornea is between *1mm* and *2mm* [177, 178], and the distance between tumour and vessels upon implant is around *3mm* [37]. Therefore, a length scale of $L = 2mm$ was taken as the initial distance between the tumour and vessels from the experiments of Folkman et al. [37]. Folkman and Klagsbrun reported that angiogenesis was initiated when this distance was *2mm*. Therefore, we took a length scale of $L = 2mm$ for the domain to simulate the angiogenesis [37].

Before non-dimensionalisation, it is useful to use a characteristic variable associated with time when choosing a scaling for time length. In other words, the initial distance between the tumour and the vessel is suitable for use as distance scaling $L$. The time scaling $\tau$ is defined as the time for TAF to diffuse across the domain. As one parameter should be taken as the standard parameter, Balding and McElwain [124] used $\tau = \frac{L^2}{4D_c}$, and Byrne and Chaplain [148] took the TAF diffusion coefficient $D_c$ as the standard parameter and used $\tau = \frac{L^2}{D_c}$. The authors called their respective values of $\tau$ as 'TAF transit time' and defined it as $\tau = \frac{L^2}{D_c}$. Later on, the TAF transit time was taken by Anderson and Chaplain [8] as the time scaling or as the length of timescale by rescaling distance $L$ between the parent vessel and tumour, so the length of timescale was defined as $\tau = \frac{L^2}{D_c}$ (where $D_c$ is the TAF diffusion coefficient). We took the length of timescale $\tau = \frac{L^2}{D_c}$.

For the coefficient of ECs induced by the chemotaxis, Stokes et al. [179] measured the chemotactic coefficient of migrating ECs in gradients of αFGF. They measured the maximum chemotactic response in concentrations of αFGF around $10^{-10}M$, and gave a chemotactic coefficient of 2,600 $cm^2s^{-1}M^{-1}$ which is equal to $0.033mm^2day^{-1}M^{-1}$. Thereby, Anderson et al. [8] in their model took $\chi^* = 2{,}600\ cm^2s^{-1}M^{-1}$, $c^* \approx 10^{-10}M$. In the absence of any available data for the haptotactic coefficient $\rho^*$, they assumed that this was of the same magnitude as $\chi^*$. As the ECs generally migrate towards the tumour, it is reasonable to assume that $\chi^* > \rho^*$. Hence, they thought the $\rho^*$ would be between 0~0.03. Terranova et al. [165] identified a phenomenon of ECs responding to a haptotactic manner in the concentrations of fibronectin around $10^{-10}M$. Anderson and Chaplain [8] took the concentrations of fibronectin as an estimation for the concentration of fibronetin $f^*$. They took EC density as $n^* = 10^{-10}M$, and TAF $c^* = 10^{-10}M$ respectively (where $n^*,\ c^*,\ f^*$ are appropriate reference variables).

Balding and McElwain [124] estimated this diffusion coefficient at around 0.29 $mm^2$ per day, based on their own simulation results. Byrne and Chaplain [148] estimated a value of $10^{-8}cm^2/day$ ($8.64mm^2/day$), but if we estimate this diffusion coefficient using $\tau = \frac{L^2}{D_c}$ with $\tau = 3.5$ days and $L = 2mm$, the diffusion coefficient will be $D_c = 2.57mm^2/day$. Sherratt et al. [180] and Bray [181] estimated the diffusion coefficient of TAF in the range of $5 \times 10^{-7} \sim 5.9 \times 10^{-6}cm^2/s$, so Anderson et al. [8] took $D_c = 2.9 \times 10^{-7}cm^2/s$, which is equal to 0.025 $cm^2/day$ or 2.5 $mm^2/day$. Hence, we took the diffusion coefficient of TAF $D_c = 2.5\ mm^2/day$.

Stokes et al. [179] and Rupnick et al. [182] estimated EC random motility coefficients $D_n$ in the range $2 \times 10^{-9} \sim 10^{-8}\ cm^2/s$ in their experiments. The estimation result was under

the assumption that the cells moved independently. However, when the movement of individual EC is constrained by surrounding cells, the random motility coefficient should be smaller than the coefficient that was estimated under independent movement. From *in vivo* experimental results, the random movement of ECs at the capillary sprout tips is very limited [129, 175]. Considering the factor that the capillary sprouts are associated with neighbouring cells due to the formation of vessel walls, the ECs are contiguous with one another. It is reasonable to expect a smaller random-motility coefficient than that observed by Rupnick et al. [182]. Anderson and Chaplain [8] took $D_n = 10^{-10} cm^2/s$, which is equal to $8.64 \times 10^{-5} cm^2/day$.

For EC random motility, the coefficients are as seen in Eq. (4.7):

$$\widetilde{D} = \frac{D_n}{D_c} = \frac{1 \times 10^{-10}}{2.9 \times 10^{-7}} = 0.00035$$

$$\tilde{\chi} = \frac{\chi^* c^*}{D_c} = 2600 \times \frac{10^{-10}}{2.9 \times 10^{-7}} = 0.896,$$

$$\text{the } \tilde{\rho} = \frac{\rho^* f^*}{D_c} = 2600 \times \frac{10^{-10}}{2.9 \times 10^{-7}} = 0.896.$$

To simulate, the modeller may have a choice between 0.1~0.9 for both the $\chi$ and $\rho$. Anderson and Chaplain [8, 152] took $\widetilde{D} = 0.00035$, $\chi = 0.38$ and $\rho = 0.34$, and we took the same magnitude of the parameters as theirs.

When considering the time scale, Addison-Smith [117] chose the value $D_c = 0.864\, mm^2/day$. This gives a value of time length for $\tau$ as 4.6 days, ($\tau = \frac{L^2}{D_c} = 4.6$) which is similar to Byrne and Chaplain's value of 3.5 days. Folkman [37] reported that approximately four days after implanting the tumour in the rabbit cornea, the tumour grew to within $2mm$ of the limbus, and angiogenesis commenced. It seems reasonable to take $\tau$ as the TAF transit time. In Anderson and Chaplain's model [8], they considered the

timescale $\tau = \frac{L^2}{D_c}$ as 1.5 days. The difference produced is due to the difference of TAF diffusion coefficient, and it maybe that the approximately four days reported by Folkman from their experiments was too long, because the time from the implanting of tumour to the commencement of angiogenesis includes a lag phase in which no TAF may have yet been secreted. Anyway, both the time scales are at the same scale. We assumed $\tau = \frac{L^2}{D_c} = \frac{2\times2}{2.5} =$ 1.6 day, so we took the timescale $\tau$ as 1.6 day.

We have simulated this model at a domain $L = 2mm$ which is related to a grid at size 100×100. To simplify the analysis and simulations, the model was non-dimensionalised as follows: tilde notation is used for the non-dimensional variables, and scaling values for the concentration of these variables in the model are indicated with star notation.

$\tau = \frac{L^2}{D_c^*}$, $\tilde{c} = \frac{c}{c^*}$ , $\tilde{f} = \frac{f}{f^*}$ , $\tilde{n} = \frac{n}{n^*}$, $\tilde{t} = \frac{t}{\tau}$ , $\tilde{D} = \frac{D_n}{D_c^*}$, $\tilde{x} = \frac{x}{L}$, $\tilde{y} = \frac{y}{L}$, $\tilde{\chi} = \frac{\chi^* c^*}{D_c^*}$ and $\tilde{\rho} = \frac{\rho_0^* f^*}{D_c^*}$, $\beta = \frac{\omega L^2 n^*}{f_0 D_c^*}$, $\gamma = \frac{\theta L^2 n^*}{D_c^*}$, $\eta = \frac{\lambda L^2 n^*}{D_c^*}$, $\theta = \frac{\theta_c \tau}{D_c^*}$, $D_c = \frac{D_c^*}{D_c^*} = 1$.

Dropping the tilde notation, we established the non-dimensional model in Eq. (4.13), Eq. (4.14), Eq. (4.15), Eq. (4.16) and Eq. (4.17) as follows:

$$\frac{\partial n}{\partial t} = D\nabla^2 n - \nabla \cdot (\chi(c) n \nabla c) - \nabla \cdot (\rho n \nabla f) + \mu M n \left(1 - \frac{n}{n_0}\right) \quad (4.18)$$

$$\frac{\partial c}{\partial t} = \nabla^2 c - \theta c \quad (4.19)$$

$$\frac{\partial f}{\partial t} = \beta n - \gamma m f \quad (4.20)$$

$$\frac{\partial m}{\partial t} = \alpha n + \varepsilon \nabla^2 m - \nu m \quad (4.21)$$

$$\frac{\partial M}{\partial t} = -\omega M m \quad (4.22)$$

The parameters in the aforementioned Eqs were set as follows:

$D = 0.00035$ , $\chi = 0.38$ , $\rho = 0$; (or $\rho = 0.34$ respectively), $\eta = 0.1$ , $\beta = 0.05$ , $\gamma = 0.1$ and , $\delta = 0.6$ [8], $\alpha = 10^{-6}$ , $\varepsilon = 0.01$ , $\nu = 3$ [6, 7]; $M_0 = 0.9$ , and $\theta =$

0.003 [176]. The doubling time of ECs was estimated at 18 hrs [8], so the proliferation coefficient of ECs can be estimated as $\mu = \frac{18}{24\times1.6} = 0.47$. Considering the death of ECs, the proliferation coefficient of ECs should be less than 0.47, so we estimate it to be $\mu = 0.3$. Chaplain gave the MDE secrete rate coefficient as $\alpha = 10^{-6}$ [152], and thus to make the simulation results of ECM visible and in an appropriate range, we estimate the ECM degradation coefficient to be $\omega = 2 \times 10^{6}$. The symbol $n_0$ represents the initial ECs concentration, from the solution of Eq. (4.24), so we take $n_0 = 0.9$ (see Figure 4.3).

### 4.3.3 Boundary conditions

Appropriate initial and boundary conditions are demanded by the model. For Eq. (4.19) the boundary conditions for the vessel and tumour side satisfy the Dirichlet condition $\mathrm{c}(0,\mathrm{y},\mathrm{t}) = 0,\ \mathrm{c}(1,\mathrm{y},\mathrm{t}) = 1$ and on the left and right side satisfy the Neumann condition $\frac{\partial \mathrm{c}}{\partial \mathrm{y}} = 0$. For Eq. (4.18) the boundary conditions should convey the idea that the ECs are issued at $x = 0$ moves from $x = 0$ to $x = 1$, and reach the tumour at the later boundary. The boundary condition of the domain subject to the non-flux conditions satisfies the Neumann condition and can be presented as follows:

For Eq. (4.18), Eq. (4.20), Eq. (4.21) and Eq. (4.22):

$\frac{\partial c}{\partial x} = 0,\ \frac{\partial c}{\partial y} = 0,\ \frac{\partial n}{\partial x} = 0,\ \frac{\partial n}{\partial y} = 0,$

$\frac{\partial m}{\partial x} = 0,\ \frac{\partial m}{\partial y} = 0\ \ \frac{\partial M}{\partial x} = 0,\ \frac{\partial M}{\partial y} = 0$

and $\frac{\partial f}{\partial y} = 0\ , \frac{\partial f}{\partial x} = 0.$

### 4.3.4 Initial condition

For the solution of Eq. (4.18), the initial condition should be described. As we discussed above, the TAF is diffused from the edge of the tumour and reaches a steady state. Its initial condition of concentration can be determined by Eq. (4.19).

Recent studies [130, 133-141] have implied that, for some invasive cancers, the fibronectin density around the stroma is higher than that of the ECM. Accordingly, cancer marks its progression through increasing the ECM density where the amount of fibrillar ECM proteins, including collagen and fibronectin, is enhanced [131]. Based on the above, we assume the highest concentration of fibronectin is at the side of the tumour line source and the lowest concentration at the side of the parent vessel. Thus, we established the equation describing fibronectin concentration as follows:

$$f(x,y,0) = ke^{-\frac{(1-x)^2}{\varepsilon_2}}, \qquad (x,y) \in [0,1] \times [0,1] \tag{4.23}$$

Eq. (4.23) represents the fibronectin concentration distribution and the gradient of fibronectin concentration is in opposite direction to that described in Eq. (4.12). In Eq. (4.23) we take the magnitude of parameters $\varepsilon_2$ and $k$ as same as that in Eq. (4.12).

The concentration of fibronectin in Eq. (4.23) is lowest at the side of $x = 0$ which represents the side of the parent vessel. The highest concentration of fibronectin is at the side of x=1 which represents the tumour

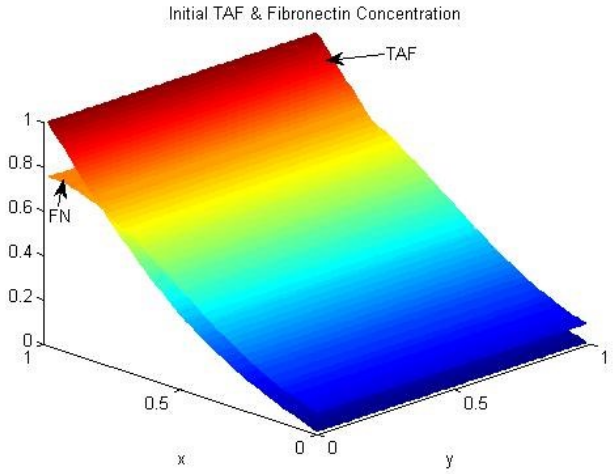


Figure 4.2. Concentrations of the TAF and fibronectin from Eq. (4.19) and Eq. (4.23) proposed in the current study

From Figure 4.2, we can observe that the gradient of TAF and the gradient of fibronectin are in the same direction.

We set four clusters of ECs at the side of the parent vessel, which has four discrete peaks of form, as the initial ECs condition. We establish a function to describe the four clusters of ECs. The function can be represented as:

$$n(x, y, 0) = e^{-\frac{x^2}{\epsilon_3}}(1 - sin^2(10\pi y)) \tag{4.24}$$

where *n* represents the concentration of ECs, $\varepsilon_3$ is a positive parameter $\varepsilon_3$ *=0.001* [8].

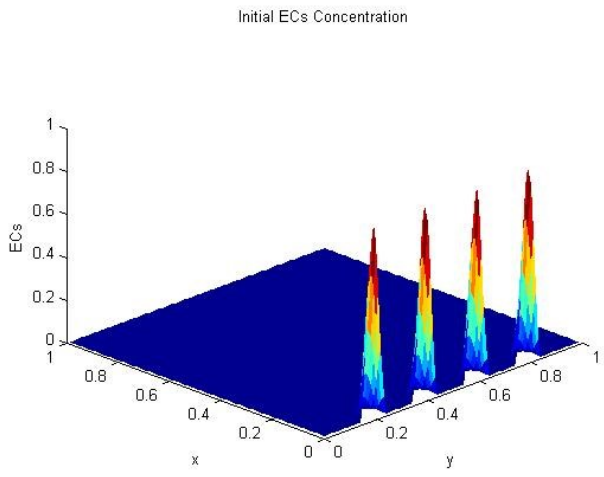

Figure 4.3. The solution of Eq. (4.26) represents the initial concentration of the four clusters of ECs.

From Figure 4.3, we can observe four clusters of ECs at the side of the parent vessel where the highest concentration of ECs $n$ is equal to one after non-dimensionallisation.

MDE is stimulated by ECs. The initial value of MDE is equal to zero. We describe the initial MDE field as:

$$m(x, y, 0) = 0 \tag{4.25}$$

We assume ECM is a homogenous density field with an initially uniform concentration of ECM components. Daub et al. [176] proposes that ECM concentration is 0.9 after non-dimensionalisation. This was taken and, therefore, the initial ECM field is presented as:

$$M(x, y, 0) = 0.9 \tag{4.26}$$

## 4.4 Simulation

All of the numerical solutions of the models presented in section 4.4 were obtained with finite difference methods. We compared the simulation results between Anderson and Chaplain's model (refer to Eqs. (4.7) - (4.12) and (4.24) [8, 152, 157] and the improved model in this study (refer to Eqs. (4.18) - (4.22)) and summarised the results as follows. The boundary conditions are described in section 4.3.3 and the initial conditions are as in Eqs. (4.23) - (4.26).

### 4.4.1 Comparison of the ECs migration between the two models without considering the effect of haptotaxis

To separately test the effects of the chemotaxis and haptotaxis factors on the model, firstly we did not include the haptotaxis factor in the models. So the migration of the ECs was mainly influenced by chemotaxis. Both Anderson and Chaplain's model and our improved model were simulated at the conditions of $\rho = 0$ (means no haptotaxis factor), and the results were shown in Figure 4.4 and Figure 4.5 respectively. From Figure 4.4 and Figure 4.5, we can observe that the ECs move towards the tumour line source with the same migration velocities for both two models. The moved distances covered by the ECs were the same at $t = 1\tau$ (1.6 days), $t = 2\tau$ (3.2 days) and $t = 3\tau$ (4.8 days) for the two models. The difference between Figure 4.4 and Figure 4.5 is shown in the ECs density. The ECs density is larger in Figure 4.5 than that in Figure 4.4 due to the term of proliferation in Eq. (4.18).

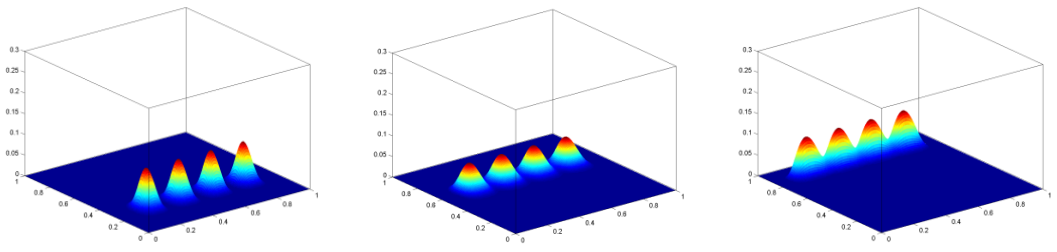

(t=1) (t=2) (t=3)

Figure 4.4. Spatiotemporal evolution of the ECs density in Anderson and Chaplain's model

The figure shows that the ECs migrate from the parent vessel $(x = 0)$ towards the tumour

line source $(x = 1)$ with the influence of chemotaxis factor and without the influence of haptotaxis factor($\rho = 0$).

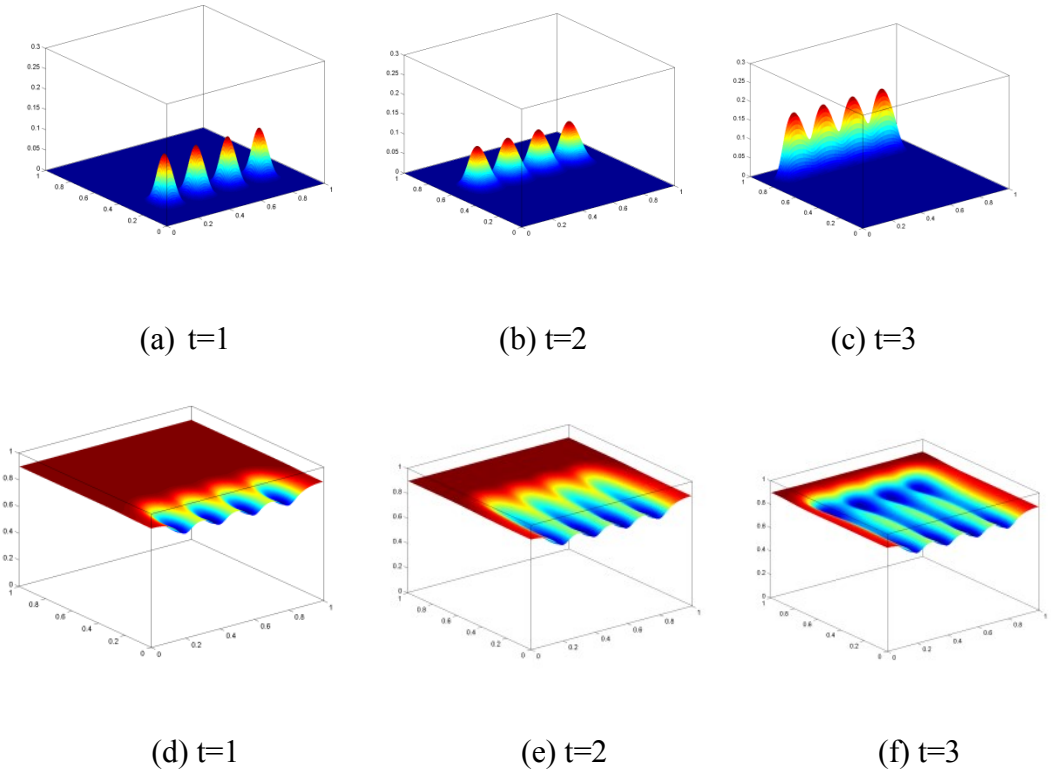

(a) t=1 (b) t=2 (c) t=3

(d) t=1 (e) t=2 (f) t=3

Figure 4.5. Spatiotemporal evolution of the ECs density in the new improved model.

(a), (b) and (c) show that the ECs migrate from the parent vessel $(x = 0)$ towards the tumour line source $(x = 1)$ with the influence of chemotaxis factor and without the influence of haptotaxis factor $\rho = 0$. (d), (e) and (f) show that the ECM is hydrolysed by the proteolytic enzyme secreted by the ECs. The four clusters of ECs move forward to the line of the tumour and correspondingly leave four ditches behind them.

The same EC velocities in the two models are due to the same chemotactic attraction. Here, chemotaxis determines the velocity of tip cell migration. We can observe that at $t = 2\tau$

(3.2 days) the ECs have passed more than halfway through the domain, and at $t = 3\tau$ (4.8 days) they have migrated across almost 80% of the domain. No significant lateral migration of the ECs is observed. The four clusters of ECs retain the shape of the initial distribution, while the density decreases to a certain extent. This is because the migration is mainly controlled by chemotaxis, and at the same time diffuses outwards, leading to a small amount of lateral movement due to random motility.

### 4.4.2 Comparison of the ECs migration between the two models with considering the effect of haptotaxis

Then we simulated the ECs migration with the influence of both chemotaxis and haptotaxis factors. If the fibronectin gradient is opposite to the TAF shown in Figure 4.1, the haptotaxis offsets the chemotaxis, and the influence on ECs velocity is negative.

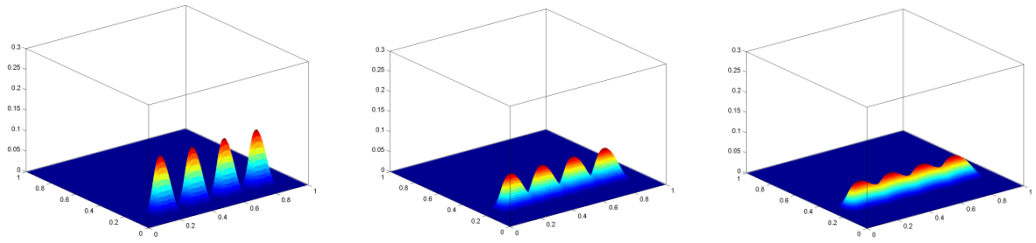

(a) t=1 (b) t=2 (c) t=3

Figure 4.6. Spatiotemporal evolution of the ECs density in Anderson and Chaplain's model [8]

The initial four clusters of ECs density are moving towards the line tumour. Eq. (4.18) including the influence of haptotaxis at $\rho = 0.34$. The fibronectin concentration distribution is based on Eq. (4.12).

In Figure 4.6 under the negative influence of haptotaxis the ECs move toward the tumour much more slowly than those as shown in Figure 4.4. The ECs only covered one third of the domain at $t = 3\tau$ (4.8 days). Significant overlaps of ECs can be observed in Figure 4.6 (c).

Compared with the results shown in Figure 4.4, without the influence of haptotaxis, the ECs move faster and take three time scaling ($t$=3$\tau$) to cover 80% domain. However, in Figure 6, with the negative influence of haptotaxis, the ECs move much more slowly and take three time scaling ($t$=3$\tau$) to cover only 30% domain. This is because TAF and fibronectin are opposite in their gradient direction and counteract the movement of the ECs. Therefore, the negative influence of haptotaxis could slow down the velocity of the ECs. On the other hand, if the fibronectin gradient is in the same direction as the TAF shown in Figure 4.2, the influence of haptotaxis on velocity is enhanced.

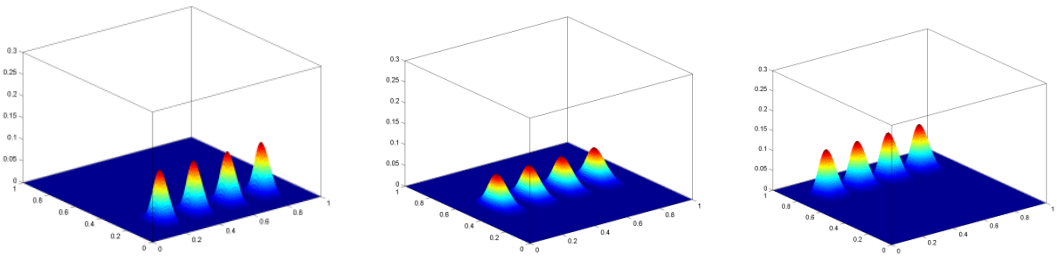

(a) t=0.5 (b) t=1 (c) t=1.5

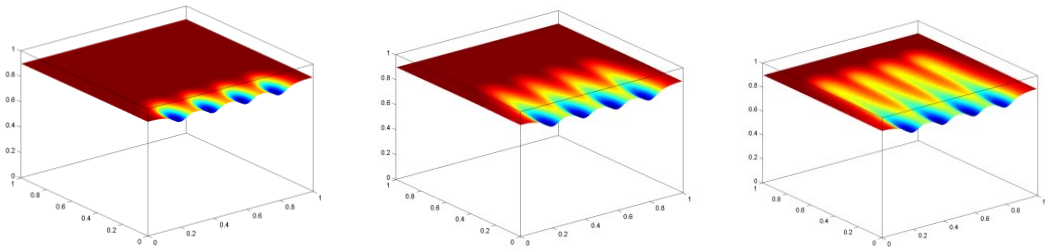

(d) t=0.5 (e) t=1 (f) t=1.5

Figure 4.7. Spatiotemporal evolution of the ECs density from the improved model

(a), (b) and (c) show that the ECs migration is influenced by chemotaxis and positive haptotaxis. (d), (e) and (f) show that the ECM is hydrolysed by the proteolytic enzyme secreted by EC migration. The ECs move forward to the tumour and correspondingly leave four ditches behind them.

The simulation of the model Eq. (4.18) is under the enhanced influence of haptotaxis. The ECs move towards the tumour line source, as shown in Figure 4.7. The four separate peaks of cells covered 80% domain at $t = 1.5\tau$ (2.4 days), as shown in Figure 4.7 (c). The velocity of the ECs is fastest because both the TAF and fibronectin gradients are in the same direction. The superposition of both TAF and fibronectin accelerates the EC migration, and the ECM changes correspondingly.

Therefore, through simulation, we obtained the important points as follows:

1. Without haptotaxis, the clusters of endothelial-cell density migrate directly across the domain to the tumour.
2. With negative haptotaxis in which the fibronectin gradient is opposite to the TAF gradient, the clusters of endothelial-cell density migrate more slowly, with lateral movement.
3. With positive haptotaxis in which the fibronectin gradient is in same direction as the TAF gradient, the clusters of endothelial-cell density migrate fastest. This means angiogenesis is promoted by the superposition of both haptotaxis and chemotaxis.

### 4.4.3 Effect of proliferation on ECs density

The change of total and average ECs density during angiogenesis can be shown in the following curves:

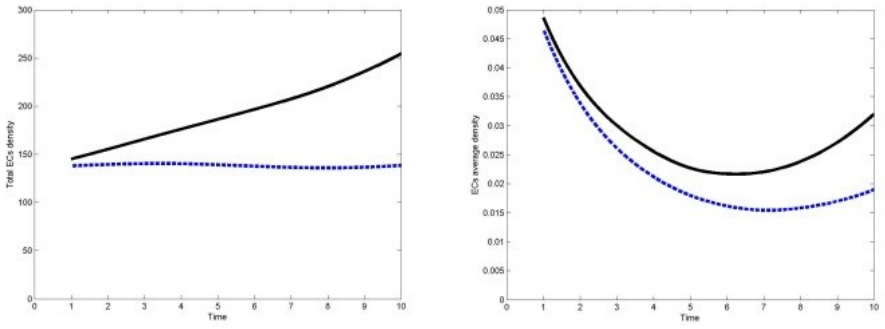


(a) (b)

Figure 4.8. Elucidation of EC density

(a) The dash curve shows the total EC density in Eq. (4.7) without proliferation and the solid curve shows the total EC density in Eq. (4.18) with proliferation. (b) The dash curve is the average density of ECs in Eq. (4.7) and the solid curve is the average EC density in Eq. (4.18).

Figure 4.8 shows the change in EC density with and without proliferation. In Figure 4.8 (a), without proliferation, its total EC density is conserved kept at conservation with proliferation, and its total EC density is increasing towards the tumour. In Figure 4.8 (b), without proliferation, the trend of its average density for each cluster is declining in Eq. (4.7). This is due to the term of random motility which makes it diffuse, and its density per unit area is declining. In Eq. (4.18) with proliferation, the trend of its average density for

each cluster remains higher than that in Eq. (4.7) and tries to retain this density.

### 4.4.4 Results of ECM

The simulation results of ECM without the influence of haptotaxis are shown in Figure 4.5 (d), (e) and (f). The simulation results of ECM with the positive influence of haptotaxis are shown in Figure 4.7 (d), (e) and (f) respectively. The ECM is proteolyzed by MDE secreted by ECs and degraded simultaneously when the ECs clusters move forward, forming a "ditch" in the ECM. This indicates that the density of the ECM decreases because of degradation. The front of the "ditches" is at the same distance from the parent vessel as that of ECs, which reveals that ECM approaches the tumour correspondingly with the ECs. It can be clearly seen that when the four clusters of ECs migrate forward, its enzymes, such as MMPs, degrade the ECM and leave the "ditch" behind them. Thus, we assume that the degradation can take place only at the front, and the four clusters of ECs are extremely actively, leaving the "ditches" behind it. It can also be clearly observed that in Figure 4.5 (d), (e) and (f) the "ditches" are deeper and wider than those in Figure 4.7 (d), (e) and (f). This indicates that the faster the ECs migrate, the shallower the "ditches" will be. The more slowly the ECs migrate, the deeper and wider are the "ditches".

### 4.4.5 Comparison of the evolution of capillary network between two models

Agent-based modelling (ABM) is a computational modelling approach providing a

systematic view of the simulation of action and interaction among autonomous individual entities [142]. Here, we use ABM to discretize the mathematical model described above, so that we can obtain the feature of the capillary sprouts and individual behaviour. The discrete capillary sprouts are shown as follows:

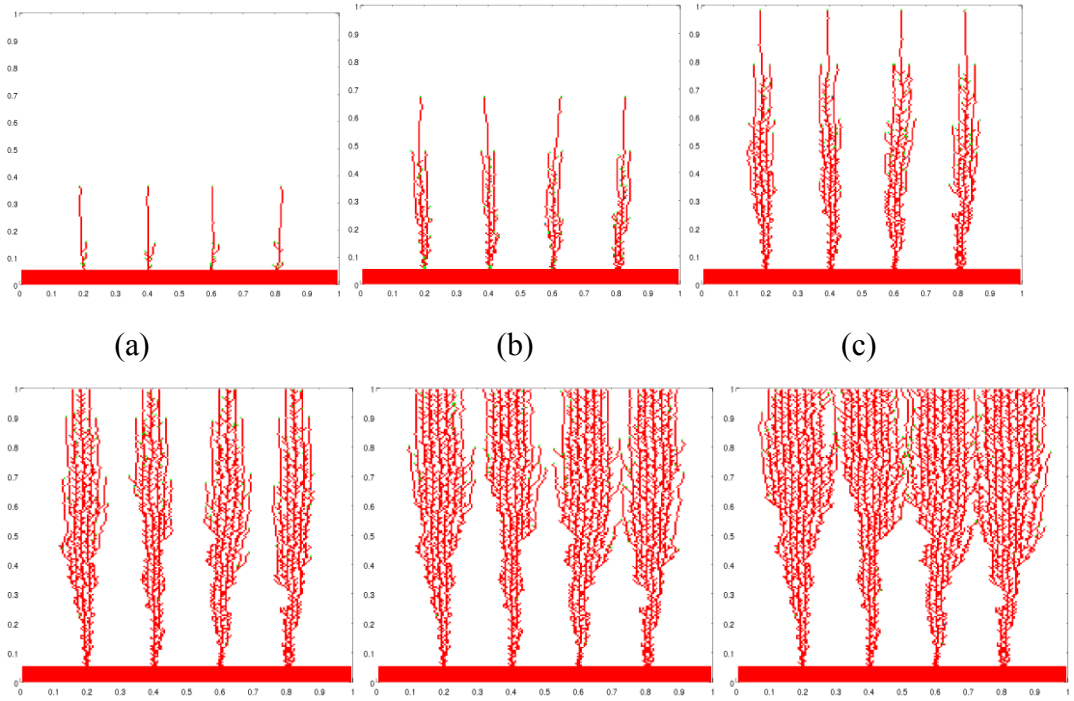

(a) (b) (c)

(d) (e) (f)

Figure 4.9. Spatiotemporal evolution of capillary network with ABMs to discretise the continuum model where the ECM degradation is not involved

Figure 4.10 shows the ECs at the capillary sprout tips migrating from the parent vessel ($x = 0$) towards a tumour ($x = 1$).

In Figure 4.9, we can observe that the four clusters of vessels develop from the parent vessel across the domain and finally reach the tumour. In front of the vessels are the sprout heads by the endothelial tip cells. In the simulation the ECM degradation is not

involved into the continuous model, so no background of degraded ECM can be observed and it seems that the capillary network formed mechanically.

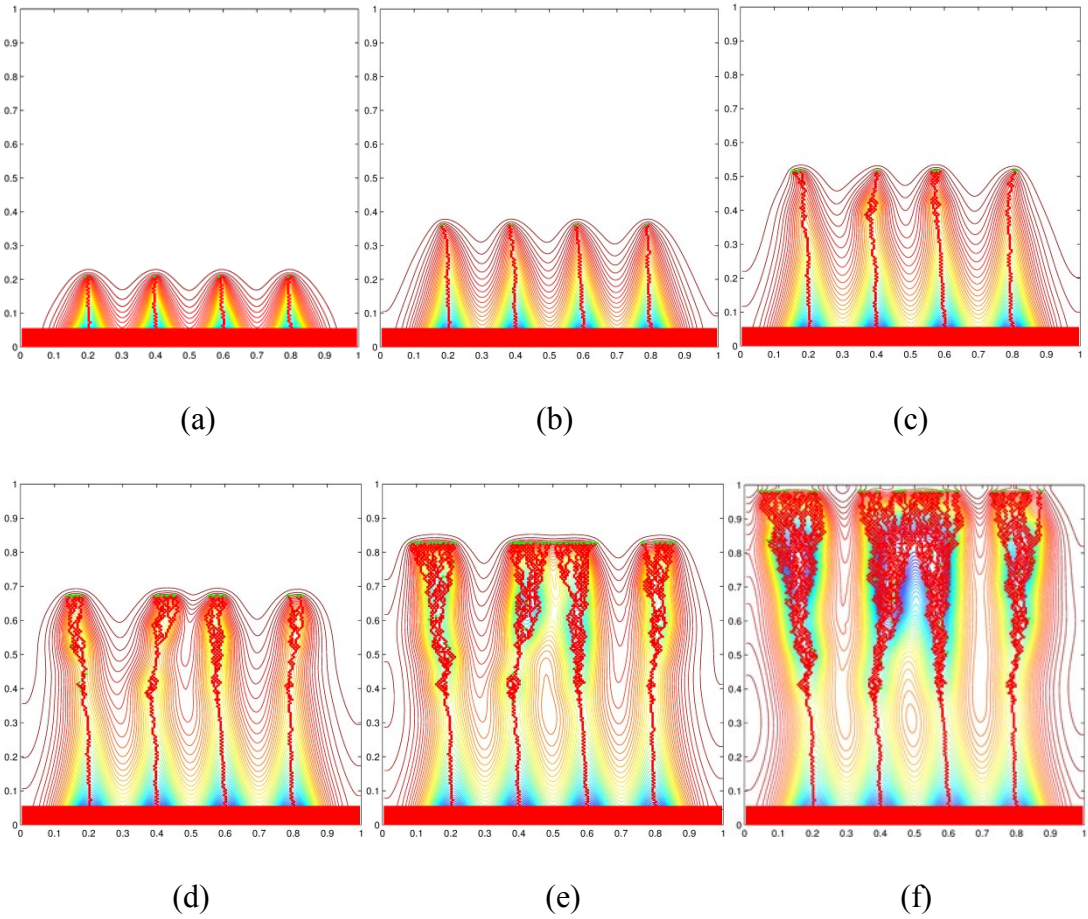

(a) (b) (c)

(d) (e) (f)

Figure 4.10. Spatiotemporal evolution of capillary network with ABM to discretize the continuum model.

Figure 4.10 shows the ECs at the capillary sprout tips migrating from the parent vessel ($x = 0$) towards a tumour ($x = 1$). The background formed with contour lines and colours shows the ECM density degraded by the MDE secreted from ECs.

In Figure 4.10, we can observe that the four clusters of vessels develop from the parent vessel across the domain and finally reach the tumour. In front of the vessels are the sprouts headed by endothelial tip cells. When the ECs approach, they secrete MDE and

proteolyse the ECM, making the density of ECM decline along in the way the ECs passed. In this way, the endothelial tip cells remove barriers and make their way for the vessels to develop. This can be observed from the background with different colours and contour lines. On the background the local density of the ECM adjacent to the vessels appears to change gradually from blue, green, yellow to red toward outside, which means the ECM density is the lowest at the vessels due to being proteolysed. At the same time, the directions of the nascent sprouts are mainly guided by the TAF gradient and also influenced by the density of local ECM, making the morphology of the vessels look tortuous. We can also observe that the density of vessels is increasing, forming a “brush border” approaching the tumour. This demonstrates the density of endothelial tip cells increasing due to the ECs proliferation.

## 4.5 Discussion

The simulation results show an accelerated endothelial tip cell migration towards the tumour when TAF and fibronectin concentration gradient are in the same direction, where the invasive tumours secrete TAF and generate fibronectin. The accelerated endothelial tip cell migration implies a possible mechanism that promotes angiogenesis in some subgroups of invasive tumours.

### 4.5.1 ECM degradation

The ECM is a major component of the microenvironment of cells. It takes part in most

basic cell behaviours, from cell proliferation, adhesion and migration, to cell differentiation [183]. The ECM is composed of a large collection of biochemically and structurally diverse components. These components include proteins, proteoglycans, and glycoproteins, such as collagen and fibronectin. They have various physical and biochemical properties. A large amount of evidence has demonstrated that ECM components greatly influence cell behaviour, such as regulating cell migration [183, 184]. The physical properties of the ECM are essential for its scaffolding role in supporting tissue structure and integrity, and for its role in migration and anchorage of the cell. In addition, ECM provides a critical framework for angiogenesis. During angiogenesis, the ECM forms the migration paths, and this releases force from the collagen assembly or cell-ECM interactions propelling cell movement [176].

During tumour-induced angiogenesis, the ECM associated with angiogenesis is continuously remodelled to create a suitable microenvironment for the survival, adhesion and migration of the vascular progress of ECs [185]. The remodelling of ECM process includes the degradation of pre-existing ECM molecules by proteolytic enzymes, such as MMP and the neosynthesis of ECM secreted by tumour cells and/or stromal cells [132]. Metalloproteinases, such as MMP families, are the most significant enzymes in ECM remodelling and they participate in cell migration [183]. EC migration depends on the expression of MMPs, which degrade the local ECM and generate a cell migration path, at the leading edge [183].

The ECs in front of the capillary network or at the top of the sprout are of the tip cell phenotype; the other ECs behind the tip cell are of the stalk cell phenotype when the angiogenesis occurs. We assume the ECs secrete the same amount of enzymes to

proteolyse the ECM, but the ECs as tip cells and as stalk cells generate different amounts of their innate inhibitor (which all proteases have to control their activity) so that the ECs in the stalk lack MDE activities to proteolyse the ECM. It is the tip cells which have characteristically high activity; the cells in the capillary vessels behind the tip cells, or in other words behind the four clusters of ECs, are stalk cells which lack activity. The secretion of enzyme proteolysis of ECM is based on the model described in Eq. (4.21) and Eq. (4.22).

According to the analysis discussed above, we assume that the activity of the MDE is central to the ECs density. The degradation rate of ECM depends on ECM, the substrate of the enzyme, and the activity of the MDE. The model also expresses that the amount of ECM degraded depends on the duration of proteolysis, which means that the longer the time lasts, the more the ECM is degraded.

Because the complexity of the constitution of the ECM, we could simply describe that the ECM is composed of components, some of which are easy to degrade, such as plasma proteins which are similar to meat, and some of which are not easy to degrade, such as collagen fibres which are similar to bone. The different ECM components may be subject to proteolysis by the different proteases secreted by the ECs during their migration. On the one hand, when the ECs in the tip cell phenotype move fast, they stay at the location for a brief time, and of course proteolysis takes place but only degrades the meat. However, when the ECs in the tip cell phenotype move slowly, they stay longer, and so there is enough time for the proteolysis to degrade both meat and bone.

Degraded at different degrees, the compositions at the adjacent microenvironment are subtly different. This makes the ECM cleave and remodel, forming migration paths. The

ECM may also provide force released from collagen assembly or cell-ECM interactions, and this propels cell movement and facilitates angiogenesis in different ways.

During the tumour invasion and induction of angiogenesis, the ECM is proteolysed and degraded. Abnormal changes in the amount and composition of the ECM can significantly affect ECM biochemical properties, enhance the tumourigenic effects, and deregulate cell functions during malignant transformation [186]. ECM also indirectly affects cancer cells by influencing the behaviour of stromal cells, including ECs and fibroblasts, which are the main initial factors triggering abnormal ECM production [186]. As a result, abnormal ECM further promotes the formation of a tumourigenic microenvironment and subsequent tumour metastasis [186].

### 4.5.2 Haptotaxis influence

According to Shekhar, Pauley and Heppner, 'the invasive carcinoma is often associated with expansion of the tumour stroma and increased deposition of ECM' [163]. Such an increased deposition of ECM in tumours is known as desmoplasia and is similar to changes that are observed during organ fibrosis. According to Folkman, solid tumours vascularize more actively than the normal tissue [163]. The fibroblast is an important stromal cell type in cancer progression [133].

Tumour can be initiated and developed by the interactions between malignant cells and cancer-associated fibroblasts (CAFs) [134, 135]. Through modulating stromal ECM, CAFs produce directional paths of fibronectin in order for tumour invasion [136]. Fibronectin is critical in many cell processes, such as cell adhesion, migration, growth and differentiation

[187]. Fibronectin is expressed in many different cell types and its expression is activated during epithelial-mesechymal transition (EMT) [137]. This is a process to facilitate cell motility and invasion [138-140].

The increased expression of fibronectin has been observed by Lundberg [130] in a subgroup of colorectal cancer (CRC) classified as CIMP-negative tumours. They point out that fibroblasts induce CIMP-negative tumour cells to produce more fibronectin. They indicate that the density of fibroblasts is higher at the front of the tumour than the normal tissue. Similar results have been reported by Derya, Yilmaz and Aytekin in Small Cell Lung Cancer (SCLC), an aggressive form of lung cancer. The ECM surrounding SCLC cells contains a great amount of fibronectin [141], and a density gradient of the fibronectin may exist so we express it as Eq. (4.23).

From Figure 4.1, we can observe the gradient of TAF and the gradient of fibronectin in an opposite direction, which means that when chemotaxis and hapotaxis take effect simultaneously, the velocity of ECs offset by both chemotaxis and haptotaxis is decelerated. This result indicates that the ECs could not reach the tumour side, as shown in Figure 4.6. From Figure 4.2, we can observe that the gradient of TAF and the gradient of fibronectin are in the same direction, which means that when chemotaxis and hapotaxis take effect simultaneously, the velocity of ECs increased by both chemotaxis and haptotaxis is accelerated. This result indicates that the ECs reach the tumour side very fast and pass the domain, as presented in Figure 4.7. Here, the quick migration of ECs approaching the tumour means that angiogenesis occurs quickly when the invasive tumour produces high concentration of fibronectin in the stroma and its adjacent microenvironment. Thus, it is possible that the fibronectin promotes the haptotaxis and facilitates the chemotaxis to

accelerate the angiogenesis.

Previous studies have suggested that fibronectin can be generated by various types of cells, including tumour cells [188]. Fibronectin enhances the secretion of MMPs and promotes the invasive migration of gallbladder cancer (GBC) cells. Stromal fibronectin is produced by tumour cells. Recent studies in human melanoma and ovarian cancer have revealed that MMPs could cleave fibronectin into shorter fragments, and facilitate fibronectin integrating adhesive interactions. This process in turn reinforces the generation of MMPs, forming a positive feedback loop for the invasive migration of GBC cells [132].

Angiogenesis plays a major role in solid tumour growth, because it links the harmless avascular growth phase and the fatal vascular growth phase [7]. Angiogenesis supplies oxygen and conveys the cancer cell. In our model, we assume that fibronectin is high at the side of the tumour line source at the malignant phase. Our hypothesis is that during the tumour malignant phase, the CAFs in some kind of caner such as GBCs create higher fibronectin concentration for the cancer cell migration, which results in an acceleration of angiogenesis. Finally, the rapid growth of the vascular tumour contributes to cancer cell progression, known as metastasis, and the establishment of a new colony in distant organs [189]. We think that there may be a density gradient of fibronectin, which is expressed as Eq. (4.23). This generates a positive haptotatic effect and augments the velocity of ECs, as shown in Figure 4.7. The quick migration of ECs approaching to tumour means that angiogenesis occurs quickly when the invasive tumour produces a high concentration of fibronectin in the stroma and its adjacent microenvironment.

According to Cao et al. [132], the overexpression of fibronectin will promote cancer progression. Their experimental results indicate that exogenous fibronectin significantly

enhances and promotes proliferation and metastasis. We think that an invasive tumour can generate fibronectin, and the fibronectin forms a gradient and enhances the haptotactic effect. The enhanced haptotaxis can cooperate with chemotaxis to accelerate angiogenesis. The formed vessels supply oxygen and nutrients which may boost the development of the tumour. Therefore, we propose a potential mechanism whereby both tumour-invasion and tumour-induced angiogenesis promote each other; this remains, as yet, unnoticed in cancer research.

## 4.6 Summary

In section 4.2, we first extended Anderson and Chaplain's work on tumour-induced angiogenesis by creating a proliferation term and combining it into Eq. (4.3). Their continuous model was developed to meet the demands of making quantitative predictions about the dynamics in the complex process of angiogenesis. Mantzaris, Webb and Othmer [125] point out that the density of the capillary network increases when it approaches the tumour during angiogenesis, so the density of the ECs should increase first. Proliferation is essential for the formation of the capillary network so that the capillary network can be formed with a sufficient population of cells. To introduce a proliferation term of ECs is a reasonable way to improve the mathematical model. We improved it in this way, and our simulation results show that EC density increases during the angiogenesis.

Secondly, we extended Anderson and Chaplain's work on tumour-induced angiogenesis in the aspect of the degradation of ECM, because the ECM should be degraded for the development of the capillary network to occur when the migration and proliferation of ECs

approach the tumour. Our simulation results clearly show that the ECM is degraded during the angiogenesis. As a result, the degradation dynamics of the ECM is catalysed by the protease enzyme [125].

Thirdly, we extended Anderson and Chaplain's work on tumour-induced angiogenesis in the aspect of fibronectin gradient direction. They assume the highest concentration of fibronectin is at the side of parent vessel and the lowest concentration is at the side of the tumour line source, with the movement rate of the ECs slowing down under the influence of Eq. (4.12). We think that there is another possibility in that the invasive tumour generates fibronectin, which enhances haptotaxis; thus, we set Eq. (4.23). Our simulation results show that during angiogenesis under the influence of enhanced haptotaxis, the ECs move much faster than that in Anderson and Chaplain's model due to the TAF and fibronectin gradient being in the same direction. The synthetic effect of both chemotaxis and haptotaxis accelerates the movement of the ECs. On this basis, we deduce that the possible mechanism of tumour-invasion and tumour-induced angiogenesis is that they promote each other to facilitate faster or malignant tumour development.

Our model improves Anderson and Chaplain's work in the continuous model in introducing the terms of proliferation, ECM degradation, and the concept of enhanced haptotaxis. Our simulation results clearly demonstrate these improvements and indicate that there is a possible mechanism. It is clear that the model successfully describes the migration of ECs guided by chemotaxis and hoptotaxis from parent vessel to the tumour; it suggests that angiogenesis promotes a malignant mechanism for some subgroups of tumour. However, there are some limitations of the mathematical model, in that the enzymes are simplified as the variable m. In fact, the enzymes are a large family consisting

of a huge number of different enzymes, such as MMPs, ADAMTS and so on. Their specificity is different, for example, different enzymes have their special target substrate. In the model, the ECM is simplified as a homogenous substrate, but in fact the ECM is a very complex tissue consisting of many different components, such as proteins, proteoglycans, and glycoproteins.

## 4.7 Conclusion

Endothelial cell (EC) migration is the crucial step in tumour-induced angiogenesis. EC migration is influenced by both chemotaxis and haptotaxis. According to recent bio-clues, tumour progression promotes overexpression of fibronectin. The overexpression of fibronectin generates a fibronectin concentration gradient which is in the same direction of TAF concentration gradient. We assume that some subgroups of invasive tumours generate fibronectin, leading to enhanced haptotaxis. Hence, we developed a mathematical model simulating the influence of haptotaxis. Our simulation results show that angiogenesis can be accelerated when the fibronectin gradient generates the positive haptotaxis which increases the velocity of ECs toward the invasive tumour. The invasive tumour enhances haptotaxis, which means angiogenesis can be synthetically and simultaneously promoted by both chemotaxis and heptotaxis. According to the consensus theory that angiogenesis supplies oxygen and nutrients to promote tumour development, by linking the relationship of tumour invasion and angiogenesis we propose that there is a possible mechanism for the cross promotion between tumour-invasion and tumour-induced angiogenesis, which would make the tumour develop faster, and thus

become more harmful for some subgroups of tumours.

Although the mathematical model could not cover all complexities of angiogenesis, it can simulate the microenvironment where many of biological phenomena are continuous. By developing the PDEs model, we can simulate the parameters which change in position and time. These parameters will be used in the establishment of a regulatory model based on a VEGF and Notch signalling pathway. The regulatory model will be discussed in detail in Chapter Six.

# Chapter 5. Modelling of Tumour-Induced Angiogenesis with Regression by Cell Cytotoxic Factor

A phenomenon observed by Folkman [39, 190] is that tumour regresses when blood vessels approach. This is the response of immune system to the tumour cells. Tumour-induced angiogenesis promotes growth of blood vessels through which host immune factors are delivered to the tumour and kill tumour cells, making tumour regress. This interaction is very complex. It is important to model them mathematically. Mathematical models can help us to better understand these procedures. Computational models can help and enhance our understanding of the immune system-tumour interactions by allowing us to simulate complex systems and behaviours that cannot be observed directly. The immune system includes the innate immune system which is quickly mobilised and triggered when recognises tumour cells. These procedures occur spatially and temporally. Therefore, we develop the mathematical models in PDE to simulate the impact of innate immune system on tumour during tumour-induced angiogenesis. In this chapter, we model and simulate large tumour load in which tumour regress and recurrence. We also simulate small tumour load in which tumour can be eliminated by immune system, and simulate the syntheses effect of immune system and drugs on large tumour.

## 5.1 Introduction

Tumour immunotherapy is a promising anticancer approach in which the patient's immune system is either stimulated or mobilied to fight tumours. Recently, the understanding of the immune system and tumour immunology has increased. This has enabled scientists to develop specific immunotherapies designed to enhance the immune response of a particular patient against a unique tumour [191]. However, because it is complicated, the exact mechanism of tumour immunity still remains unclear. Tumour immunoediting is the process whereby immune cells protect against tumour formation by sculpting the immunogenicity of developing tumours. The process is hypothesized as three phases: elimination, equilibrium, and escape called the three Es of tumour immunoediting [192, 193]. In the elimination phase, the tumour cells are successfully recognized and eliminated by the immune system, thus returning the tissues to their normal function [194]. However, the immune rejection of cancer is not clear and there is still much to be learned about the specifics of immune tumour elimination. Tumour cells that are not completely eliminated by the immune system are predicted to proceed into a phase of equilibrium, in which the immune system is hypothesized to control tumour development but not completely eliminate the transformed tumour cells. It was hypothesized that in the equilibrium phase, the constant interaction of the immune system with tumours may sculpt or edit the phenotype of developing tumours, resulting in tumours no longer being susceptible to immune attack and thus able to progress into the third phase of the immunoediting process, termed as escape. Numerous experimental data have shown that tumours in the escape phase destroy the immune system to aid growth and recurence [195].

The immune system has an innate and adaptive immunity, the former responding fast and the latter taking time to respond. Innate immunity can manifest tumour immunoediting activity in the absence of adaptive immunity. This activity requires natural killer (NK) cells and interferon γ (IFN-γ), which mediate the induction of M1 macrophages to cancer immunoediting [196]. P101, p102,

Mathematical modelling and simulation of the tumour cytotoxic influence can promote the development of an immunotherapy strategy. Based on the mathematical model established in Chapter 4, we have developed another mathematical model further by incorporating the formation of vessels, tumour loads, immune tumour cytotoxic factor, and a tumour cytotoxic drug. In this chapter, we present our mathematical models of tumour-induced angiogenesis with tumour regression by immune tumour cytotoxic factor, and simulate the influence of immune tumour cytotoxic factor on different tumour loads. Although the tumour cytotoxic immune factor can be delivered to the tumour by either blood vessel tips or by vessels, the immune factor identified by Folkman et al. (1975) is described as being delivered by the blood vessel tips and only to the areas within about 0.5 mm of the tips [37]. In our model, we assume the immune tumour cytotoxic factor is the innate immunity which responds immediately to the tumour cells, and the innate immune cells are delivered to the tumour by the blood vessel tips during tumour-induced angiogenesis. Hence, our model describes the delivery of tumour cytotoxic immune factor as being limited to the tips. The simulation results provide a possible form of tumour therapy by improving and enhancing the patients' immune system.

## 5.2 Modelling of tumour-induced angiogenesis with regression by cell cytotoxic factor

The immune system is a collection of cells and molecules that can respond and generate resistance to disease, especially infectious disease. There are many indications that tumours can be influenced by the immune system. Enhancing a patient's immune system to augment conventional therapies has been a clinical practice for a long time. In this chapter, we establish a mathematical model involving the immune system and its effect on tumours. We consider that the immune factor generated in the host is delivered from the limbus to the tip position. Further, we believe the modelling of tumour-induced angiogenesis with regression by tumour cytotoxic immune factor delivered through formed vessel tips will facilitate a better understanding of tumour-induced angiogenesis. Hence, in this section, we develop the mathematical model established in section 4.2 with another three PDEs describing tumour, vessel, and cytotoxic factor, to simulate the regression, recurrence, or clearance of the tumour by involving tumour cytotoxic factor, including the immune system and drugs delivered through the vessels formed during angiogenesis.

It should be acknowledged that tumours interacting with immune system are very complex and that the mathematical model established in this chapter is simplified. This simplification is to make it more easily and clearly to illustrate the influence of tumour-induced angiogenesis on tumour load. Even though there are few biological evidences to support the assumption,we assume that: 1) the immune factor is a kind of innate cells and is tumour cytotoxic factor which can recognize and interact with tumour cells immediately then kill the tumour cells once they meet together; 2) only the tip cells

can recruit the tumour cytotoxic factor and the only one immune factor is involved as the tumour cytotoxic factor in our model; 3) the immune factor level declines during the simulation.

The interactions of tumours with the host immune system are very complex and very difficult to be mathematically described in detail. Hence, simplification is necessary for mathematical modelling. Although simplifying a model would make it not absolutely suitable to reflect the whole reality *in vivo,* mathematical models can generate visual output and help us to better understand the interactions, and the simulation results of the model could be qualified to a certain extent.

### 5.2.1 Establishing the mathematical model

Back to 1974, the tumour immune phenomenon was firstly observed by Folkman et al. They observed that angiogenesis commenced when the tumour was in the range of 2 mm, and the tumour began to regress when the front edge of the vessel was 0.5 mm from the tumour[190]. This implies that there is a kind of cytotoxic factor which can kill the tumour cells. The tumour cytotoxic factor could be delivered to the front edge of the vessel where the tip cells are and diffuse towards the tumour cells. When both meet together, the tumour cells may be killed and the tumour regresses. Once the tumour regresses, the vessel front regress and then tumour develops again to maintain equilibrium. This tumour cytotoxic factor could be part of the immune system, leading to the supposition that some tumour cytotoxic drugs could be delivered by the formed vessels, and that this may be a helpful method to assist the body as it tries to fight tumours. The kinetics of tumour cytotoxic factor should be investigated, and therefore simulating this kinetics is valuable. Folkman et

al. [37, 192], observed that after the tumour regressed, the vessel also decayed. This means that there is a mechanism by which these influence each other. In the aspect of tumour cytotoxic immune simulation, it should be mentioned that in 2010 Addison-Smith developed and proposed a mathematical model in a one dimensional domain, considering factors such as the immune system's influence on the development of vessels and tumour cells [117]. Some of the parameters we have used come from her thesis.

We take the model established in section 4.2.1.1. Eq. (4.18) as the basis of the model. For simplicity, in section 5.1, we ignore the influence by haptotaxis, so the term haptotaxis in Eq. (4.18) is excluded and the relative equation Eq. (4.20) is eliminated. The ECs described in Eq. (4.18) are also assumed to undergo a random motility, chemotaxis, and proliferation. The change rate of endothelial tip cells is described in Eq. (5.1).

$$\frac{\partial n}{\partial t} = D\nabla^2 n - \nabla \cdot (\chi(c) n \nabla c) + \mu M n \left(1 - \frac{n}{n_0}\right) \qquad (5.1)$$

where $n$ represents the concentration of ECs, $n_0$ represents the initial concentration of ECs, c represents TAF concentration, $M$ indicates ECM density. On the right of the Eq. (5.1), the first term represents the EC diffusive flux with the diffusion coefficient D, the second set of terms represent the EC flux by chemotaxis, and the third set of terms represent the proliferation with the proliferation coefficient $\mu$. All the meanings of the variables and coefficients are the same as those described in section 4.3.

For modelling the tumour, it is assumed to develop as the tumour cells increase. The increasing rate of tumour $\frac{\partial T}{\partial t}$ is proportional to the load of total tumour cells $T$. This is to describe its development as a simple exponential growth. The tumour cells are also subject to physical spread in two dimensions based on Fick's diffusion law, called random motility. In addition, we assume that the formed vessel can deliver nutrients to supply the

development of the tumour, so the tumour growth rate is promoted by interactions with the blood vessels. In the model, the tumour cells are assumed to die on interaction with the tumour cytotoxic cells described as tumour cytotoxic factors in modelling. Tumour cytotoxic factors have been found in the human immune system, such as natural killer (NK) and CD8+ T cells, both of which can kill tumour cells. These would eventually be able to defeat the tumour. Based on this assumption, once the host's immune system responds and develops effectively, and the tumour is defeated or regresses to an extent, further tumour-induced angiogenesis will regress and no further vascularization will occur. According to the behaviour of the tumour and immune system, in the two dimensional domain, the equation of a tumour influenced by a generalized tumour cytotoxic factor $I$, delivered through the formed blood vessels b, can be described in Eq. (5.2) as follows.

$$\frac{\partial T}{\partial t} = D_T\left(\frac{\partial^2 T}{\partial x^2} + \frac{\partial^2 T}{\partial y^2}\right) + k_1 T b - k_2 T I + k_3 T \qquad (5.2)$$

Where $T$ represents tumour cells, $I$ represents immune cytotoxic factor, and $b$ is the formed blood vessels respectively. On the right of Eq. (5.2), the first term represents the random motility of tumour cells with diffusion coefficient $D_T$, the second term represents tumour development rate enhanced by blood vessel density b and the density of tumour cells with the rate constant $k_1$, the third term indicates the killing rate of tumour cells by immune cytotoxic factor with the rate constant $k_2$, the fourth term refers to the natural tumour growth rate with the rate constant $k_3$.

The capillary vessels, $b$, are laid down by migration of the tips. The length of capillary vessels is the trail of tip cell migration, so the rate of generating new vessels by tips is assumed to be proportional to the total tip flux at rate of $k_4$. The term $n\left(\frac{\partial c}{\partial x} + \frac{\partial c}{\partial y}\right)$ means the total tip flux. If no new tips are produced, the capillary vessels will undergo a natural

decay. The decay rate is $k_5$ and the natural decay is proportional to the length of vessels, *b*. It is described in Eq. (5.3).

$$\frac{\partial b}{\partial t} = D_b\left(\frac{\partial b}{\partial x} + \frac{\partial b}{\partial y}\right) + k_4 n\left(\frac{\partial c}{\partial x} + \frac{\partial c}{\partial y}\right) - k_5 b \qquad (5.3)$$

where *b* represents blood vessel density, *c* represents TAF respectively. On the right of Eq. (5.3), the first term represents the random motility of blood vessels with diffusion coefficient $D_b$, the second term represents blood vessels development rate enhanced by ECs with the rate constant $k_4$, the third term indicates the decay rate of blood vessels with the rate constant $k_5$.

To model the tumour immune factor, we denote the immune factor as *I* and assume that the immune factor is recruited by the tip cells and delivered through the vessels formed, so the increasing rate $\frac{\partial I}{\partial t}$ is proportional to the density of the endothelial tip cells *n* at the rate of $k_6$. The immune factor is diffused into the two dimensional domain based on Fick's law. The diffusion coefficient is $D_I$. The immune factor also decays at an exponential rate with the coefficient of $k_7$. Hence, it is described in Eq. (5.4).

$$\frac{\partial I}{\partial t} = D_I\left(\frac{\partial^2 I}{\partial x^2} + \frac{\partial^2 I}{\partial y^2}\right) + k_6 n - k_7 I \qquad (5.4)$$

where *I* represents immune cytotoxic factor, and *n* represents ECs respectively. On the right of Eq. (5.4), the first term represents the random motility of immune cytotoxic factor with diffusion coefficient $D_I$, the second term represents immune cytotoxic factor recruited by tip ECs with the rate constant $k_6$, the third term indicates the decay rate of immune cytotoxic factor with the rate constant $k_7$.

The governing equations for tip cell density is denoted as *n*, tumour cells load as *T*, immune factor density as *I*, tumour angiogenic factor TAF concentration as *c*, and the formed vessel density as *b*. These have been described above by the set of PDEs which are Eq. (5.1), Eq.

(5.2), Eq. (5.3), and Eq. (5.4), respectively. Other equation in the model is taken directly from Eq. (4.19). We use the solution result of Eq. (4.19) to generate a steady state concentration gradient profile of TAF, and use it as the initial condition of TAF concentration to simulate the main model.

#### 5.2.1.1 Parameters and non-dimensionalisation

For the non-dimensionalisation of Eq. (5.1), Eq. (5.2), Eq. (5.3), and Eq. (5.4), we set a square domain for the model in the range of $2 \times 2mm^2$, and the tumour is at one edge opposite to the pre-existing limbus vessel. The distance L from the tumour to the vessel at the onset of angiogenesis is $2mm$. The timescale is $\tau = \frac{L^2}{D_c}$, the parameters including the diffusion coefficient of endothelial tip cells is $D_n$, and the chemotactic function of coefficient $\chi$ have been non-dimensionalised in the same way as in section 4.3.

Scaling values for concentration of these parameters and variables of the model are indicated with star notation. That is $\tilde{T} = \frac{T}{T^*}$, $\tilde{I} = \frac{I}{I^*}$, $\tilde{n} = \frac{n}{n^*}$, $\tilde{c} = \frac{c}{c^*}$ and $\tilde{b} = \frac{b}{b^*}$ respectively. We take the diffusion coefficient of TAF as the standard coefficient. The other diffusion coefficients are non-dimensionalised by division of TAF coefficient $D_c^*$. Tilde notation is used for the non-dimensionalised variables. The definitions of the parameters in Eq. (5.5), Eq. (5.6), Eq. (5.7), and Eq. (5.8) for non-dimensionalisation is described as follows:

$\tau = \frac{L^2}{D_c^*}$, $\tilde{t} = \frac{t}{\tau}$, $\tilde{x} = \frac{x}{L}$, $\tilde{y} = \frac{y}{L}$, $\tilde{T} = \frac{T}{T^*}$, $\tilde{I} = \frac{I}{I^*}$, $\tilde{n} = \frac{n}{n^*}$, $\tilde{c} = \frac{c}{c^*}$, $\tilde{b} = \frac{b}{b^*}$, $\widetilde{D_n} = \frac{D_n}{D_c^*}$, $\tilde{\chi} = \frac{\chi^* c^*}{D_c^*}$, $\widetilde{D_T} = \frac{D_T}{D_c^*}$, $\widetilde{D_b} = \frac{D_n L^2 n}{D_c^* b}$, $\widetilde{D_I} = \frac{D_I}{D_c^*}$, $\tilde{k}_1 = k_1 \tau b^*$, $\tilde{k}_2 = k_2 \tau I^*$, $\tilde{k}_3 = k_3 \tau$, $\tilde{k}_8 = \frac{k_6 \tau n^*}{I^*}$, $\tilde{k}_9 = \frac{\chi^* c^* L^2 n^*}{D_c^* b^*}$, $\tilde{k}_{10} = k_5 \tau$, $\tilde{k}_{14} = k_7 \tau$ [117].

Where $\tau$ is the timescale and the definition of timescale is $\frac{L^2}{D_c^*}$. $D_c^*$ is the diffusion

coefficient of TAF. $\chi^*$ is the chemotactic coefficient. $L$ is the length of domain.

The values of parameters for Eq. (5.6), Eq. (5.7), and Eq. (5.8) after non-dimensionalisation are described as follows:

$\widetilde{D_T} = 0.0005,\ \widetilde{D_b} = 20D_n,\ \widetilde{D_I} = 0.05,\ \tilde{k}_1 = 2.0,\ \tilde{k}_2 = 1.0,\ \tilde{k}_3 = 0.055,\ \tilde{k}_8 = 40,$ $\tilde{k}_9 = 2.5,\ \tilde{k}_{10} = 1.0,\ \tilde{k}_{14} = 1.0$ [117].

The definitions and values of parameters for Eq. (5.5), and Eq. (4.19) after non-dimensionalisation are described in detail in section 4.3.

The model with five PDEs described below is in a two-dimensional domain. In the five equations, the Eq. (4.19) comes from the model established in section 4.3, and the other four equations, Eqs. (5.5)-(5.8), are developed by introducing the concept of tumour cytotoxic factor. After non-dimensionlisation, the set of equations can be given as follows:

$$\frac{\partial n}{\partial t} = D\nabla^2 n - \nabla \cdot (\chi(c) n \nabla c) + \mu M n \left(1 - \frac{n}{n_0}\right) \tag{5.5}$$

$$\frac{\partial T}{\partial t} = D_T\left(\frac{\partial^2 T}{\partial x^2} + \frac{\partial^2 T}{\partial y^2}\right) + k_1 T b - k_2 T I + k_3 T \tag{5.6}$$

$$\frac{\partial I}{\partial t} = D_I\left(\frac{\partial^2 I}{\partial x^2} + \frac{\partial^2 I}{\partial y^2}\right) + k_8 n - k_{14} I \tag{5.7}$$

$$\frac{\partial b}{\partial t} = D_b\left(\frac{\partial b}{\partial x} + \frac{\partial b}{\partial y}\right) + k_9 n\left(\frac{\partial c}{\partial x} + \frac{\partial c}{\partial y}\right) - k_{10} b \tag{5.8}$$

where Eq. (5.5) governs the tip cell density $n$, Eq. (5.6) governs the tumour cell density $T$, Eq. (5.7) governs the tumour cytotoxic immune cell density $I$ and Eq. (5.8) governs the blood vessel density $b$ respectively.

### 5.2.1.2 Boundary condition

To simulate the model, we should set appropriate initial and boundary conditions for equations respectively. The boundary conditions at the vessel and tumour side satisfy the Dirichlet condition $c(0, y, t) = 0$, $c(1, y, t) = 1$ and at the left and right side satisfy the Neumann condition $\frac{\partial c}{\partial y} = 0$ for Eq. (4.19). For Eq. (5.5), Eq. (5.6), Eq. (5.7), and Eq. (5.8), the boundary conditions should convey the idea that the ECs are issued at $x = 0$, moving from $x = 0$ to $x = 1$. The boundary conditions of the domain subject to the non-flux conditions satisfy the Neumann condition and can be presented as follows:

Eq. (5.5), Eq. (5.6), Eq. (5.7), and Eq. (5.8),

$\frac{\partial c}{\partial x} = 0, \frac{\partial c}{\partial y} = 0, \frac{\partial n}{\partial x} = 0, \frac{\partial n}{\partial y} = 0, \frac{\partial b}{\partial x} = 0, \frac{\partial c}{\partial y}$ $\frac{\partial I}{\partial x} = 0, \frac{\partial I}{\partial y} = 0$ *and* $\frac{\partial T}{\partial y} = 0, \frac{\partial T}{\partial x} = 0.$

### 5.2.1.3 Initial condition

For the ECs, we are going to set three clusters of cells at the parent vessel by setting Eq. (5.9), and take three clusters of EC concentration as the initial condition for the simulation of the model.

$$n(x, y, 0) = e^{-\frac{x^2}{\epsilon_3}} sin^2(10\pi y) \tag{5.9}$$

The initial conditions for other variables are:

$$I(x, y, 0) = 0 \tag{5.10}$$

$$b(x, y, 0) = 0 \tag{5.11}$$

Simulation and discussion

Before simulation, we set the tumour load adjacent to the border of the domain. The domain is divided into a 100×100 grid with $101 \times 101$ net nodes. From *x=0.97* to *x=1*, *y=0~1*, *t=0*, the tumour density is set at each node as 1. We designed two tumour load situations. One is a relatively large tumour load which can be described as *T* (0.97~1, 0~1, 0)=1, so the total large tumour load is $4 \times 101 \times 1 = 404$. The other is a relatively small tumour load which can be described as *T* (0.97~1, 48~52, 0)=1, so the total small tumour load is $4 \times 5 \times 1 = 20$.

For the big tumour load, we assume that the tumour is large and the domain is relatively small so the tumour source is a line at the edge of the domain. Angiogenesis is introduced by a tumour line source and the regression of the tumour is triggered by the angiogenesis. In this assumption, the tumour is set at the opposite side of the pre-existing vessel. Because the tumour is large enough, it can be described as a line tumour at one edge of the domain. For the small tumour load, the tumour is in the middle position adjacent to the edge.

#### 5.2.1.4 Simulating large tumour load regression and recurrence by immune tumour cytotoxic factor

We assume the large tumour load is a great one and forms a line TAF source. The TAF is secreted and diffused to the side of the vessel based on Eq. (4.19), and forms a TAF concentration gradient at a steady state. The distribution of TAF is shown in Figure 5.1.

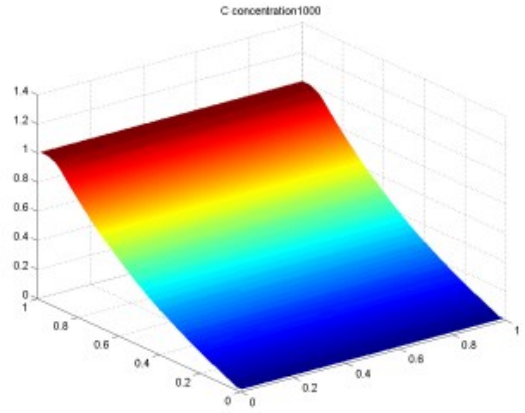


Figure 5.1. The steady state TAF concentration gradient is generated by a line tumour. This figure is obtained by numerically simulating Eq. (4.19).

We take the steady state TAF concentration gradient shown in Figure 5.1 as the initial condition for the simulation of Eq. (5.5), Eq. (5.6), Eq. (5.7), and Eq. (5.8). In this section, 5.1.2.1, we set a large tumour load T=400. The simulation results are shown as follows.

*1) The tip cell density (ECs)*

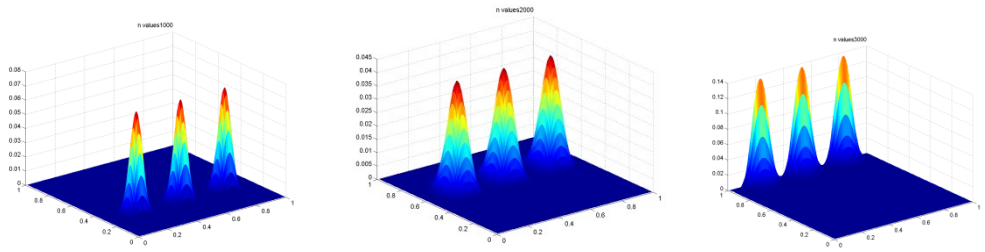

(a) t=1 (b) t=2 (c) t=3

Figure 5.2. Spatiotemporal evolution of EC density *n*

The initial three clusters of EC density are moving towards the line tumour. The figure shows the evolution result of EC density towards the tumour line source by numerically simulating Eq. (5.5).

From Figure 5.2 shown above, we can observe that the ECs (tips), *n*, migrate up the gradient of TAF under the influence of chemotaxis. The position of the tip cell reach represents the position of the front edge of the vessels, through which the immune factor is delivered at the same time, recruited by the tip cells.

*2) The tumour cytotoxic immune factor*

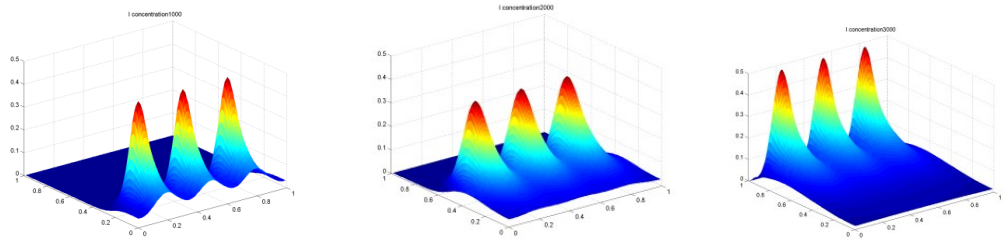

(a) t=1 (b) t=2 (c) t=3

Figure 5.3. Spatiotemporal evolution of an immune factor density *I*

These are the same EC steps as the profile view. The three clusters of immune factor density are moving through the vessel or may be recruited by the ECs towards the line of the tumour. The figure shows the evolution result of immune factor density towards the tumour line source by numerically simulating Eq. (5.7).

From Figure 5.3 shown above, we can observe that the tumour immune factor, *I*, migrates up the gradient of TAF in the same position of tip cells, *n*. The position of the tip cell reach represents the position of the front edge of the vessels, through which the immune factor is delivered at the same time, as recruited by the tip cells. The immune factor is diffused into the surroundings, making the immune factor reach the tumour ahead of the front edge of

the vessel. This is in line with Folkman's [190] observation. He found that the tumour began to regress when the vessel was within *0.5mm* from it. The regression is the consequence of the tumour cells making contact with the immune factor.

*3) The vessel density*

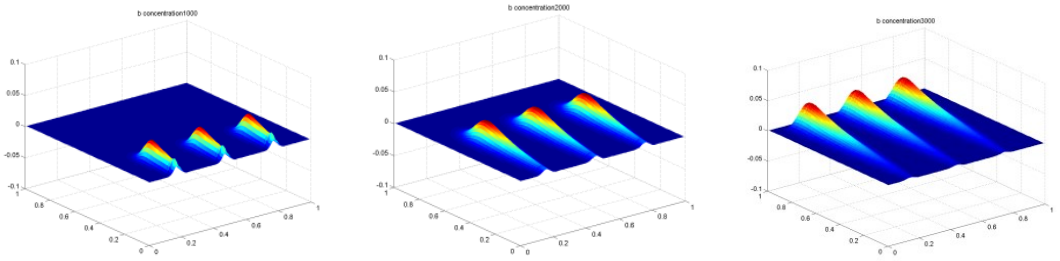

(a) t=1 (b) t=2 (c) t=3

Figure 5.4. Spatiotemporal evolution of a vessel density *b*[8][8]

The three clusters of vessel density are moving through the trail of tip cells towards the line tumour. The figure shows the evolution result of vessel density towards the tumour line source by numerically simulating Eq. (5.8).

From Figure 5.4 above, we can observe the vessel density, *b*, migrates up the gradient of TAF under the influence of chemotaxis. The vessels are laid down on the trail of tip cells, through which the immune factor is delivered at the same time, as recruited by the tip cells. The vessel density can be dynamically observed. When the vessels approach the tumour, the density of the vessels becomes higher and higher, which is consistent with what is called the 'brush border' phenomenon [8].

*4) Tumour influenced by the cytotoxic immune factor*

The change in tumour load is calculated by integrating the tumour densities at each time

step across the domain. The tumour load increases until the immune factor or the tumour-cytotoxic factor reaches the position of tumour. These make the tumour regress, and the rate of regression depends on the coefficient. If the $k_2$ in Eq. (5.6) increases, the term $k_2TI$ becomes significant and the tumour load becomes lower. Thus, we can consider the parameter $k_2$ as a sensitive parameter of the tumour to the tumour cytotoxic factor. If the coefficient $k_8$ in Eq. (5.7) increases, the term $k_8nI$ will increase and make the rate of generating immune factor increase, make the total magnitude of immune factor increase significantly, and finally influence the tumour load. The profile of the tumour load changing via time steps can be observed in Figure 5.5.

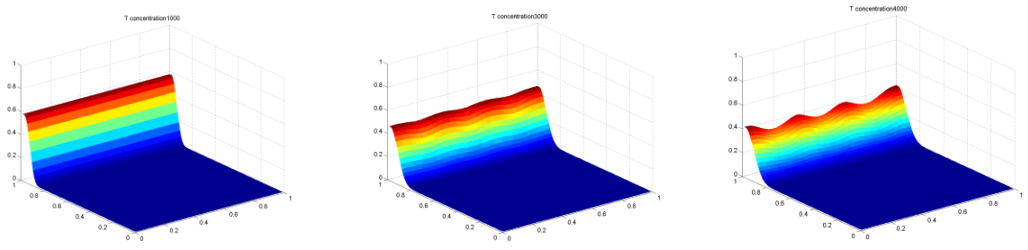

(a) t=1 (b) t=3 (c) t=5

Figure 5.5. Spatiotemporal evolution of a line tumour *T*

From the profile view of the tumour, it can be seen to regress when the vessels reach it. In the time step (*t*=5), the three clusters of vessels pass through tumour, making the tumour regress at the positions where the vessel passed. The figure shows the evolution result of the line tumour load by numerically simulating Eq. (5.6).

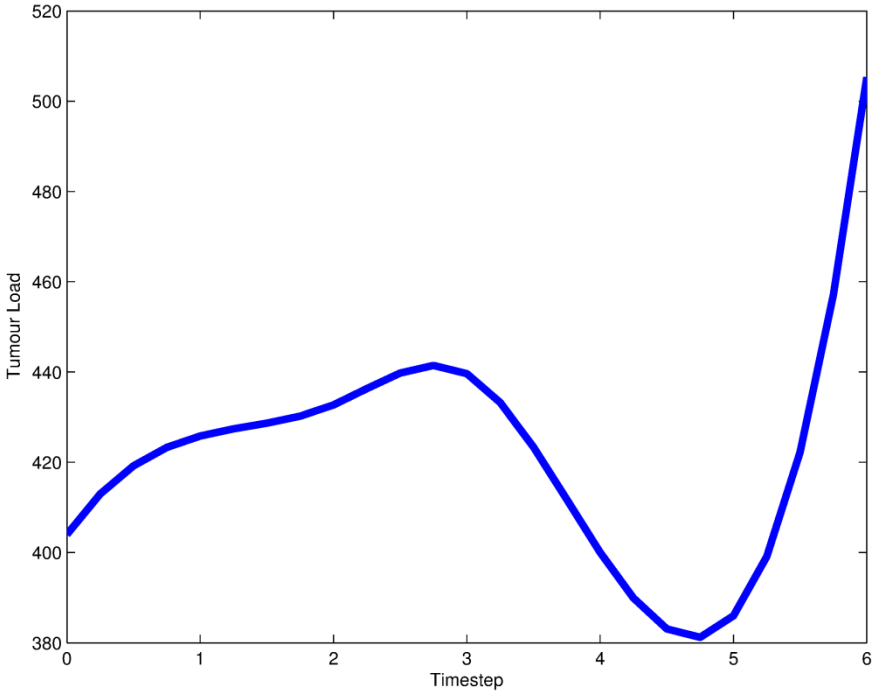


Figure 5.6. Profile of the large tumour load changing via time steps

In this case, at $t=0$, the original tumour load is set to be 404. During the simulation, the tumour load develops from the original load of 404 to the load of 440 at time step 3, then after the tumour cytotoxic factor reaches the tumour position, the tumour load decreases to the load of 390 at time step 5. After time step 5, with no tumour cytotoxic factor again, the tumour load increases and recurs.

Figure 5.6 shows the profile of change in the tumour load. The tumour mass develops from the very beginning to the time 3, each time step represents the length of timescale $\tau$. From time 3 when the immune cytotoxic factor reaches the tumour, it kills the tumour cells and makes the tumour regress, so the tumour load becomes lower and lower. After time 5, the tumour load increases again, which is called recurrence. This is due to the disappearance of the immune factor, because in the model, the immune cells is assumed only delivered by the tips in front of vessels when tips disappeared the immune cells disappeared. The

surviving tumour cells then begin to recur. This indicates that the tumour may not develop again. To make it easier to understand, we have plotted simulation results in the following sequence of images.

*5) The sequence of images extracted from animation results.*

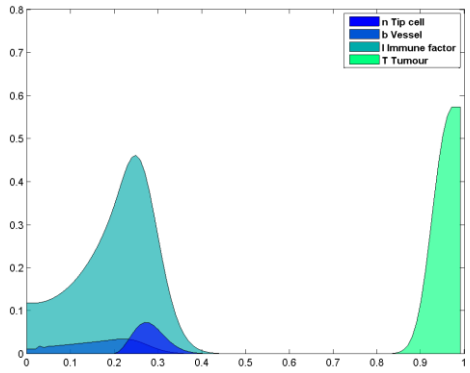


(a) t=1

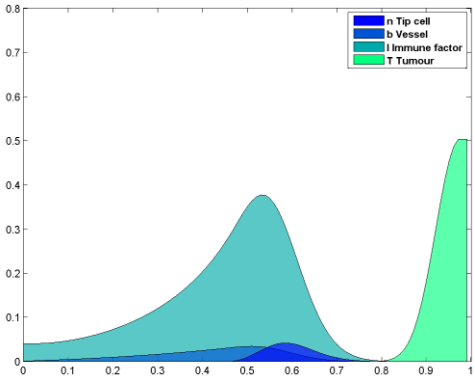


(b) t=2

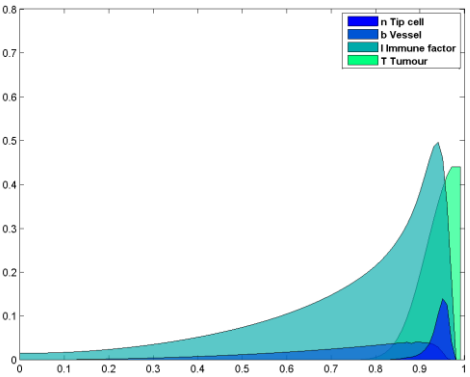


(c) t=3

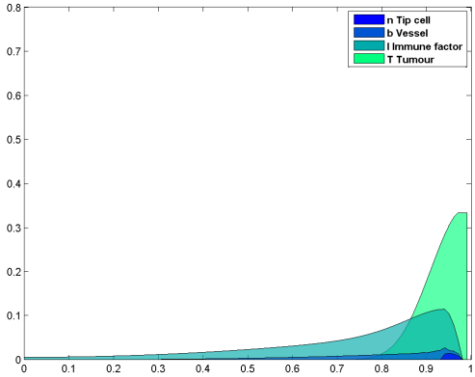


(d) t=4

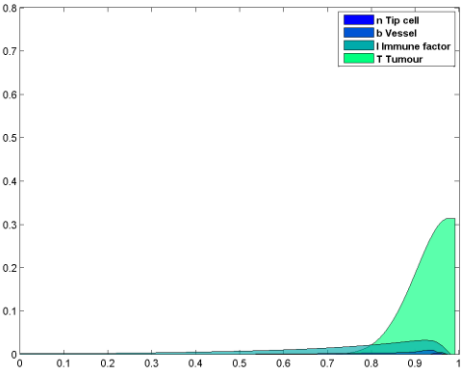


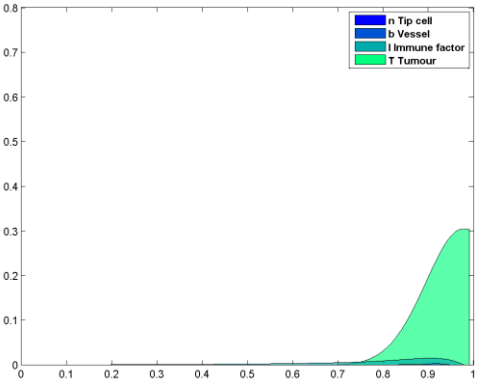

(e) t=5 (f) t=6

Figure 5.7. Animation profile of large tumour load, tip, vessel and immune factor profile in different time steps

From the sequence of images shown above, it is clear that in $t$=1 and $t$=2, the tip cells do not reach the tumour, so the immune factor is also far from the tumour, and the tumour is developing. At $t$=3, the immune factor reaches the tumour and begins to kill tumour cells. After $t$=4, the tip cells pass the position of the tumour, and the concentration of the immune factor decreases and finally disappears. After the tip cells have passed the tumour, the density of immune factor decreases simultaneously. Lacking the immune factor, the tumour begins to recur and develops again after the time $t$=5 shown in Figure 5.5, Figure 5.6, and t=1

(b) t=2

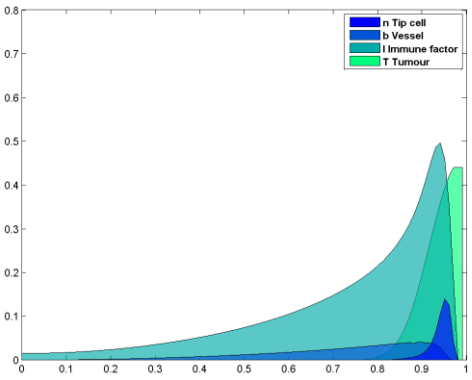


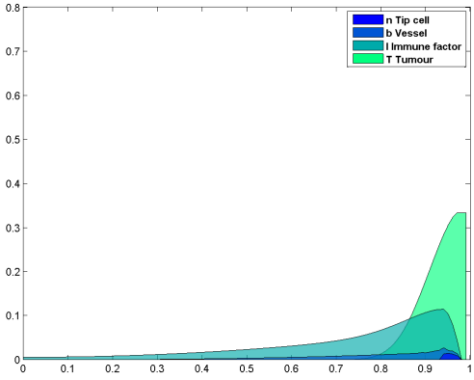


(c) t=3 (d) t=4

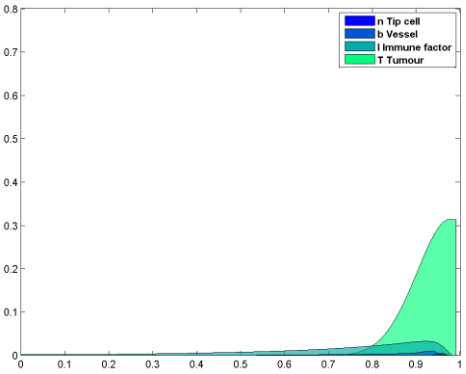


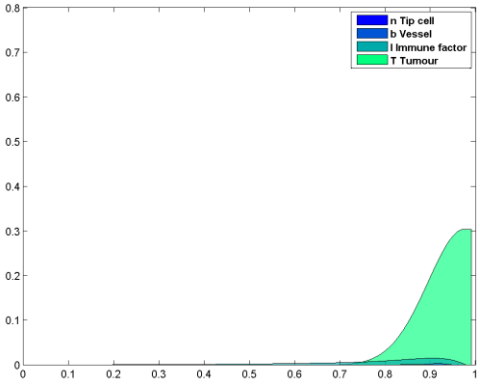


(e) t=5 (f) t=6

Figure 5.7.

#### 5.2.1.5 Modelling of drug delivery through the vessel

From the simulation above, we can find that when the tumour cytotoxic factor reaches the tumour, it will kill the tumour cells and make the tumour regress. However, after the tumour cytotoxic factor disappears in tumour mass, the tumour begins to develop again. This is the recurrence phenomenon of a tumour. Thus, we should consider how to continuously deliver the tumour cytotoxic factor into the tumour. We set the drug equation as follows:

$$\frac{\partial d}{\partial t} = D_d\left(\frac{\partial^2 d}{\partial x^2} + \frac{\partial^2 d}{\partial y^2}\right) + k_{15} b\left(\frac{\partial c}{\partial x} + \frac{\partial c}{\partial y}\right) \qquad (5.12)$$

where $d$ represents tumour cell cytotoxic drugs, $b$ represents formed blood vessel density and $c$ represents TAF respectively. On the right of Eq. (5.12) the first term represents diffusion of tumour cell cytotoxic drugs by random motility with diffusion coefficient $D_d$, the second term represents the tumour cell cytotoxic drugs delivered through the formed

vessels with the rate constant $k_{15}$, in which the rate of drug delivered is proportional to the vessel density $b$.

In Eq. (5.12) the molecular component drug may diffuse faster than the cellular component immune factor. The diffusion coefficient $D_d$ of the drug should be greater than that of $D_I$, but would be in the same scale. Considering the possibility that the drug is delivered following the formation of vessels and the immune factor is recruited by the tip cells, we assume that the drug and the immune factor reach the tumour at almost the same time, so the magnitude of the drug diffusion coefficient $D_d$ is taken to be the same as $D_I$ to Eq. (5.12). The drug is delivered through the capillary vessels, so the flux of the drug is proportional to the density of the vessel denoted as $b$. We assume the concentration of drug delivered is in the same scale as the immune factor, but it could be higher because the drug can be delivered artificially to a certain extent. Thus, we take the magnitude of the coefficient $\mathrm{k}_{15}$ in Eq. (5.12) as high as five times of $k_9$ in Eq. (5.8) in our simulation.

For the equation of the tumour, we think that the tumour cytotoxic factor consists of two parts. The first is the immune factor delivered from the host immune system throughthe vessels formed. The immune factor reaches the tumour at the same time as the tip cells. The second is the drug which is delivered from the vessels. The drug reaches the tumour along with the vessel development. Both of the cytotoxic factors have a synthetic effect on the tumour. The former makes the tumour cells more sensitive to the drug. The tumour cytotoxic drug coefficient is $\mathrm{k}_{16}$. The magnitude of $k_{16}$ is taken to be the same as $k_2$. We assume that the killing rate is proportional to the concentration of drug and tumour cells. It is described as Eq. (5.13).

$$\frac{\partial T}{\partial t} = D_T(\frac{\partial^2 T}{\partial x^2} + \frac{\partial^2 T}{\partial y^2}) - k_2 TI - k_{16} Td + k_{11} Tb + k_3 T \qquad (5.13)$$

where *T* represents tumour cells, *I* represents immune cytotoxic factor, *d* represents tumour cell cytotoxic drugs and b is the formed blood vessels respectively. On the right of Eq. (5.13), the first term represents flux of tumour cells by random motility with diffusion coefficient $D_T$, the second term represents the killing rate of tumour cells by immune cytotoxic factor with the rate constant $k_2$, the third term indicates the killing rate of tumour cells by tumour cell cytotoxic drugs with the rate constant $k_{16}$, the fourth term refers to the tumour development rate enhanced by blood vessels with the rate constant $k_{11}$ the fifth term refers to the natural tumour growth rate with the rate constant $k_3$.

Based on the analysis above, we set another simulation assuming that a tumour cytotoxic drug is delivered through the vessels formed. In this simulation, the condition of the tumour and TAF are the same as discussed above, which is a line tumour and a steady state TAF distribution. Except for the immune factor, the different point from above is that we simulate the delivery of a tumour cytotoxic drug through the vessels in Eq. (5.12). The variables denoted as *d* represent the tumour cytotoxic drug. The influence of the drug on the tumour is described in Eq. (5.13). The result of simulation is as shown in Figure 5.8. The figure for the tip cells, vessel density, and the immune factor concentration is the same as that simulated above, so here we only present the tumour cytotoxic drug concentration profile and the simulated tumour profile.

#### 5.2.1.6 Simulating large tumour load regression by both immune factor and cytotoxic drug

We assume the large tumour load is a great one and forms a line TAF source. The TAF is secreted and diffused to the side of the vessel based on Eq. (4.19), and forms a TAF concentration gradient at a steady state. The distribution of TAF is shown in Figure 5.1. We take the steady state TAF concentration gradient shown in Figure 5.1 as the initial condition for the simulation of Eq. (5.5), Eq. (5.6), and Eq. (5.8). In addition, the two equations which describe the drug delivery and tumour response to the drug, Eq. (5.12) and Eq. (5.13), are involved in the simulation. We set the large tumour load to be the same as that in section 5.2.2. The simulation results are shown as follows.

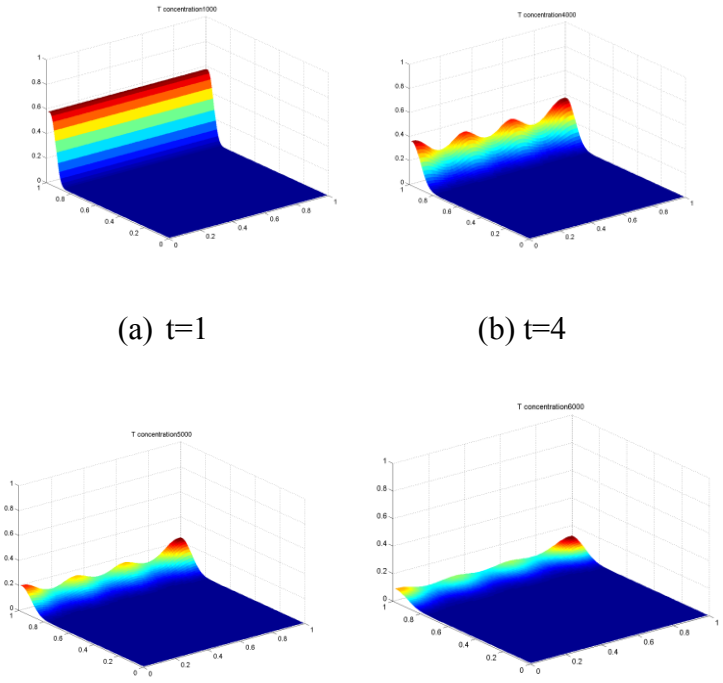

(a) t=1 (b) t=4

(c) t=5 (d) t=6

Figure 5.8. Spatiotemporal evolution of a line tumour *T* influenced by immune factor and drug

From the profile view, the tumour regresses when the vessels reach the tumour. In time step ($t$=5), the three clusters of the immune factor pass through the tumour, and the drug remains in range of the tumour, making the tumour regress. The figure shows the evolution result of line tumour load by numerically simulating Eq. (5.13).

*1) Simulation of tumour cytotoxic drug concentration.*

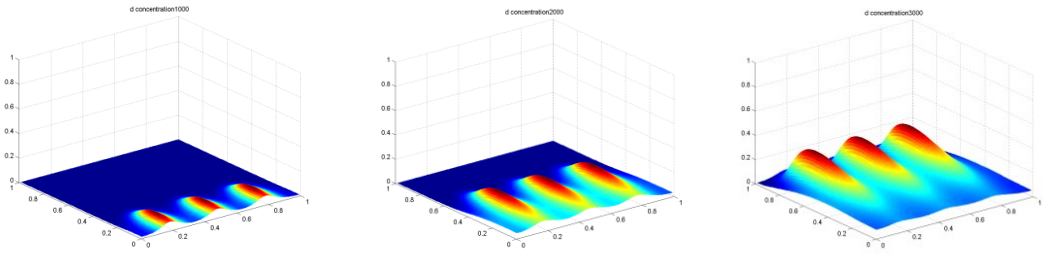

(a) t=1 (b) t=2 (c) t=3

Figure 5.9 Spatiotemporal evolution of the tumour cytotoxic drug $d$

The drug concentration corresponds with the density of the vessels formed. It is in the same step with the vessels from the view of profile. The three clusters of tumour cytotoxic drug are moving through the vessels towards the line tumour. The figure shows the evolution result of tumour cytotoxic drug delivered towards the tumour line source by numerically simulating Eq. (5.12).

From Figure 5.9, we can observe the change of tumour cytotoxic drug, denoted as $d$ in Eq. (5.12). The drug is delivered through the vessels, through which the immune factor is also delivered at the same time. The tumour cytotoxic drug can be observed dynamically, consistent with the density of vessels.

*2) The sequence of images extracted from animation results*

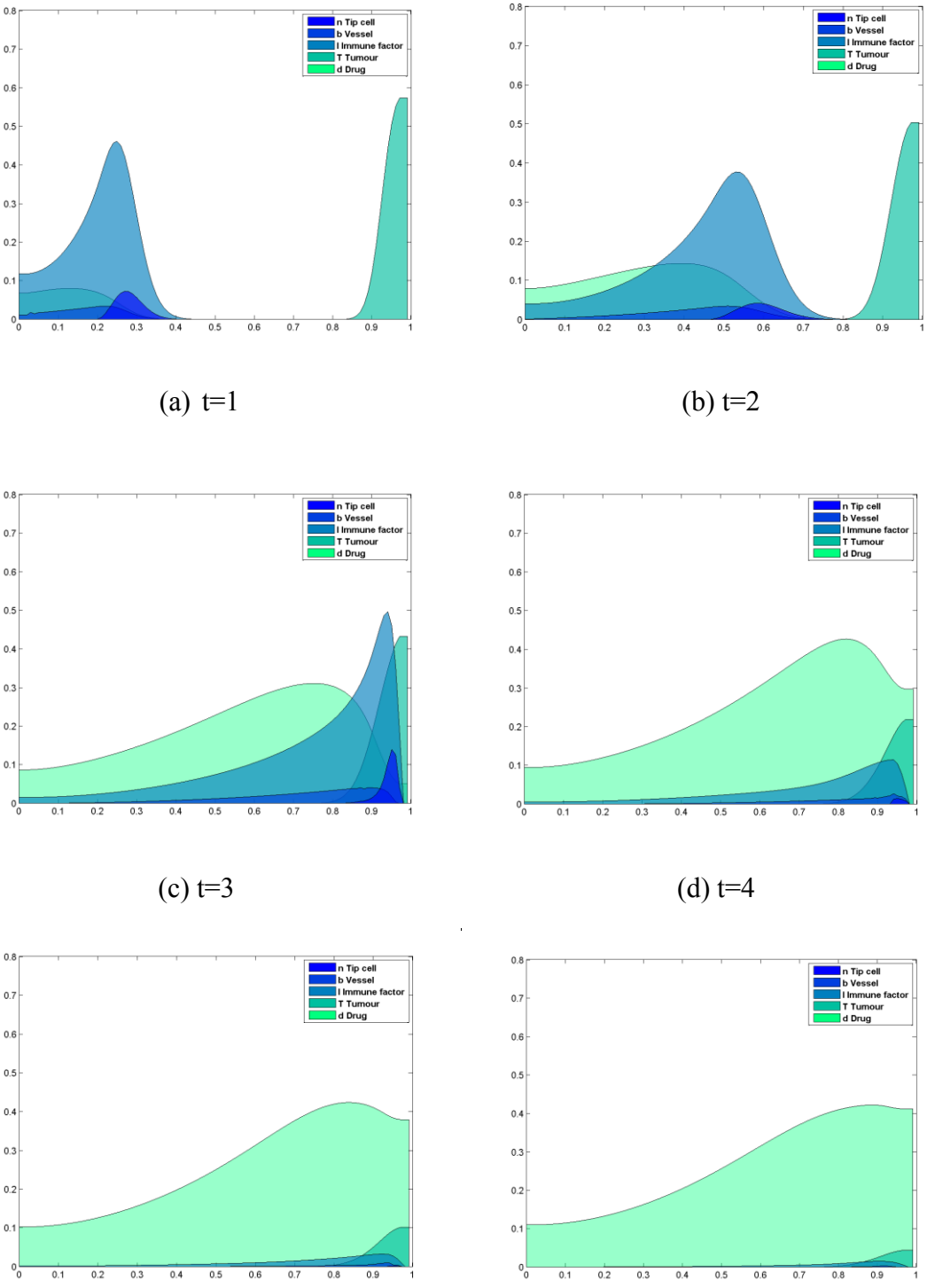


(a) t=1 (b) t=2

(c) t=3 (d) t=4

(e) t=5 (f) t=6

Figure 5.10 Animation profile of the tumour, tip, vessel, immune factor, and drug profile at different time steps

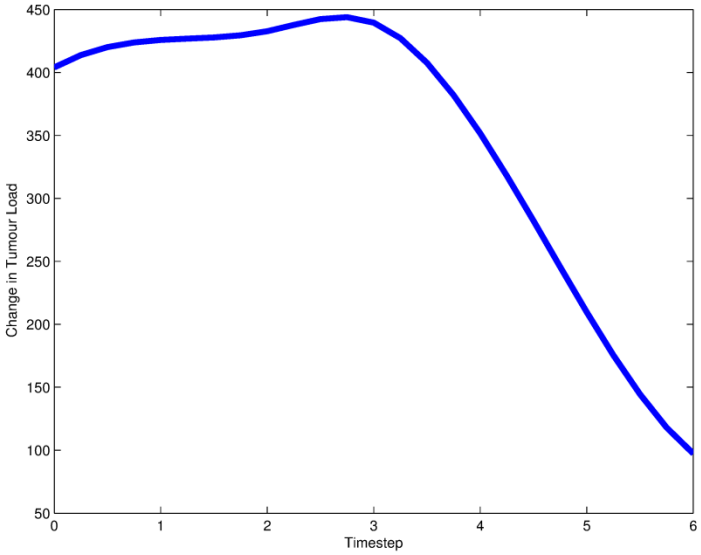


Figure 5.11 Profile of the large tumour load change via time steps influenced by immune factor and drug

In the profile, the original tumour load of 404 developed to 440 at time step 3, then after both the cytotoxic factor and drug reached the position of tumour, the tumour load decreased significantly to the load of 100 at time step 6. Which mean that tumour regressed significantly When the synthetic effect of tumour immune cytotoxic factor and drug occurred simultaneously and the drug effect remained.

In Figure 5.8, t=1 (b) t=2

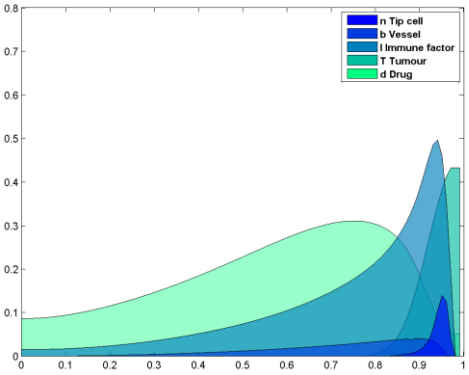


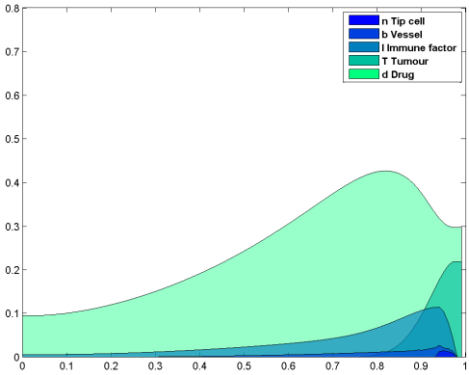


(c) t=3 (d) t=4

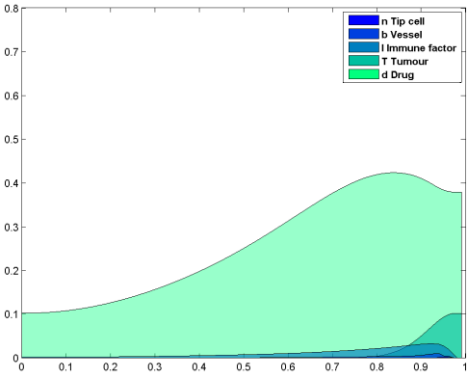


(e) t=5

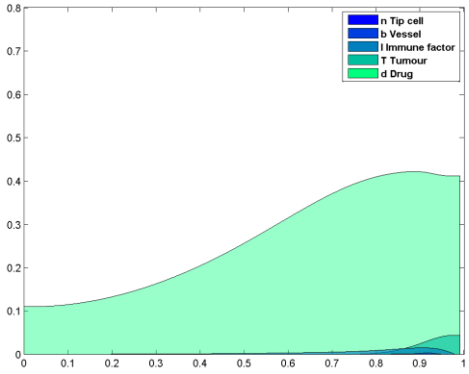


(f) t=6

Figure 5.10, and Figure 5.11, it can be observed that the tumour is reduced from the system significantly after the immune factor reached the tumour mass. The drug delivered through the vessels reaches the tumour mass later and remains for a longer time. This means that the killing effect of the drug is maintained longer and the tumour continuously regresses. At time step ($t$=6), the tumour mass becomes a smaller one and is still regressing. This is because the drug remains there. The vessels reach the tumour before significant effects occur. The model simulation results show that the drug reaches the tumour a little later than that of the immune factor. This may be because the tip cells recruit the cytotoxic immune factor but the drug should be delivered after the formation of the vessel. Usually, drugs are molecular components and they diffuse faster than cellular components, such as the cytotoxic immune factor. However, in the simulation, the drug reaches the tumour mass later. This could be due to the drug being delivered through the vessels, but the immune factor being carried by tip cells.

#### 5.2.1.7 Simulating a small tumour load clearance by immune tumour cytotoxic factor

Now, we assume that there is a tumour which is relatively small. The tumour load is set as $4 \times 5 \times 1 = 20$. We put the small tumour in the middle adjacent to the edge opposite to the vessel. For the simulation domain, no tumour line source exists, and only a small tumour is put in the mid-point adjacent to the side of domain opposite to the pre-existing vessel. The TAF is secreted by the small tumour and diffused into the microenvironment. After the TAF reaches a steady state, the contribution of TAF can be shown as follows in Figure 5.12.

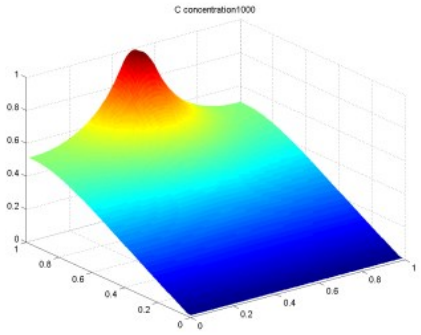


Figure 5.12 The steady state TAF concentration gradient generated by a small tumour. This figure is obtained by numerically simulating Eq. (4.19)

In the same way as shown in section 5.2.1, we take the steady state TAF concentration gradient shown in Figure 5.12 as the initial condition for the simulation of Eq. (5.5), Eq. (5.6), Eq. (5.7), and Eq. (5.8). In this section, we set a small tumour load T=20. The simulation results are shown as follows in Figure 5.13, Figure 5.14, Figure 5.15, Figure 5.16, Figure 5.17, and Figure 5.18.

Based on the assumption, we set three clusters of ECs on the side of the vessel which is the same as the simulation above. Under the influence of chemotaxis, the ECs migrate from the

side of pre-existing vessel to the tumour in the midle of the opposite side. The migration of tip cells and their change in density are shown in Figure 5.13. The three clusters of ECs migrate due to the attraction of the chemotaxis.

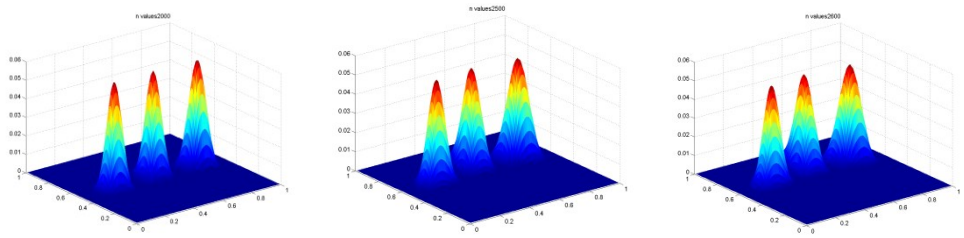

(a) t=2 (b) t=2.5 (c) t=2.6

Figure 5.13 Spatiotemporal evolution of ECs density *n*

The initial three clusters of EC density are moving towards the line tumour. The figure shows the evolution result of EC density towards a small tumour source by numerically simulating Eq. (5.5).

*1) Tip cells (ECs) migration attracted by a small tumour*

From Figure 5.13, we can observe that from time step ($t$=1, $t$=2) to $t$=2.5, the movement velocity of endothelial tip cells in three clusters remains almost the same. The distance covered by the ECs is only two thirds of the domain. This means that the velocity of the move is relatively low because the gradient is low. From time step ($t$=2.5) to time step ($t$=3), the movement velocity of endothelial tip cells in three clusters accelerates and covers the rest of the domain. It takes less than half a time step to cover one third of the domain. This is due to the precipitous gradient of TAF concentration approaching the small tumour. We can observe that the three clusters of ECs get closer to the centre and move faster towards

the tumour. At this local range, the gradient becomes steeper and leads to a strong chemotactic influence. When the ECs approach the tumour, the three clusters of ECs gather and overlap, leading to higher local density.

*2) The vessel density induced by a small tumour*

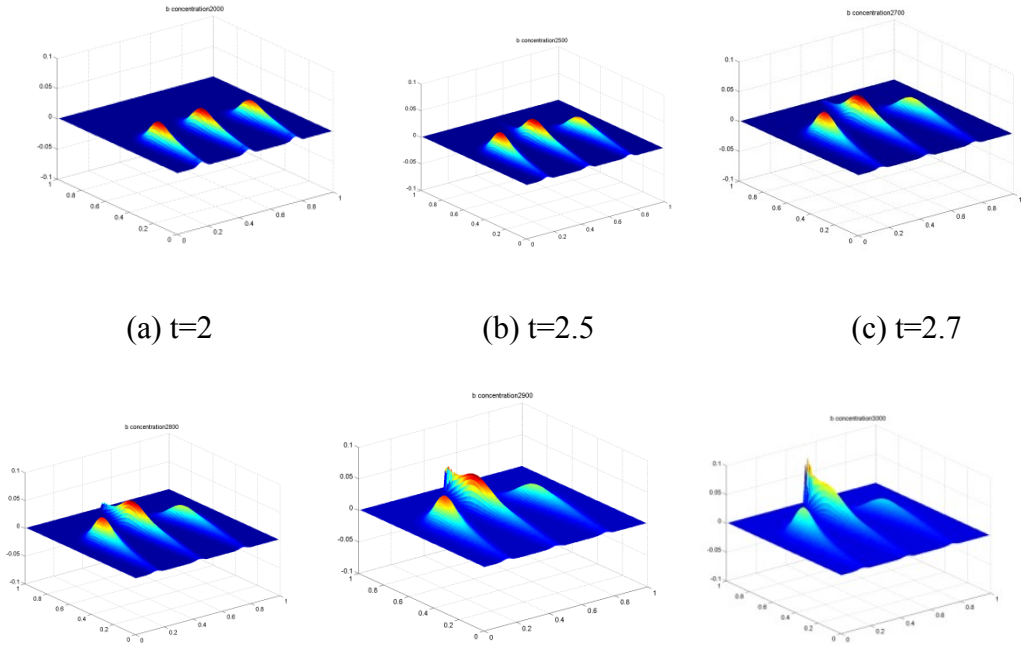

(a) t=2 (b) t=2.5 (c) t=2.7

(d) t=2.8 (b) t=2.9 (c) t=3

Figure 5.14 Spatiotemporal evolution of vessel density *b*.

The three clusters of vessel density are moving towards the small tumour. The figure shows the evolution result of vessel density towards a small tumour source by numerically simulating Eq. (5.8)

From Figure 5.14 shown above, we can observe that the vessel density is the highest at the tumour at time step ($t$=3). The position it reaches represents the position of the front edge of the vessels, through which the immune factor is delivered at the same time, which would be recruited by the tip cells.

*3) Immune factor attracted by the small tumour*

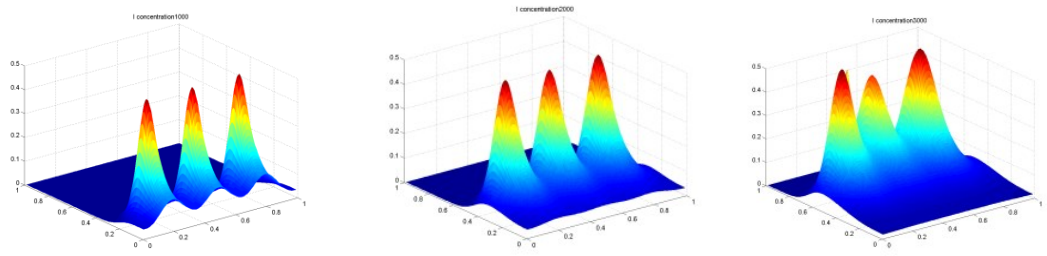

(a) t=1 (b) t=2 (c) t=3

Figure 5.15 Spatiotemporal evolution of an immune factor density *I*.

The three clusters of immune factor density are moving towards the small tumour. The figure shows the evolution result of immune factor density towards a small tumour source by numerically simulating Eq. (5.7).

*4) A small tumour clearance by the immune factor*

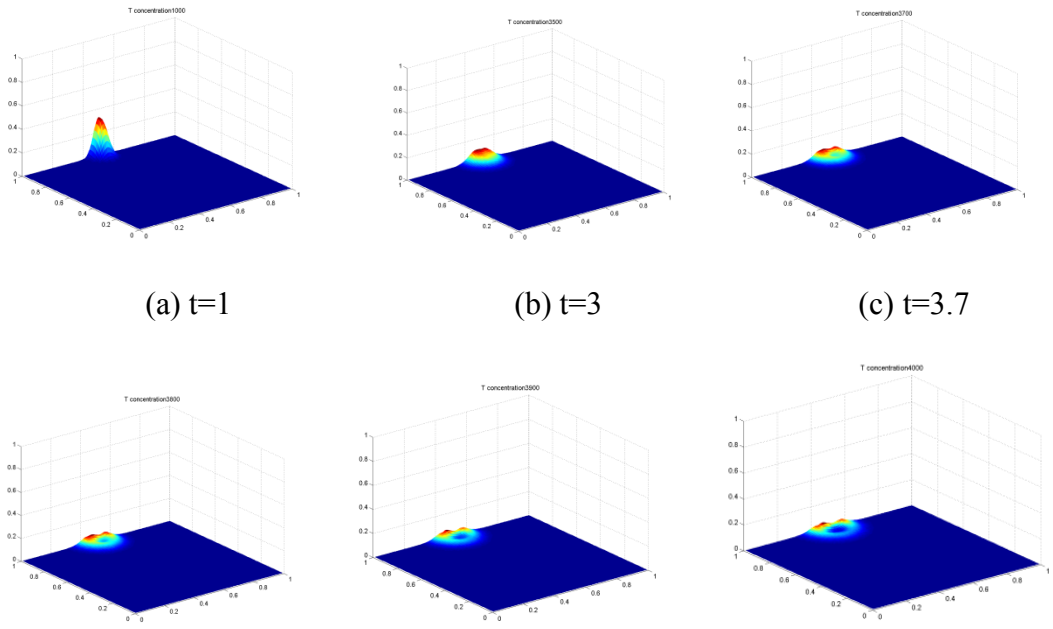

(a) t=1 (b) t=3 (c) t=3.7

(d) t=3.8 (e) t=3.9 (f) t=4

Figure 5.16 Spatiotemporal evolution of a small tumour load *T* cleared by immune factor

From the profile view, the tumour regresses when the vessels reach the tumour. In time step ($t$=4), the three clusters of overlapping vessels pass through tumour, making the tumour regress significantly at time step ($t$=4). The figure shows the evolution result of small tumour load by numerically simulating Eq. (5.6).

*5) Sequence images extracted from animation results*

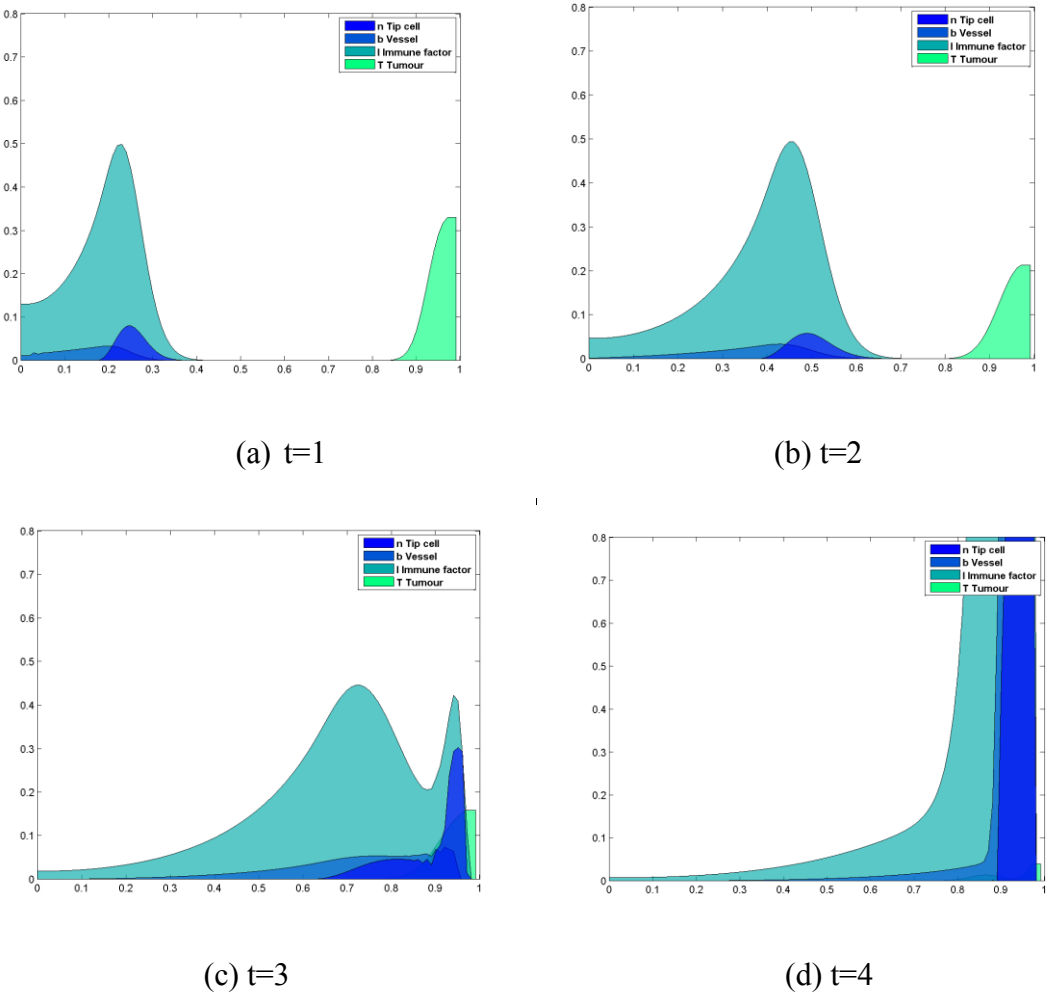


(a) t=1 (b) t=2

(c) t=3 (d) t=4

Figure 5.17 Animation profile of a small tumour, tip, vessel, immune factor profile at different time steps

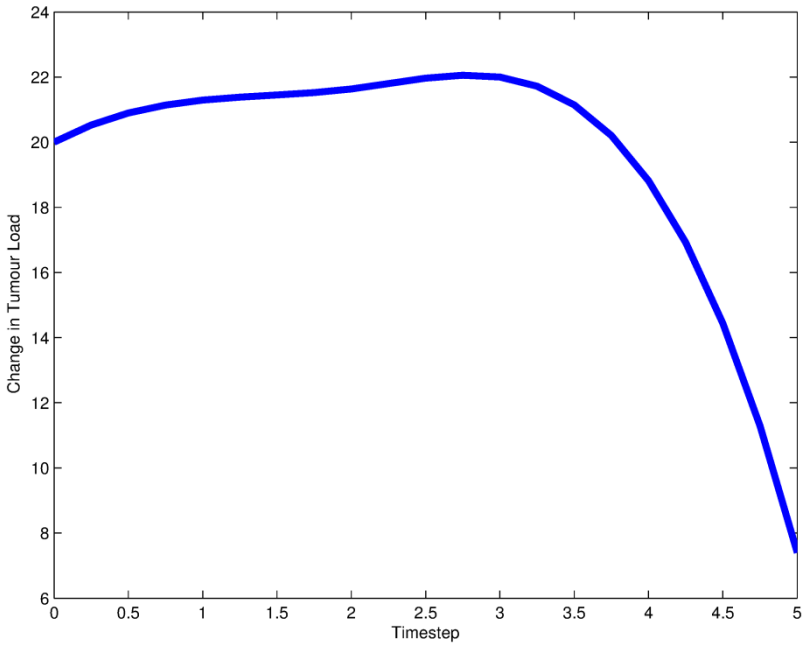


Figure 5.18 Profile of the tumour load change via time steps

The tumour developed from the original small load of 20 to 23 at time step 3, then after the tumour cytotoxic factor generated by immune system reached the position of the small tumour, the tumour load decreases to the load of 7 at time step 5. The trend remained. This means that a very small tumour load could be eliminated by the immune factor if the tumour cytotoxic factor can be focused enhanced on it.

In Figure 5.16, Figure 5.17, and Figure 5.18, it can be observed that the small tumour is reduced significantly after the immune factor passed the tumour mass after time step ($t$=3). At time step ($t$=5), the tumour mass has been eliminated. This is because the immune factor from three clusters of vessels gathers and enhances the tumour cytotoxic effect. The results imply that if the tumour is small enough, the tumour load would probably be eliminated, such as when the tumour cells have metastasis from a primary tumour and appear close to a limbus vessel, and when the immune factor generated by the limbus vessel is strong

enough.

Tumours can raise the function of the immune system, as the immune system interacts with tumours. The immune system can kill the tumour cells and regress the tumours. At the same time, it can partly sculpt the cancer phenotype, making the tumour cells less immunogenic and ultimately aiding tumour growth [195]. The dual functions of the immune system hinder and facilitate tumour growth, leading to the theory of cancer immunoediting [193]. The tumour immunoediting process hypothesis consists of three phases: elimination, equilibrium, and escape, termed the three Es of tumour immunoediting [192, 193].

In the elimination phase, the tumour cells are successfully recognised and eliminated by the immune system, thus returning the tissues to their normal state of function. Numerous studies have now demonstrated this phenomenon of the immune system for such a phase [194, 197]. The tumour cells that are not completely eliminated by the immune system proceed into a phase of equilibrium, in which the immune system controls tumour cell growth but not completely eliminate the cells. In the phase of equilibrium, the constant interaction of the immune system with tumours over a long period of time may finally edit or sculpt the cells of developing tumours, resulting in tumour cells shaped into a less-immunogenic state, which leads to being less susceptible to immune attack. Thus, the tumour progresses into the third phase of the immunoediting process, termed escape. The tumours in the escape phase destroy the immune system to facilitate their growth through different mechanisms [194, 197]. Now, numerous experiments and intensive research work are being carried out to develop strategies that can target these mechanisms of escape, as this represents new means of cancer immunotherapy [198].

In our simulation, we find that when the tumour is small, the immune factor can eliminate the tumour completely, but when the tumour becomes large, the immune factor can only make the tumour regress then recur. Our model and simulation results are consistent with the tumour immunoediting process described in recent research [192, 193]. In our model, for the therapy of a large tumour, we have developed two equations described in Eq. (5.12) and Eq. (5.13). The two equations involve the variables I and d. The simulation results in

Figure 5.8, t=1 (b) t=2

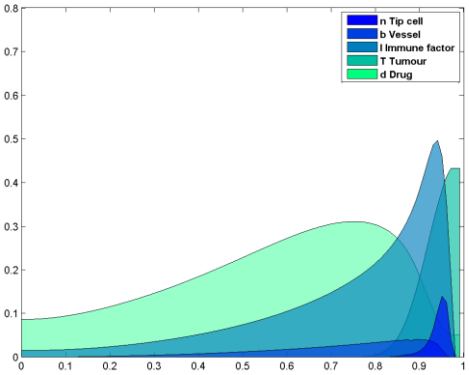


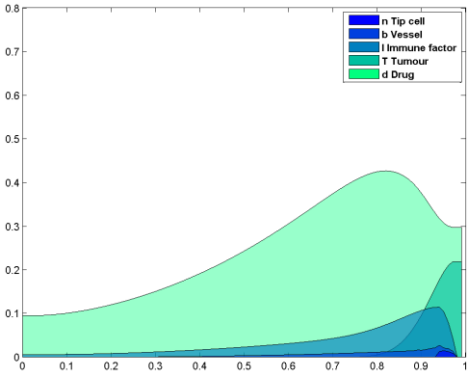


(c) t=3 (d) t=4

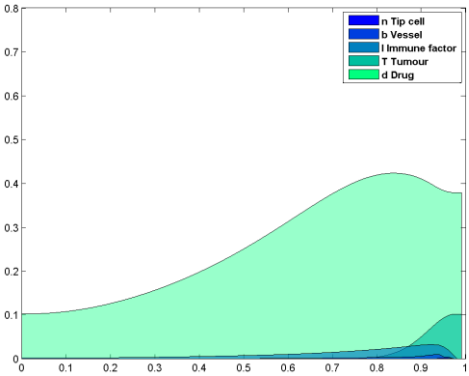


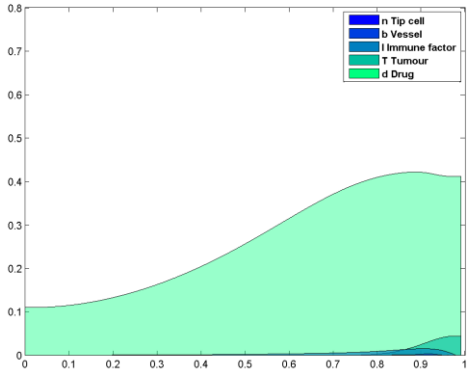


(e) t=5 (f) t=6

Figure 5.10 and Figure 5.11 show that the large tumour regresses and does not recur by the influence of *I* and *d*. Here, the variable *d* can be a tumour cytotoxic drug or some kind of immune therapy substance delivered through the formed vessels. From the simulation

results, we can imagine that if we can mobilise, recruit the tumour cytotoxic immune factor, and focus it on a tumour, the immune factor will be strong enough to defeat the tumour. These simulation results imply that there may be possible ways progress: by improving the patients' immune system; by mobilising and recruiting patients' immune factor; or by superimposing immune factor and drug effects together. These are possible forms of early tumour therapy and in some cases the tumour might be cured completely. The simulation results indicate the potential for tumour therapy.

## 5.3 Summary

In section 5.1, we further developed the model established in section 4.2 by involving another three PDEs and simulating the tumour regression, recurrence, and clearance by cytotoxic factor delivered through the vessels formed by tumour-induced angiogenesis under different conditions. The model is able to simulate a sequence of tumour-induced angiogenesis, the delivery of a tumour cytotoxic factor, including innate tumour cytotoxic immune factor such as natural killer (NK) cells and macrophages, or a tumour cytotoxic drug through the newly formed capillary vessels, and consequently the regression of the tumour. In the model, we assume that based on the steady state of concentration gradient of a tumour angiogenesis factor (e.g. VEGF), the angiogenesis from a pre-existing limbus vessel commences. The main equation used to describe the density of capillary tip cells both spatially and temporally is a nonlinear PDE. The development of capillary tip cells governs the density of blood vessels and the concentration of cells of the immune system. The density of tumour cells is also described by using a PDE. From the simulation, we can

observe that the tumour regresses when the tip cells lead the approach of vessels. This is the reason why tip cells carry the immune factor approaching at the same time and make the tumour regress. Here we call it a system approaching. If the tumour cell loading is relatively low and the immune tumour cytotoxic factor enhanced, the system approaching can eliminate the tumour by itself. If the tumour cell loading is relatively high, the immune factor cannot eliminate the tumour by itself, so the tumour recurs. We also developed a PDE to describe the delivery of tumour cytotoxic drug. By simulating the model, we can observe that the tumour regresses significantly by introducing drugs. We can observe the synthesis effect of immune factor generated in the body and the tumour cytotoxic drug delivered through the vessels formed from the simulation.

The computational modelling approach is of a lot of benefits in describing the interactions of tumours between immune factors for the results come out fast and visually, but *in vivo* experiments the results are usually very costly and can take months or years for an experienced team to perform. The interactions between tumours and immune factors are also very complex to follow since it is difficult to observe them without disrupting the ongoing process. Therefore, *in silico*, computer modelling can help our understanding of the tumour-immune factor interactions by allowing us to simulate the behaviours that cannot be observed directly *in vivo*. Computer models can simulate experiments lasting years in real time in a far shorter time even days and give access to information which is normally hidden during *in vivo* studies. The precision of these simulations depends on the model established.

## 5.4 Conclusion

In this chapter, we have presented and discussed our mathematical models of tumour-induced angiogenesis with tumour regression by cell immune tumour cytotoxic factor.

We developed the model by involving cytotoxic factor under different conditions to describe the tumour regression, recurrence, and clearance. The simulation demonstrates the synthesis effect of immune factor generated in the body and the tumour cytotoxic drug delivered through the formed vessels. The results show that a small tumour load can be eliminated completely by enhancing the immune factor, and a large tumour load can be regressed by the immune factor but recur again. Here we would like to emphasize that it is oversimplified for the model that the precision of the simulation results are limited and it is necessary to carry out much more biological research to make this model more useful.

# Chapter 6. Modelling of VEGF/Notch regulatory mechanism in angiogenesis

Signal transduction plays a vital role in tumour-induced angiogenesis in which cells divide, differentiate, migrate and proliferate. The VEGF/Notch signalling pathways are the important regulatory mechanism for the proper formation of capillary vessel networks. Tumour-induced angiogenesis usually starts at the subcellular level. This subcellular level is marked by events that occur within and between ECs, such as transduction of chemical signals between VEGF ligand and VEGF receptors or Dll4 ligand and Notch receptors. A large number of intracellular components regulate activities at the cellular level, such as tip and stalk cell differentiation. This cellular level can be referred to as the microscopic scale. It is a challenging task to modelling the regulatory mechanism of VEGF and Notch signalling pathways which make the capillary vessels formed in an appropriate network. Mathematical models can help us to better understand these mechanisms.

This chapter firstly presents the VEGF signalling pathway regulatory model in angiogenesis, then demonstrates the Notch signalling pathway regulatory model in angiogenesis, and also discusses the VEGF-Notch feedback regulatory mechanism in angiogenesis. Finally, it analyses the developed enzymatic catalysed kinetic model in ODE hybrid with ABM to simulate the regulatory mechanism.

## 6.1 Introduction

This chapter presents our innovative models involving the regulatory mechanism of a VEGF/Notch signalling pathway, which is crucial in the selection of tip and stalk cells during the angiogenesis process and influences the morphology of the capillary network. The mechanism of sprouting and branching is also simulated in this chapter.

## 6.2 Establishing the VEGF signalling pathway regulatory model in angiogenesis

Based on the bio-evidence described in section 2.3.4.1, when the ligand VEGF-A binds the receptor VEGFR-2 on the surface of ECs, they form receptor-ligand complex. The formation of receptor-ligand complex triggers the VEGF signalling pathway and generates the VEGF signals. For simplicity, we described VEGF-A as VEGF and VEGFR-2 as VEGFR, so the receptor-ligand complex here is described as VEGF-VEGFR. The reaction of forming VEGF-VEGFR complex is catalysed by tyrosine kinase. We describe the VEGF as substrate, denoted as S, and the VEGF-VEGFR complex formed by enzymatic catalysed reaction as product, denoted as P. In the triggering of VEGF signalling pathway, VEGFR-1 suppresses angiogenesis by trapping VEGF-A and suppressing the local concentration of VEGF-A near VEGFR-2 on the surface of ECs [95]. Thus, VEGFR-1 can act as a competitive inhibitor in the expression of VEGF signalling. We assume that co-receptors, VEGFR1 etc., are the competitive inhibitors in our model during the reaction, denoted as I, which can competitively inhibit the combination of VEGF with VEGFR-2.

Therefore, we assume that VEGFR-1 competitively inhibits the reaction rate of forming VEGF-VEGFR complex. According to the theory of enzymatic catalysis, we use the Michaelis-Menten enzymatic reaction kinetics model, described as follows:

$$v = v_{max_1} \frac{[S]}{[S] + K_{M_1}\left(1 + \frac{[I_1]}{K_{I_1}}\right)} \tag{6.1}$$

$$\because\ v = -\frac{d[S]}{dt} \quad or \quad v = \frac{d[P]}{dt} \tag{6.2}$$

$$\therefore \frac{d[S]}{dt} = -v_{max_1} \frac{[S]}{[S] + K_{M_1}\left(1 + \frac{[I_1]}{K_{I_1}}\right)} \tag{6.3}$$

Where v is the enzymatic catalysed reaction rate, $v_{max_1}$ is the maximum reaction rate, $[S]$ is the concentration of substrate, the VEGF. $K_M$ is the Michaelis constant. $K_I$ is the inhibition constant and $I_1$ is the concentration inhibitor. From the equation, if the $I_1$ increases or the inhibition constant $K_I$ decreases, the reaction rate will decrease. We use $[S_0]$ to represent the local original VEGF concentration and $[P_1]$ to represent the concentration of reaction product, the VEGF-VEGFR. The relationship can be described as:

$$[P_1] = [S_0] - [S] \tag{6.4}$$

$$\frac{d[P_1]}{dt} = -\frac{d[S]}{dt} \tag{6.5}$$

Therefore, we obtain the equation as follows:

$$\frac{d[P_1]}{dt} = v_{max_1} \frac{[S_0] - [P_1]}{([S_0] - [P_1]) + K_{M_1}\left(1 + \frac{[I_1]}{K_{I_1}}\right)} \tag{6.6}$$

Considering the decay of $P_1$ with the time elapse, the rate of degradation is proportional to its concentration, with the coefficient of $k_1$. As a result, Eq. (6.6) can be rewritten as follows:

$$\frac{d[P_1]}{dt} = v_{max_1} \frac{[S_0] - [P_1]}{([S_0] - [P_1]) + K_{M_1}\left(1 + \frac{[I_1]}{K_{I_1}}\right)} - k_1[P_1] \quad (6.7)$$

The complex is formed based on the equations described above during the VEGF and VEGFR reaction under the tyrosine kinase catalysis. Once the complex is formed, the VEGF signalling is expressed. The increasing rate of $P_1$ represents the expressing rate of VEGF signalling. The higher the magnitude of $P_1$, the stronger the strength of VEGF signalling is expressed and the faster the tip cells are formed. The EC differentiation towards the tip cells is accelerated. VEGF signalling stimulates a series of reactions to generate Dll4 on its surface.

From Eq. (6.7), where $[S_0]$ represents the original local VEGF concentration, $[P_1]$ represents the VEGF signalling, and $[I_1]$ represents the inhibition of VEGFR-1 triggered by the Notch signalling, it is clearly shown that the increasing rate of $[P_1]$ is determined by $[S_0]$ (the local original VEGF concentration), and also inhibited by the expression of inhibition $[I_1]$. $[I_1]$ will be described in detail later in section 6.4.

## 6.3 Establishing Notch signalling pathway regulatory model in angiogenesis

Based on the bio-evidence described above in 2.3.4.2, the Notch signalling pathway starts from the receptor-ligand interaction between adjacent cells. This interaction triggers a series of proteolytic cleavages of the Notch receptor inside the cell. There are several Notch receptors and ligands. As the Dll4 ligand is the most important ligand and the only protein in the Notch signalling pathway, we assume that Notch signalling begins with

receptor-ligand interactions between neighbouring cells to form a Dll4-Notch complex, which in turn triggers a series of proteolytic cleavages of the Notch receptor and is a very complicated reaction inside the cell. The Notch pathway must be tightly regulated to ensure proper vascular formation during angiogenesis.

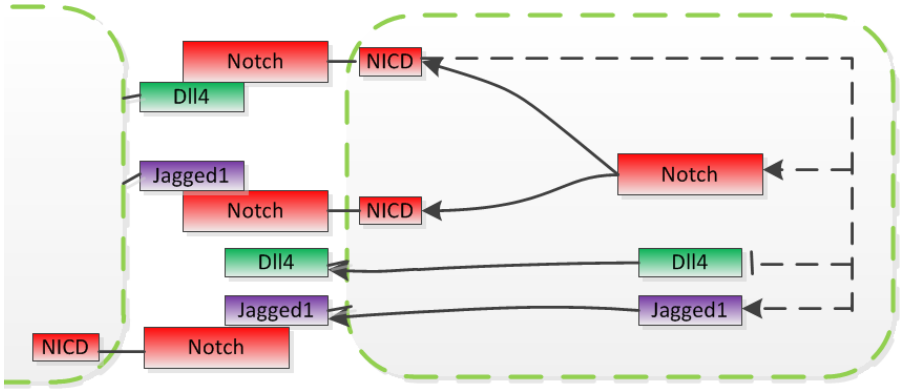


Figure 6.1. Elucidation of Notch signalling pathway

Notch signalling begins with Notch receptor-Dll4 ligand interaction between neighbouring cells. This interaction triggers a series of proteolytic cleavages of the Notch receptor, releasing NICD from the cell membrane, promoting Notch signalling and releasing Jagged1 as a competitive ligand. The Dll4 ligand is also a target gene regulated by the Notch signalling pathway [4].

Based on Figure 6.1, we assume that the Notch signal is generated by enzyme catalysed interactions between ECs. They regulate adjacent cells to specify different characteristics during sprouting angiogenesis. The strength of the signal depends on the reaction rate.

Since Dll4 is the principal ligand in the Dlls family and Jagged1 is the principal ligand in the Jagged family (see 2.3.4.2), for simplicity the Dlls ligand family is denoted as Dll4 ligand, and the Jagged ligand family is denoted as Jagged1 ligand. To establish the model,

thereby, we describe the complicated system as the reaction of Dll4 ligand with the Notch receptor and this reaction is catalysed by on enzyme (glycosyltransferase Fringe) [4] on the surface of adjacent ECs.

Once the Dll4-Notch receptor complex is formed, it triggers a series of complicated reactions inside the ECs and produces the Notch signal which makes the cell itself turn into a stalk cell without sprouting; at the same time, it sends the Notch signal to regulate the adjacent cells in front of it. This is a chain reaction representing the Notch signalling pathway. Once the reaction happens, it means the Notch signalling pathway is expressed. To describe the Notch signalling pathway regulation model, we assume that the reaction rate implemented inside the cells is faster than the reaction rate on the surface. Hence, the limited reaction rate depends on the reaction route shown in Eq. (6.8).

$$Dll4\ ligands + Notch\ receptor \overset{enzyme}{\longleftrightarrow} Dll4/Notch\ complex \tag{6.8}$$

Then, the expression of Notch signalling pathway depends on the reaction route shown in Eq. (6.9).

$$Dll4\ Notch\ complex \xrightarrow{trigger\ series\ of\ reaction\ inside\ ECs} Notch\ signaling \tag{6.9}$$

We describe the reaction in Eq. (6.10) to represent the whole Notch signalling pathway kinetic. Once the Notch signalling pathway is expressed strongly, it makes the reaction happen inside the ECs. As a result, the ECs turn into stalk cells and trigger the enzyme (Fringe) to catalyse the Jagged1 ligand to combine with the Notch receptor. In this way, the reaction competitively inhibits the combination of Dll4 with the Notch receptor, and finally lowers the Notch expression strength, whereas the Notch receptor shows strong activation by Dll4 and competitive inhibition by Jagged1.

We use $S_2$ to denote Dll4 which is the substrate of the reaction. $[S_2]$ represents the concentration of Dll4. $I_2$ denotes the coreceptor Jagged1 which acts as the inhibitor during the reaction. $[I_2]$ represents the concentration of Jagged1. $I_2$ can combine with enzyme E during the reaction. The magnitude of $I_2$ is influenced by the Notch signal. $P_2$ represents the Dll4-Notch receptor complex and $[P_2]$ represents the concentration of the Dll4-Notch receptor complex. The increasing rate of $P_2$ is consistently promoted by the strength of VEGF signal.

When the strength of Notch signal increases, the magnitude of $I_2$ increases and so does the down-regulation effect; when the Notch signal decreases, the magnitude of $I_2$ decreases and so does the down-regulation effect. It is a cell autonomous regulation. During the procedure, the balance decreases the rate of generating $P_2$ and the activation of $I_2$ depresses the expression of Notch signalling pathway by adjusting the inhibition. As a result, the cells can realise the regulation of the Notch signalling pathway autonomously.

Considering Jagged1 as a competitive inhibitor, we obtained the competitive inhibition dynamic balance based on the concept of enzymatic catalytic kinetics. In the same way as described above in VEGF signalling pathway, we derived the competitive/inhibitive kinetic equation as follows:

$$\frac{d[P_2]}{dt} = v_{max_2} \frac{[S_2]}{[S_2] + K_{M_2}\left(1 + \frac{[I_2]}{K_{I_2}}\right)} \tag{6.10}$$

where $K_{i_2}$ is the inhibitor constant, because Dll4 is produced by the expression of the VEGF signal pathway. The higher the magnitude of the VEGF expression, the higher is the Dll4. Hence, in magnitude we can assume that Dll4 is proportional to that of the VEGF-VEGFR2 complex which can be described as $[S_2] \propto [P_1]$ or $[S_2] = k[P_1]$. To

eliminate the symbol $[S_2]$ we used $k[P_1]$ to substitute $[S_2]$ in Eq. (6.10) and obtained Eq. (6.11).

$$\frac{d[P_2]}{dt} = v_{max_2} \frac{k[P_1]}{k[P_1] + K_{M_2}\left(1 + \frac{[I_2]}{K_{I_2}}\right)} \tag{6.11}$$

Considering the decay of $P_2$ with the time elapse, the rate of degradation is proportional to its concentration, with the coefficient of $k_2$ and $k_M = k \cdot K_{M_2}$. As a result, Eq. (6.11) can be rewritten as follows:

$$\frac{d[P_2]}{dt} = v_{max_2} \frac{[P_1]}{[P_1] + K_M\left(1 + \frac{[I_2]}{K_{I_2}}\right)} - k_2[P_2] \tag{6.12}$$

We assume the Notch receptor on the surface of the cell adjacent to the tip cell reacts with the Dll4 which is produced in the tip cell. Dll4 is generated by the VEGF signalling pathway expression catalysed by enzymes. We suppose that the reaction rate depends on Dll4. Based on the equation described above, during the Dll4 and Notch receptor reaction under the enzyme catalysis, the Dll4/Notch receptor complex is formed, and thereby the Notch signalling pathway is expressed. With the reaction carried out, the concentration of the complex is accumulated and then increased; the strength of Notch signalling pathway expression is increased, and the ECs differentiation towards stalk cells is accelerated. When the stalk cell is formed, it sends a signal to stimulate a series of reactions to lower VEGFR. From Eq. (6.12), it is clearly shown that the increasing rate of $[P_2]$ is determined by $[P_1]$ (adjacent Dll4 concentration), and also inhibited by the expression of inhibition $[I_2]$ which is triggered by the Notch signalling pathway.

The activation of Notch signalling promotes tip cell formation. The overexpression of Notch signalling inhibits the tip cell characteristics. Thus, the activation level of Notch signalling expression quantitatively determines the ability of individual EC differentiation

to tip or stalk cell during sprouting.

Jagged1 enhances differential Notch activity by competitively interfering with the ability of Dll4. The Notch signalling pathway can be modulated not only by the quantity of individual ligands, but also by their activity profile when Dll4 or Jagged1 interacts with the Notch receptor.

VEGF-A and Notch signalling pathways are key players governing tip and stalk cell behaviour. VEGF and Notch signalling regulate tip and stalk specification during pathological angiogenesis, such as cancer [17, 97]. Dll4 ligand has been observed to be strongly expressed in the tumour vasculature. The overexpression of Dll4 and increased Notch activation result in reduced tumour sprouting and angiogenesis. Notch signalling acts as a negative regulator of VEGF-induced angiogenesis and is essential for proper vascular morphogenesis.

The VEGF and Notch signal pathways are both key regulators of the angiogenic process and both are involved in the specification of the tip and stalk cell phenotypes. These two pathways work together to achieve functional patterning during sprouting angiogenesis. Several lines of evidence indicate that VEGF signalling acts upstream of the Notch signalling pathway during physiological and pathological angiogenesis to control the expression of different Notch components [21, 23, 98]. In addition to VEGF-A acting as the upstream of Dll4, it has become clear that Notch, in turn, controls VEGF signalling. In general, all observations support the concept that Notch signalling via Dll4 principally acts as a negative feedback regulator to control VEGF-induced angiogenesis.

## 6.4 Establishing the VEGF-Notch feedback regulatory mechanism in angiogenesis

### 6.4.1 Modelling the VEGF-Notch signalling feedback loop inside each cell

Inside each EC, both VEGF and Notch signalling feedback occur simultaneously. The VEGF and Notch signalling pathways cooperate tightly to specify and balance the tip and stalk cell phenotypes between the ECs that constitute the sprouts during angiogenesis process. To this end, Notch signalling acts in a negative feedback loop with VEGF signalling during sprouting angiogenesis.

From the VEGF signalling pathway and Notch signalling pathway described above, we obtained two equations, Eq. (6.7) and Eq. (6.12), both of which are regulatory mechanisms. For simplicity, we put both Eq. (6.7) and Eq. (6.12) together and mark them as Eq. (6.13) and Eq. (6.14), expressed as follows:

$$\frac{d[P_1]}{dt} = v_{max_1} \frac{[S_0] - [P_1]}{(S_0 - P_1) + K_{M_1}\left(1 + \frac{[I_1]}{K_{I_1}}\right)} - k_1 P_1 \tag{6.13}$$

$$\frac{d[P_2]}{dt} = v_{max_2} \frac{[P_1]}{[P_1] + K_{M_2}\left(1 + \frac{[I_2]}{K_{I_2}}\right)} - k_2 P_2 \tag{6.14}$$

$$I_1(VEGFR1, Nrp1, etc.) = f(P_2) \tag{6.15}$$

$$I_2(Jagged1) = g(P_1) \tag{6.16}$$

Considering our assumption that the inhibitors $I_1$ and $I_2$ play negative feedback roles and are triggered by the variables $P_2$ and $P_1$ respectively, we establish another two equations Eq. (6.15) and Eq. (6.16). In Eq. (6.15) and Eq. (6.16), both inhibitors $I_1$ and $I_2$ are described as function of $P_2$ and $P_1$ in which both are triggered by $P_2$ and $P_1$ respectively,

leading to down-regulation of $P_1$ and $P_2$.

Till now, we have established a pair of ODEs in Eq. (6.13) and Eq. (6.14) and two inhibitive regulation equations in Eq. (6.15) and Eq. (6.16), respectively. The four equations compose the VEGF and Notch signalling model. At each time step, the regulated results are obtained using the Euler method to solve the ODEs in Eq. (6.13) and Eq. (6.14) at each time step, and by using ABM to update data, to compare P values with C values, to judge how to take $I_1$ or $I_2$, to make decisions on cell state, and then reiterate the process. The down-regulation of Notch signalling to VEGF signalling is implemented by $P_2$ which triggers the expression of $I_1$ in Eq. (6.15), which is realised by the ABM method. In this way, the down-regulation of $P_2$ to $P_1$ is realised in our model. As a result, we established the VEGF-VEGFR-Dll4-Notch-VEGFR regulatory feedback loop mechanism inside each EC, described as Eq. (6.13), Eq. (6.14), Eq. (6.15), and Eq. (6.16).

In Eq. (6.13), $P_1$ represents the concentration of VEGF-VEGFR complex. We assume the Dll4 is proportional to the VEGF-VEGFR complex, so the formed Dll4 is logically represented as $P_1$. In Eq. (6.14), $[P_1]$ represents the concentration of Dll4 which is generated through a series of complicated reactions triggered by the formation of VEGF-VEGFR complex.

### 6.4.2 Regulation of specification of tip/stalk between adjacent ECs in angiogenesis

The specification of tip and stalk is the interplay between adjacent ECs. Any EC activated by VEGF-A and not directly inhibited by a neighbour expressing high levels of Dll4 can be

developed into the tip cell phenotype, and thus initiate a new sprout. The model described above in Eq. (6.13) and Eq. (6.14) happens not only inside each cell, but also between adjacent cells. This is a competitive/inhibitive feedback regulatory mechanism in which VEGF is up-regulatory signal pathway and Notch is down-regulatory signal pathway between the tip cell and stalk cell selection during sprouting.

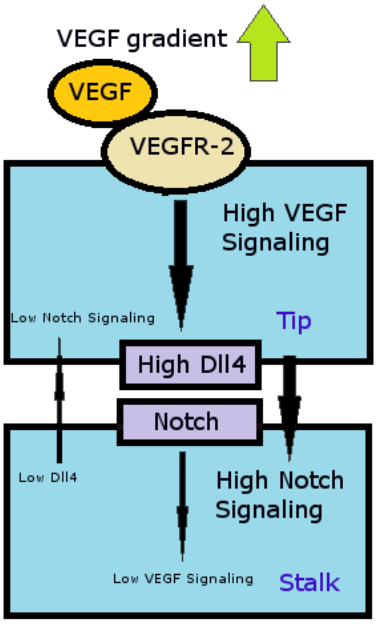


Figure 6.2. Tip and stalk cell specification during sprouting angiogenesis under the VGEF/Notch regulatory mechanism [4]

Figure 6.2 shows the regulatory mechanism formed from the implementation of VEGF and Notch signalling pathway between adjacent cells in which the tip and stalk cells are specified. High VEGF signalling generates high concentration of Dll4 on the surface of the tip cell.

When the VEGF signalling increases, the ECs in front which are specified into tip cells generate Dll4. The higher the VEGF signal is, the higher Dll4 is in magnitude. Dll4 is up-regulated in the tip cells by the VEGF signalling. Dll4 generates high Notch signalling

by triggering the reaction between the Dll4 and Notch receptor on the surface of the adjacent cells following the tip. The Notch signalling inhibits the tip characteristic and makes itself turn into a stalk cell. Consequently, once Dll4 is formed, it acts as the ligand triggering the reaction with the Notch receptor on the surface of adjacent cells. The reaction is catalysed by enzymes in the stalk cells which suppresses the tip cell phenotype. Notch signalling activation reduces VEGFR2 expression and increases VEGFR1/sVEGFR1 levels which are expressed in the equation as $I_1$, meaning the inhibition of the VEGF signal.

When the tip cell receives low Notch signalling, it allows a high expression of VEGFR2 and Nrp1, but low expression of VEGFR1. By contrast to Dll4, at the same time Jagged1 ligand is expressed by the stalk cells. Jagged1 antagonises Dll4-Notch signalling in the front of sprout when the Notch receptor is modified by the glycosyltranferase (Fringe), which is expressed as $I_2$ in Eq. (6.14). It is the competitive inhibition of Dll4. Thereby, the competitive inhibition enhances differentiation of Notch activity between tip and stalk cells.

What is described above is the computational model of the VEGF-Dll4-Notch-VEGFR regulatory feedback loop mechanism between ECs. Up to now, we have established the enzymatic catalysed kinetics computational model, based on the evidence of the VEGF signal and Notch signal pathways described above and the VEGF-Notch-VEGFR regulatory feedback loop mechanism theory. We have summarised several fundamental rules of the mechanism, as follows:

(1) The VEGF signalling pathway up-regulates sprouting. It is necessary to induce the tip characteristic which makes ECs appear as a tip phenotype. Blocking VEGF prevents tip cell formation.

(2) VEGF signalling pathway is upstream of the Notch. It positively up-regulates to promote the Notch signalling pathway consistently.

(3) Notch signalling pathway critically regulates the ratio of tip and stalk cells by suppressing tip cell formation in adjacent cells and turning them into stalk cells. Jagged1 enhances differential Notch activity by competitively interfering with Dll4.

(4) Notch signalling pathway down-regulates the VEGF signalling pathway and forms a feedback loop regulatory mechanism during sprouting angiogenesis.

(5) The VEGF and Notch signalling pathways cooperate to adjust the specification of tip cell and stalk cell instantaneously.

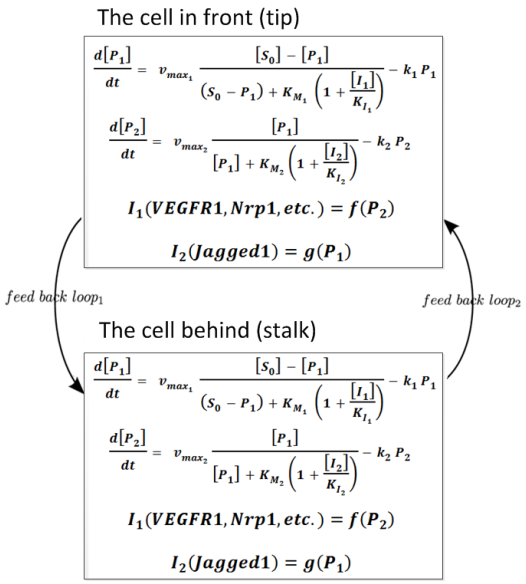


Figure 6.3 Regulation procedure of sprouting Eq. (6.13), Eq. (6.14), Eq. (6.15) and Eq. (6.16)

Figure 6.3 describes the regulation procedure of tip/stalk cell differentiation inside and between adjacent ECs at the spearheading point during sprouting angiogenesis. Each rectangle represents a cell which includes two equations representing the VEGF and Notch signal respectively. The regulation takes place inside each cell by the solution of the four equations. The two rectangles represent two adjacent cells, and the regulation occurs by the established feedback mechanism between the two cells, as described above. Figure 6.3 elucidates the relationship between VEGF and Notch signalling pathways which are implemented in the differentiation of tip and stalk cells in the vascular endothelium.

In the front cell Eq. (6.13) represents the VEGF signalling pathway. It demonstrates the interaction between VEGF and VEGFR2 on the surface of ECs. The bind of VEGF and VEGFR2 triggers the VEGF signalling and generates Dll4 ($P_1$). $P_1$ value represents the VEGF signalling. The increasing $P_1$ value promotes the increase of $P_2$ value which

represents the Notch signalling. Eq. (6.14) reveals the relationship that the Notch signalling is up-regulated by the VEGF signalling.

In the back cell, the mechanism of the regulation is the same as that in the tip cell. The front cell sends the signal back to the cell behind it to enhance Notch signalling by the high Dll4 ligand. Notch signalling in the cell behind takes the competitive inhibitors denoted as $I_1$. This is realised using the ABM method. Thus, the Notch signalling reduces VEGF signalling inside itself, which reduces $P_1$. The low VEGF signalling generates low Dll4, which makes the front cell lower the Notch itself. Consequently, the front cell is characterized as tip and the back cell as stalk. The regulation procedure of sprouting is shown in Figure 6.3. Here, the competitive receptors VEGFR1/sVEGFR1 are denoted as $I_1$ and the Jagged1 as $I_2$ in the cells. The solution of Eq. (6.13), Eq. (6.14), Eq. (6.15), and Eq. (6.16) results in the change of $P_1$ and $P_2$ values, both of which influence the cell behaviour.

## 6.5 Establishing discrete model by Agent-based Modelling (ABM)

### 6.5.1 ABM

#### 6.5.1.1 The rationale

Agent-based modelling (ABM) is a computational modelling approach providing a systematic view for the simulation of action and interaction between autonomous individual entities [142]. A network of cellular automata (CA) is another framework for

defining the interacting components in a system [146]. Since CA is not capable of representing a large amount of data transformation between entities due to the increasing complexity of the input symbols and the number of states, to model tumour-induced angiogenesis we have applied an agent-based approach which provides a more powerful state machine to allow an intuitive exploration of the dynamics and complexity of biological systems.

#### 6.5.1.2 The implementation

Finding and representing a realistic agent representation is the main focus of ABM. Maes [199] defines agent architecture as the methodology of building agents. The architecture encompasses techniques and algorithms to specify the agent into a set of component modules and define the interaction between modules. The interaction between modules determines the current internal state of the agent and future agent actions. In addition, agent architecture is famous for its particular decision making characteristics. Müller [200] summarised some of the main types of agent architecture as follows.

- **Reactive-based architectures**

  The decision making procedure is based on a very limited amount of information and simple situation action rules. It focuses on producing robust behaviour rather than correct or optimal behaviour. This type of architecture allows its decisions determined by the limited input information without other information from environment.

- **Deliberative-based architectures**

Different from the reactive agents, its decision making procedure is based on the explicit information from environment. The agent takes into account all the available environment information and integrates it with the internal knowledge before making a plan of action. The desire is to achieve the goals that an agent wishes to achieve. Intentions are the drives that propel agents to achieve their goals. The belief-desire-intention (BDI) architecture is a well-known type of deliberative architecture. The BDI agent takes into account the information about its surrounding environment and other agents.

- **Interaction-based architectures**

  The decision making procedure is attained by explicitly reasoning about the environment via different software layers. This type of architecture originates from distributing artificial intelligence.

The development process of an agent-based model involves creating agents that mimic the attributes and behaviours of their environment. In this study, agents represent the different types of ECs. Each EC has been built to have a cognitive process dictating its decision, while staying in the microenvironment during tumour-induced angiogenesis.

MASON [201] is a computational modelling toolkit used in developing the agent-based model. There are two different kinds of interactions: cell-cell and cell-ECM. The former is the interaction between ECs, while the latter is the interaction between the EC and its environment. Agents representing ECs are the core of the MASON model, so they are the main decision-making components in this model. Finally, the model consists of active, autonomous agents (i.e. ECs), and passive entities representing the surrounding environment in tumour-induced angiogenesis.

#### 6.5.1.3 A hybrid ABM approach

Modelling the individual cell behaviour in the process of angiogenesis is a challenging and complicated task. It involves interdisciplinary processes and concepts, such as theories from biology, mathematics, and computer engineering. In addition, the local heterogeneity of important factors, such as VEGF, MDE, ECM, and EC distribution in the microenvironment, makes the model more challenging. We have used ordinary differential equations (ODEs) to simulate regulation signalling, providing a signalling system model. We have used partial differential equations (PDEs) to simulate the vital factors which dynamically and simultaneously change in spatial and temporal dimensions, providing a microenvironment model. Now, we have to use the agent behaviour concept to describe how to realise the signalling communication and make decisions, especially the signalling generation and communication inside and between different ECs, which should be solved by the use of ODEs, PDEs and ABM iteratively at every time step.

In this sense, our research seeks to elucidate the complexity of building a cell behaviour model including cell interaction, specification of tip and stalk from ECs, migration of tip, and proliferation of stalk etc. Accordingly, this research proposes a novel agent-based model approach combining the microenvironment model and signalling system model. In comparison with the existing architecture reported in the literature, this research adapts a combined architecture based on a dynamic angiogenesis process.

### 6.5.2 The ODEs regulatory mechanism

To explore the mechanism of tumour-induced angiogenesis, we have introduced the discrete modelling approach to capture the features of the cell behaviours which could represent the cell-cell interaction and cell-ECM interaction in an easy way. The ABM method is a discrete modelling approach capable of representing features such as cell behaviours, ECM remodelling, and cell signalling. We are going to present and discuss a hybrid multi-scale model integrating with ABM and incorporating with the ODEs and PDEs in this section.

In the discrete model, each lattice point can be occupied by an agent representing the cell at any situation and at any time. The continuum model integrates with a VEGF layer, a MDE layer, and an ECM layer. We assume that every lattice site is associated with a field describing the concentrations of VEGF, MDE, and ECM. Agent states can be quiescent, proliferative, and migratory, and transitions between the states are regulated by the rules described later in section 6.5.3 and 6.5.4. Transitions to a state of migration or proliferation go through a series of regulations, the number of which depends on the result of VEGF/Notch regulation mechanism. The change of states is influenced by the local chemical environment and the agents nearby.

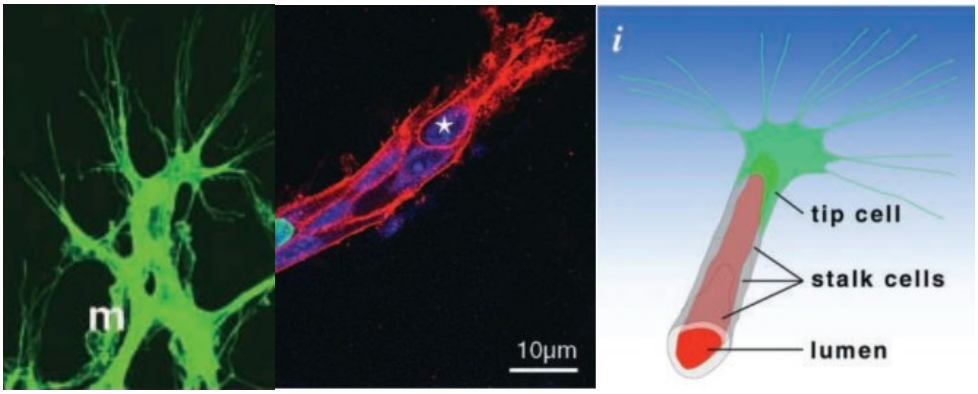


(a) (b) (c)

Figure 6.4. Illustration of the structure of sprouting [16]

Filopodia, tip and stalk are in a queue. Filopodia extends forward from the tip cell. The stalk cell is behind the tip cell，in (a) the mark m is macrophage, in (b) the mark star (*) represents tip cell [16].

The intercellular communication occurs through the field. The local and global concentrations change the agent state inside. The reaction diffusion equations govern the evolution of VEGF, MDE, and ECM. The PDEs we described above allow agents to determine which characters will be performed.

Based on Figure 6.4, we designed the sprouting model. The tip extends filopodia in front and the stalk follows the tip. Proliferation is confined by the stalk cells, and tip cells do not proliferate but can migrate [16]. MDE is secreted by the agent at the tip state and this degrades the ECM. The generation rate of MDE and the degrading rate of ECM are based on the following two equations described in Chapter 4:

$$\frac{\partial m}{\partial t} = \alpha n + \varepsilon \nabla^2 m - \nu m \qquad (4.21)$$

$$\frac{\partial M}{\partial t} = -\omega M m \qquad (4.22)$$

where n represents the tip cell density, m represents the activity of MDE, M represents the density of ECM, the coefficients are described in detail in section 4.3.2. The rate of MDE produced by the tip cell is proportional to the tip cell. The generated MDE is diffused toward its environment, based on Fick-Diffusion law. The decay of MDE also takes place. M represents the ECM, and the rate of degradation is proportional to the MDE generated. The proliferation and migration of cells require sufficient room; if there are too many cells, there will not be enough room for the cell to move and proliferate. By accounting for the empty lattices around it, the cell determines where to implement migration or proliferation. If there is not enough room left, the ability of proliferation and motility will be affected. According to Anderson and Chaplain's work [6-8, 152] on molecular layers, the soluble chemical substance VEGF concentrations are solved at each time step. The agent entities are updated in a random order. At every time step of the simulation, each agent is updated according to the agent behaviour flowchart in Figure 6.5, as follows:

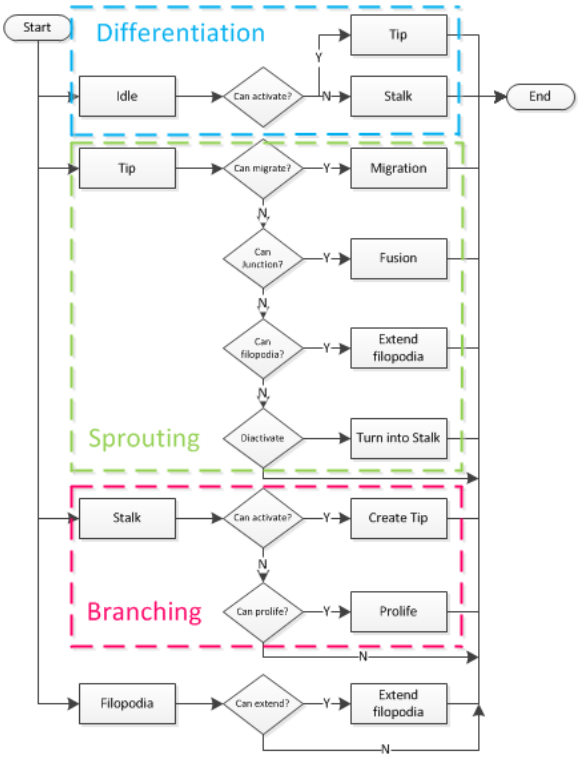


Figure 6.5 Schematic cell behaviour flowchart overview

A cellular level basic transition of agent decisions for both tip and stalk phenotype selection in sprouting and branching for every time step.

Our tumour-induced angiogenesis model was designed on three scales: at the tissue level such as branching and sprouting, at the cellular level such as the tip and stalk selection, and at the molecular level, including VEGF, MDE diffusion, and ECM density. The cellular level flow chart shown in Figure 6.5 represents agent decisions for both tip and stalk cells behaviours at each time step.

We use a two-dimensional space to represent the simulation domain in a grid net of 200×200. The location of the ECs is determined by a set of coordinates (x, y), considering each EC occupying every other lattice point. The MDE is secreted by each tip cell which takes a lattice at the front position and degrades the local ECM. The soluble VEGF secreted

by the tumour engages in the regulatory mechanism of tip and stalk state selection. We assume VEGF-A diffuses based on Fick's law. Hence, its concentration is different at different positions, forming a gradient stretch from the side of the tumour to the parent vessel.

Rules for behaviours were created from the literature [5, 30, 142-144, 202-206], relating each cell action to its local concentrations of VEGF physical properties. We systematically assume the way cells interact with one another. We introduce the background for how we approached the model and characterized cell behaviours. After identifying cell behaviours, we defined the rules computationally and described how the rules interact with each other, as shown in Figure 6.5.

The position of tip agents at the front edge of the capillary network is consistent with the position of the ECs simulated from Eq. (4.18). The consistency of both is realised by the iteration simulation between the continuum and discrete model. At every time step of the simulation, each agent position is updated according to the ECs position in the simulation of continuum model.

The tip cells are in front of the capillary network. They generate filopodia which probes into the ECM in front of it to check the gradient of VEGF-A. The filopodia generated by the tip determines the route of migration by sensing the VEGF gradient and local ECM density. Based on the filopodia role and function discussed in section 2.3.2, we set the agent at the filopodia state's extending direction, depending on VEGF and ECM density at the microenvironment around itself. As shown in Figure 6.6 (a), the agent at the filopodia state makes its selection of extending destination based on the comparison of both VEGF and ECM density weight from the seven empty grids (white) around it.

### 6.5.3 Sprouting

Sprouting is the most important process in angiogenesis. During sprouting, this very complicated procedure involves the specification of tip and stalk phenotype from ECs, the migration of tip cells, the proliferation of stalk cells, and the determination of the approaching route, which is sensed and led by filopodia. Filopodia are generated by the tip and extend into the ECM. We designed a model which is schematically presented in Figure 5.4 to elucidate the procedure of sprouting. Here, filopodia, tip, and stalk are designed in the agents and marked in green, blue, and red respectively. The continuous development of sprouting finally forms a capillary vessel in which the only tip is at the spearhead point of the vessel, and following the tip, the stalks are joined to form the whole body of the vessel.

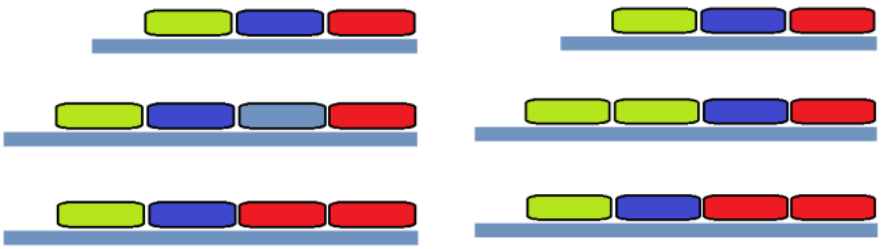

(a) (b)

Figure 6.6 Illustration of cell movements.

Cell movements are illustrated in a 2D domain and represented by rules in the model. The tip cell movement is represented by a blue grid. The filopodia is represented by a green grid. The stalk cell is represented by a red grid. The grey grid represents the stalk cell activated by VEGF-A. (a) represents the migration of tip cell directed by its filopodia

(green). The stalk cell (red) proliferates and generates a cell (grey) in front of itself in an idle state. The tip cell triggers the VEGF/Notch signalling to make the cell adjacent behind it and turn into stalk. (b) represents the extension of the filopodia.

The extending direction of the filopodia is based on VEGF and ECM density at the microenvironment around itself. The grid selected is by the comparing the magnitude of introducing factor, which is determined by both VEGF and ECM density. The magnitude takes both in individual weight. The procedure is shown in Figure 6.7 (a), in which the seven grids in white represent the possibility of choice, and the grid in green represents the agent in filopodia state

The transition limitation conditions are as follows: (a) there is VEGF adjacent to it; (b) there is no agent at tip state adjacent to it. The agent in the tip state expresses Dll4. Dll4 influences the adjacent grids in which the Notch becomes high in expression. Once the conditions described above are satisfied, the agent in the idle state turns into the tip state. Once an agent becomes tip, induced by its local VEGF, it generates an agent in filopodia state which probes into the grid nearby. After the time interval it becomes mature and turns into tip state (blue). The grid occupied by the agent in the tip state turns into the agent in the stalk state (red), as shown in Figure 6.6. The change happens based on the comparison of Notch signalling.

The tip cell migration is guided and pulled by its filopodia, which extend into the ECM and adhesion with the astrocyte. The moving is sensed by the stalk cell right behind it, then the stalk triggers the proliferation and produces a new cell in front of itself, so the new cell

partly has some tip cell characteristics and engages in the battle for the tip [16].

### 6.5.4 Branching

Branching is a special state of sprouting. When a stalk in the vessel is activated due to the change of VEGF and Notch signals and thereby obtains the tip characteristic, it begins to sprout. This procedure continuously forms a new vessel. From this point, a new branch is formed. We designed the agents to elucidate the procedure schematically in Figure 6.7 (b), in which we can observe that the branching occurs from the point where a stalk is activated. The grids in white around the tip represent the possible directions for the new sprouting to develop.

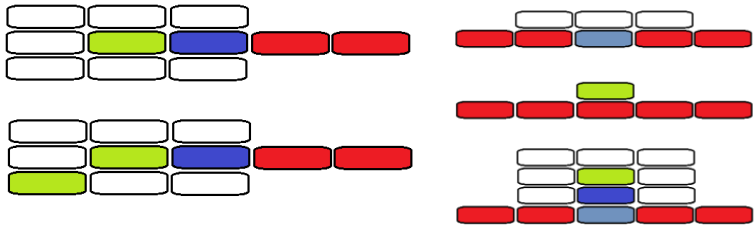

(a) (b)

Figure 6.7 The schematic design of the agent-based model: sprouting and branching

In Figure 6.7, the sprouting and branching of angiogenesis is illustrated in a 2D grid and ruled by the rules set in the model. The tip cell is represented by a blue grid. The filopodia are represented by a green grid. The stalk cell is represented by a red grid. The grey cell represents the cell proliferated by the stalk behind it. The white grid represents the possible directions in which the filopodia could extend. (a) represents the extension of filopodia

(green) during the sprouting procedure. Filopodia will extend to the empty grid nearby (white). (b) represents the branching procedure when one of the stalk cells is in activated state (grey) and it proliferates and generates a cell (blue). The blue one is a tip because there are no cells in front of it. The tip cells extend filopodia (green), which extend into the empty grid nearby (white), and they begin to sprout when a new sprouting occurs and a new branch is formed. The process of sprouting and its special state branching iterates continuously, leading to the formation of a capillary network, which is the mechanism of angiogenesis.

## 6.6 Simulation and discussion

### 6.6.1 Solution of the ODEs using the Euler method and ABM

We discretized Eq. (6.13) and Eq. (6.14) as follows and used the Euler method to solve the initial valued ODEs. The solution is to discretize the time scale and take the first existing value to calculate the second value, and then to use the second value to calculate the third value. This iterates, and finally a solution of ODEs can be obtained. This is the famous Euler method. In our model, we used two ways to solve the regulatory model. One is to use the Euler method to solve the ODEs in Eq. (6.13) and Eq. (6.14) and obtain the smooth curves which were used as the criteria values shown in Figure 5.2; the other way is to use the Euler method combined with the ABM to solve Eq. (6.13), Eq. (6.14), Eq. (6.15), and Eq. (6.16).

Our solution is described as follows. We firstly discretized the time scale then used the Euler method and ABM alternatively at every time step. By using the first set of values of Eq. (6.13) and Eq. (6.14) to calculate the second set of values, we then used ABM to compare the set of second values with the criteria values and made judgments and decisions. Next, we triggered the solution to Eq. (6.14) and Eq. (6.15), and triggered the inhibitors $I_1$ and $I_2$, leading to the curves $P_1$ and $P_2$ oscillating in the period. In this way, we realised the modelling of the VEGF/Notch regulatory mechanism.

$$P_1^{T+1} = P_1^T + \Delta t \left( \frac{v_{max_1} \left( S_0 - P_1^T \right)}{\left( S_0 - P_1^T \right) + K_M \left( 1 + \frac{I_1^T}{k_{i_1}} \right)} - k_1 P_1^T \right) \tag{6.17}$$

$$P_2^{T+1} = P_2^T + \Delta t \left( \frac{v_{max_2} P_1^T}{P_1^T + K_M \left( 1 + \frac{I_2^T}{k_{i_2}} \right)} - k_2 P_2^T \right) \tag{6.18}$$

Here is the description of how the state of the system changes during the simulations for each of the variables of the model. The state at $t = (T + 1)\Delta t$ is obtained from that at $t = T\Delta t$, where $\Delta t$ is the local cell time step and $T$ is an integer index. The superscripts $T$ and $T + 1$ here indicate the values at $t = T\Delta t$ and $t = (T + 1)\Delta t$ respectively.

The simulation time $t$ is then incremented by $\Delta t$, and the cycle is repeated using the newly calculated $P_1$ and $P_2$ concentrations. $I_1$ and $I_2$ are then updated based on the regulation. The solution of Eq. (6.17) and Eq. (6.18) is shown as follows:

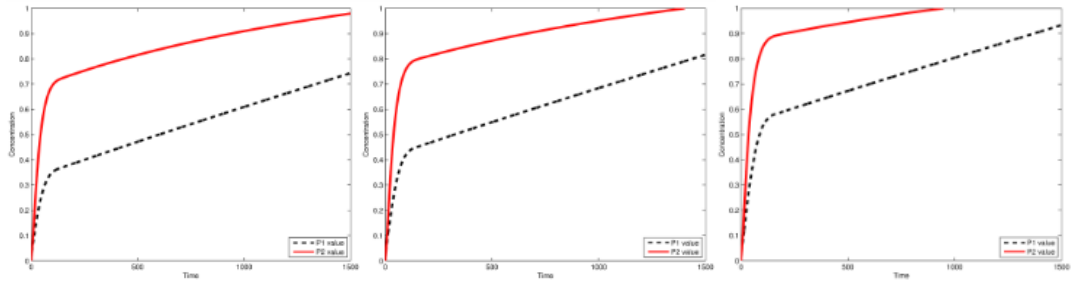

(a) (b) (c)

Figure 6.8 The results of the solutions to Eq. (6.17) and Eq. (6.18)

The dashed line represents the $P_2$ curve; the solid line represents the $P_1$ curve; (a), (b) and (c) represent the results of the solution at $S_0 = 0.2$, $S_0 = 0.4$, $S_0 = 0.6$ respectively

From Figure 6.8, the two curves are the results of the solution of Eq. (6.17) and Eq. (6.18). The values of $P_1$ and $P_2$ depend on the local VEGF concentration expression, which is denoted as $S_0$. From the three figures, we can observe that both the $P_1$ curve and $P_2$ curve are based on the local $S_0$. When $S_0$ increases from $0.2$ to $0.6$, the $P_1$ and $P_2$ values increase slightly.

Eq. (6.17) is in the upstream position and Eq. (6.18) is in the downstream position. Eq. (6.17) positively regulates Eq. (6.18). As the two equations are not negatively feedback regulated, the solution results show that the two curves appear continuously and smoothly, and increase in the same trend. At the very beginning, the $P_1$ value increases fast, which promotes the $P_2$ value to increase fast spontaneously. Then, the $P_1$ and $P_2$ values increase gradually. Both curves appear lower in slope with time elapse, and they dynamically change with time. Dynamic change criteria were created to compare with the values regulated instantaneously. Hence, we used the solution results of Eq. (6.17) and Eq. (6.18) as the local criteria which change dynamically at different positions.

### 6.6.2 Regulation of sprouting

We used the solution of Eq. (6.13) and Eq. (6.14) which exhibit two smooth curves as dynamic criteria. Figure 6.9 illustrates that the solution of the model comprised of Eq. (6.13), Eq. (6.14), Eq. (6.15), and Eq. (6.16) exhibits two oscillating curves $P_1$ and $P_2$. The $P_1$ and $P_2$ curves regulated by VEGF and Notch signalling oscillate around their own criteria curves ($C_1$ and $C_2$). Both the $P_1$ and $P_2$ values are updated based on their state and the regulatory results.

The curve represented in the solid red line is based on the result solved by Eq. (6.14). The curve represented in the dashed black line is based on the result solved by Eq. (6.13). Both curves are used as criteria in the later analysis. The solid green line with star markers represents the $P_1$ curve, which denotes the VEGF signalling. The dashed blue line with cross markers represents the $P_2$ curve which denotes the Notch signalling. Both curves are the solution to the regulatory model shown in Figure 6.9.

From Figure 6.9, the $P_1$ and $P_2$ values fluctuate during the procedure. We took the critical $C_1$ value and the critical $C_2$ value as the criteria respectively, by comparison with the relative magnitude. There are two different compositions:

$$P_1 \geq C_1 \quad \text{and} \quad P_2 < C_2 \tag{6.19}$$

$$P_1 \leq C_1 \quad \text{and} \quad P_2 > C_2 \tag{6.20}$$

We define that $P_1 > C_1$ represents high VEGF signalling and high Dll4; $P_1 < C_1$ represents low VEGF signalling and low Dll4; $P_2 > C_2$ represents high Notch signalling; $P_2 < C_2$ represents low Notch signalling.

ECs are specified into tip at high VEGF signalling, high Dll4 and low Notch signalling. In our model, once ECs satisfy the condition of Eq. (6.19), they will be specified into a tip. In the same way, high Notch and low VEGF signalling specify as a stalk. In our model, once ECs satisfy the condition of Eq. (6.20), they will be specified into the stalk phenotype. Hence, we define that the cell satisfying Eq. (6.19) is the tip cell, and the cell satisfying Eq. (6.20) is the stalk cell.

According to the theoretical analysis above, we simulated the regulatory model in Figure 6.3, in which the adjacent cells regulate each other during sprouting angiogenesis, making the $P_1$ and $P_2$ values of the cells fluctuate. The results are shown in Figure 6.9 1, in which both $P_1$ and $P_2$ values fluctuate around their own critical standard values respectively. The $P_1$ curve (the dashed blue line with cross markers) fluctuates around the $C_1$ curve (the solid red line) dynamically. The $P_2$ curve (the solid green line with star markers) fluctuates around the $C_2$ curve (the dashed black line) dynamically. The fluctuation is influenced by the adjacent cell sending a Notch signal. Thus, we divided the cell cycle into three different stages. Stage *I* (from a to b) is of tip characteristics (hereafter called tip); stage II (from b to c) is the transition state; and stage III (after c) is the stalk stage.

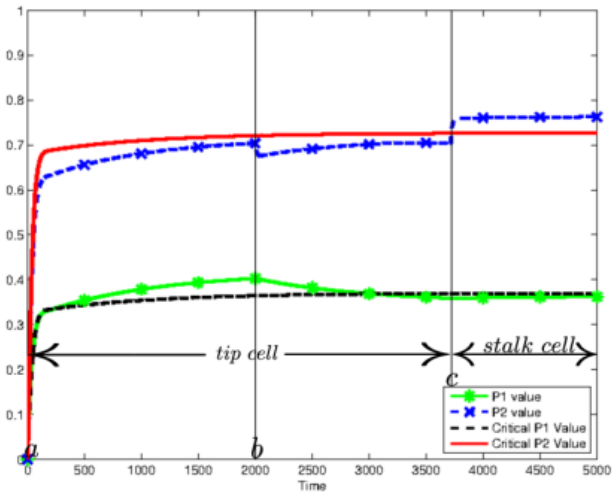


Figure 6.9 1Regulation procedure of sprouting analysis

Stage I (from a to b) is the transition state. Stage II (from b to c) is the sprouting state. Stage III (after c) is the stalk state. Tip cells include Stage I and II.

We divided the curve into two zones (tip and stalk), as shown in Figure 6.9. The cell differentiation is triggered by the successful combination of VEGF and VEGFR. This enzyme catalysed combination generates the VEGF signalling. The VEGF signalling promotes the generation of Dll4 which promotes the increase of Notch signalling in the cell shown as $\mathrm{Arrow}_1$. This is an up-regulation mechanism which can be observed in the range from point a to b where $P_1$ and $P_2$ increase at the same trend. When the Notch signalling begins to be up-regulated by the front cell through high Dll4, it down-regulates the VEGF signalling by controlling the expression of $I_1$ which makes the VEGF lower. This can be observed in the range from point b to c where $P_2$ increases but $P_1$ decreases in the opposite trend shown as $\mathrm{Arrow}_2$. Both of $\mathrm{Arrow}_1$ and $\mathrm{Arrow}_2$ show the VEGF-VEGFR-Dll4-Notch-VEGFR feedback loop regulation mechanism in the same EC. Between the cells, the Dll4 on the surface of the front cell reacts with the Notch receptor on

the surface of the back cell to promote its Notch signalling which is an up-regulation. This regulation is shown in $\mathrm{Arrow}_3$ where VEGF signalling in the front cell simultaneously increases the Notch signalling in the back cell in the same trend. From Figure 6.10, we can observe that when the front cell $P_1$ value increases, the $P_2$ value in the back cell increases simultaneously in the same trend in the range from point b to c. The lower VEGF signalling in the back cell regulates the Notch signalling in the front cell, shown as $\mathrm{Arrow}_4$, indicating a trend to make the Notch lower in the front cell in the range after point c. Both the VEGF and Notch signal regulate to promote the sprouting of the new cell.

Through the period of tip, $P_1 > C_1$ represents a higher VEGF signalling, and a higher Dll4 is generated. $P_2 < C_2$ means that the Notch is modulated by Jagged1 and a lower Notch signalling is generated. Thus, when $P_1 > C_1$ and $P_2 < C_2$, it is in the tip cell stage. $P_1 < C_1$ represents a lower VEGF signalling and $P_2 > C_2$ represents a higher Notch generated. Accordingly, when $P_1 < C_1$ and $P_2 > C_2$, it is in the stalk cell stage.

At the inference of VEGF signalling, when the front cell begins to migrate, it generates high Notch signalling back to the back cell. During the procedure, Notch signalling triggers the reaction of co-receptors such as VEGFR1, Nrarp etc., which are denoted as the competitive inhibitor $I_1$. This is a competitive inhibition which makes the $P_1$ curve turn down (at point b).

According to the literature, the Notch receptors can be combined by either Dll4 or Jagged1, whereas Dll4 has a competitive relationship with Jagged1. When Dll4 wins over the combination with the Notch receptors, the Notch signalling is enhanced; when Jagged1 wins over the combination with the Notch receptors, the Notch signalling is weakened [4]. In our model, when the $P_1$ curve intersects with the $C_1$ curve (at the point c), Jagged1 is

weakened by the feedback mechanism, leading to the enhancement of the Notch signalling. The reaction is catalysed by glycosyltranferase (Fringe) [4]. The magnitude of inhibition is denoted as $I_2$.

From Figure 6.10, we can observe that after point c, $P_2 > C_2$ and $P_1 < C_1$. This means that the cell turns into the stalk cell state. After the tip cell receives low Notch signalling, the front cell expresses high VEGFR2 and Nrp1, and makes itself become a tip cell.

From Figure 6.10, we can observe that the $P_1$ curve turns down slightly (at b point). This is because the cell takes the signal from the cell in front of it and triggers their cell inhibitor $I_1$. In the $P_1$ curve, the magnitude of $I_1$ depends on competitive coreceptors. The higher inhibitor $I_1$makes the $P_1$ curve turn down more significantly.

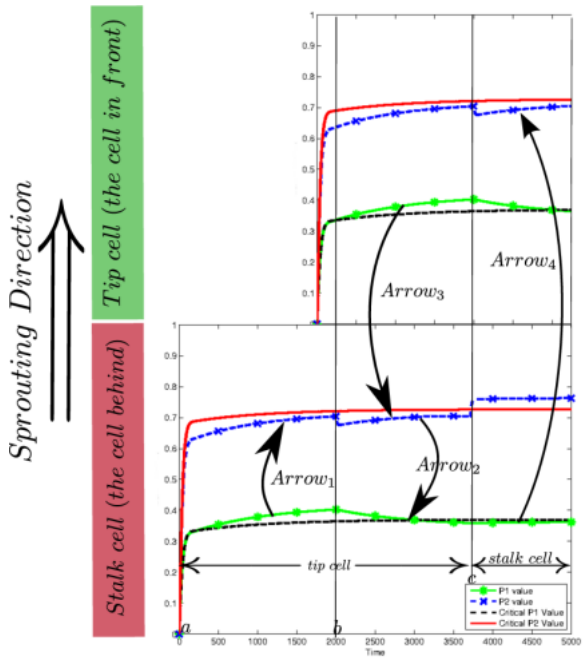


Figure 6.10 Regulation procedure of sprouting angiogenesis based on the VEGF signalling pathway and Notch signalling pathway

Stage I (from a to b) shows the up-regulation of VEGF to Notch inside the cell. Stage II (from b to c) shows the down-regulation of Notch to VEGF inside the cell and the

up-regulation of VEGF to Notch. Stage III (after c) shows the differentiation of the cell.

Our model delineates a molecular pathway of tip-stalk cell selection that is controlled by the interplay of three ligands, VEGF, Dll4 and Jagged1. According to the description above, the Notch changes and promotes the differentiation of tip and stalk. This result is produced by the change of Notch signalling co-expressed by Jagged1, which leads to the formation of a tip or stalk cell.

Being suppressed, the $P_1$ decreases. When the $P_1$ curve intersects with the $C_1$ curve (at point c), it triggers the release of inhibitor Jagged1, which competitively binds with the Notch receptor and increases the Notch activity. This makes the cell move into the stalk stage. At the same time, the front cell is regulated by the back cell which is low in Notch and high in VEGF. Thereby, the regulatory mechanism enhances the differentiation between tip cell in front and stalk cell behind.

Figure 6.10 shows the sprouting procedure regulated by VEGF signalling pathway and Notch signalling pathway. The VEGF and Notch signalling pathways cooperate tightly to specify and balance the tip and stalk cells between ECs that constitute the sprouts. Notch signalling acts in a negative feedback loop with VEGF signalling during sprouting angiogenesis.

### 6.6.3 Regulation of branching

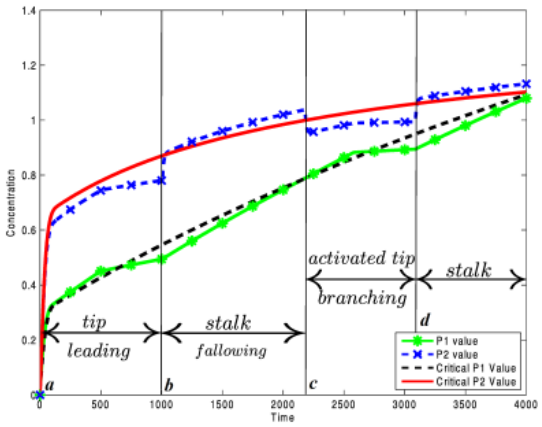


Figure 6.11 Regulation procedure of sprouting angiogenesis based on the VEGF signalling pathway and Notch signalling pathway.

Stage I (from a to b) is the tip cell. Stage II (from b to c) is the stalk cell. Stage III (from c to d) is the activated cell with tip characteristic. Stage IV (after d) is the stalk cell.

For the mechanism of regulation during the branching of angiogenesis, we assume that when a stalk cell in the vessel is activated, it obtains the characteristic of a tip cell, which can sprout. When a sprout is formed and a new vessel is successfully developed from the cell, a new branch is formed and then emerges from this point. This is the procedure of branching during angiogenesis.

We assume that in a stalk cell, the binding of co-receptors (VEGFR1, Nrp1, Nrp2, etc.) with VEGF weakens with the time elapse. This increases the reaction of VEGF and VEGFR2 to enhance the VEGF signalling. It is shown in our model that when the competitive inhibitor $I_1$ weakens, the VEGF signalling increases. The curve $P_1$ rises and finally intersects with curve $C_1$, this leadsto $P_1 > C_1$, so high VEGF signalling appears at

point c, shown in Figure 6.11. At the same time Notch changes with the expression of Jagged1. This makes the Notch signalling decrease and $P_2 < C_2$, so low Notch signalling appears. High VEGF and low Notch signalling appear simultaneously, satisfying the condition of the tip cell. Thus, the stalk cell is activated and obtains the characteristic of the tip cell. This result is consistent with the phenomenon that tip cells are at intervals with stalk cells, which is called 'salt and pepper'. From this point, the activated cell begins to sprout and form a new branch. The regulation procedure described above is shown in Figure 6.11.

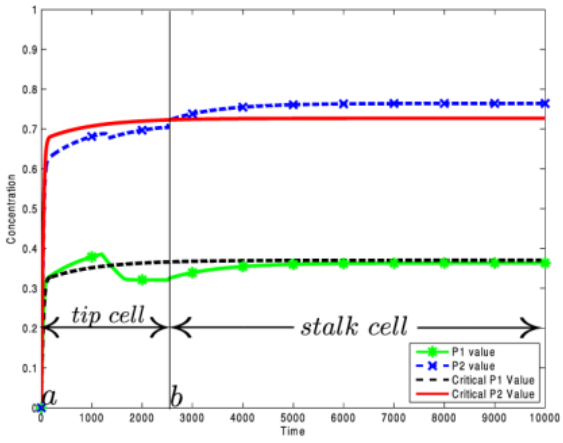


Figure 6.12 Regulation procedure of sprouting angiogenesis based on the VEGF signalling pathway and Notch signalling pathway

Stage I (from a to b) is the tip cell. Stage II (from b to c) is the stalk cell.

Based on the assumption described above, only if a stalk cell in the vessel is activated can it obtain the characteristic of a tip cell. The cell has the ability to sprout and develop a new branching. However, if there is no stalk cell activated, no cell will obtain the characteristic of tip cells and there will not be a new sprout formed. The angiogenesis finally develops

into a single vessel with no branching at all.

In a stalk cell, the binding of co-receptors (VEGFR1, Nrp1, Nrp2, etc.) with VEGF weakens with the time elapse. This increases the reaction of VEGF and VEGFR2 to enhance the VEGF signalling. It is shown in our model that the competitive inhibitor $I_1$ weakens and the VEGF signalling increases near the point b. The curve $P_1$ rises, but is never high enough to intersect and become higher than curve $C_1$. The VEGF signalling remains low and maintains $P_1 < C_1$. Under this condition, the VEGF signalling is not high enough to trigger the Notch. The Notch signalling keeps high and maintains $P_2 > C_2$. This state continuously satisfies the condition of the stalk cell, and thus it will never be activated and branching (extra sprouting beside the vessel) will never appear. This procedure is described in Figure 6.12.

### 6.6.4 Simulation of angiogenesis

According to the analysis described above, in this section we are going to implement the simulation of angiogenesis based on the regulation of VEGF and Notch signalling pathways. Under the regulation, ECs are specified into tip and stalk cells, respectively. This procedure forms the sprouting at the spearhead of the vessel and makes the vessel grow forward continuously. If the condition of the tip is satisfied in a stalk, it will be activated, obtain the tip cell characteristic, and begin to sprout, forming a new branch. In this way, a capillary network is formed.

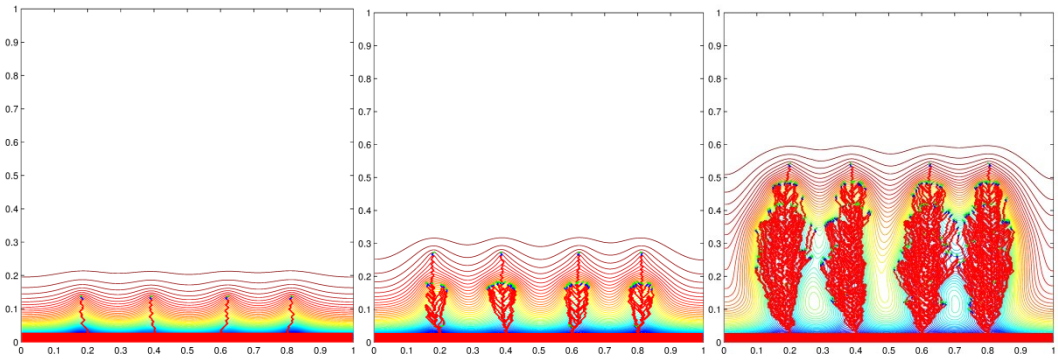

(a) (b) (c)

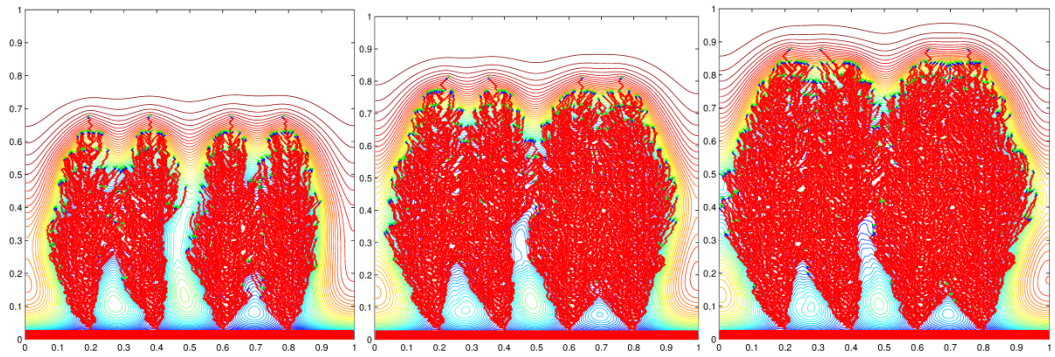

(d) (e) (f)

Figure 6.13 Spatiotemporal evolution of the capillary network using the agent-based method to discretize the continuum model under the regulation of VEGF/North signalling pathways

The background formed with contour lines and colours shows the ECM density degraded by the MDE secreted from tip cells.

Figure 6.13 shows the simulated vessels regulated by the VEGF and Notch feedback regulatory mechanism. The regulation process is shown in Figure 6.11, from which we can observe the periodic alternation of tips and stalks, governed by VEGF and Notch signalling. The simulation results come out under the regulation process shown in Figure 6.13.

Sprouting is regulated by VEGF and Notch in the specification of tip and stalk, which forms vessels, whereas the branching that appears at intervals is the result of the tip and stalk in the so called ‘salt and pepper’ pattern. New branches are formed from the tips and finally result in the generation of a capillary network.

The background formed with contour lines round the tips represents ECM density degraded by the MDE secreted by the tip cells. The ECM density is different around the location of the tips. At each spearhead, we can observe three colours of grids, including green, blue, and red. The green ones represent filopodia tips, which are located at the front. Following the green grids are the blue grids representing the tip cells. The red ones follow the tip and represent the stalk cells.

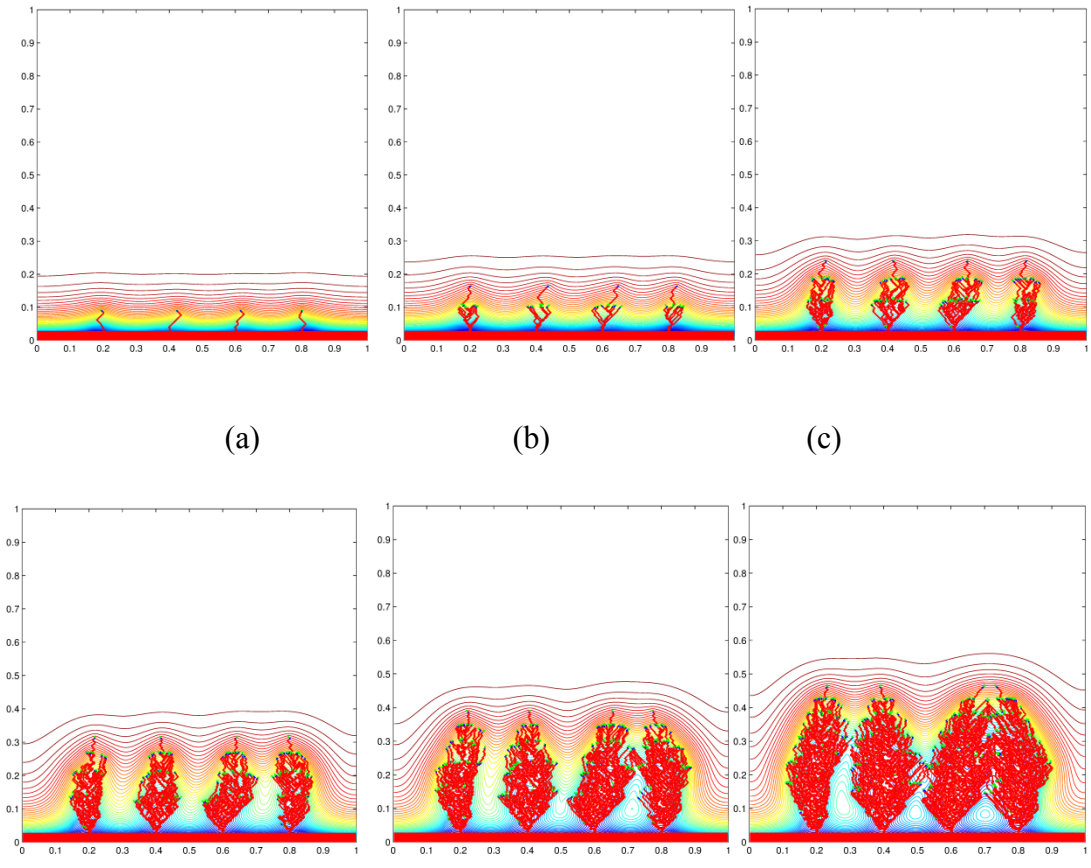

(a) (b) (c)

(d) (e) (f)

Figure 6.14 Spatiotemporal evolution of capillary network with agent-based method to

discretize the continuum model under the regulation of VEGF/North signalling pathways

The background formed with contour lines and colours shows the ECM density degraded by the MDE secreted from ECs.

Figure 6.14 shows the simulated vessels regulated by the VEGF and Notch feedback regulatory mechanism. The regulation process is shown in Figure 6.11, from which we can observe the periodic alternation of tips and stalks, which are governed by VEGF and Notch signalling. The simulation results come out under the regulation process shown in Figure 6.11, in which VEGF and Notch cooperate throughout the simulation. Tips and stalks are at intervals, and are called 'salt and pepper.' The branches formed by tips finally result in the generation of a capillary network. In this simulation, we changed the magnitude of $I_1$ and $I_2$ in Eq. (6.13) and Eq. (6.14), leading to the extension of regulation periods. The simulation results of angiogenesis appear denser in net and slower in growth.

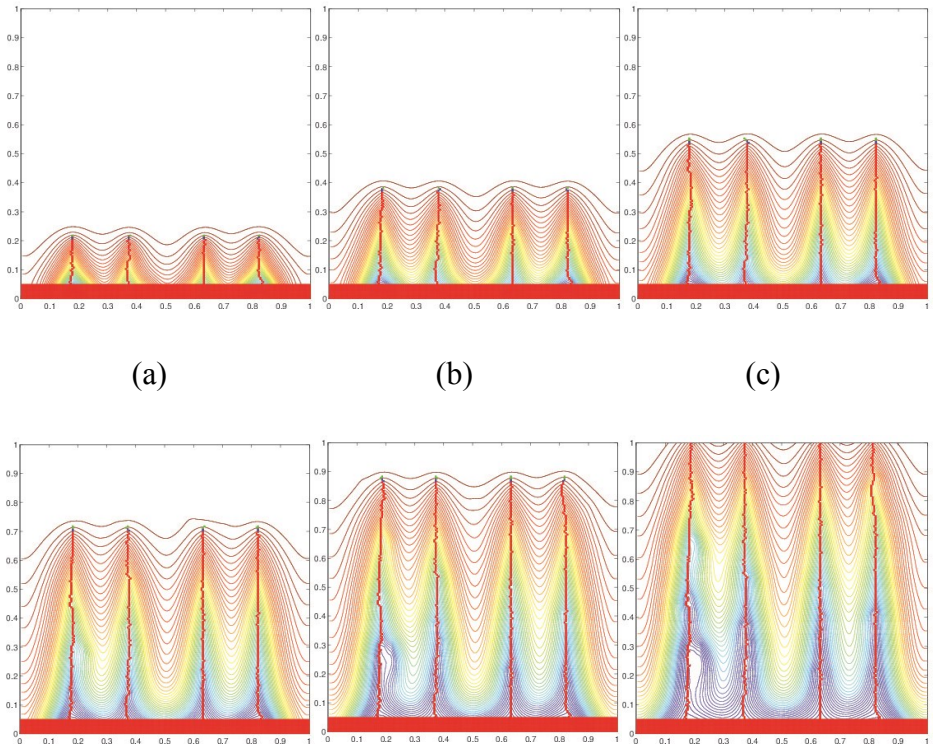

(a) (b) (c)

(d) (e) (f)

Figure 6.15 Spatiotemporal evolution of capillary network with agent-based method to discretize the continuum model under the regulation of VEGF/North signalling pathways in which Notch signalling is overexpressed

Figure 6.15 shows the simulated vessels overexpressed in Notch. The simulation results come out under the regulation process shown in Figure 6.12 in which Notch is overexpressed ($P_2 > C_2$) throughout the simulation. Only a tip cell emerges at the very beginning, then sprouts and becomes a vessel without any branches during the angiogenesis procedure. Here, VEGF and Notch satisfy the condition of stalk cells. No more tip cells emerge and the vessels appear like snail-trailing. The simulation results show no branches at all.

From the simulation results, we can see the regulatory mechanism works well. The results

are consistent with the bio-clues and bio-theory of regulation, as discussed in section 2.3.4.1, section 2.3.4.2, and section 2.3.5.1. The results arise from the complicated bio-system angiogenesis process which involves many scales solved by the integration of ODE, PDE, and ABM.

## 6.7 Conclusion

As the VEGF and Dll4/Notch signalling regulatory mechanism determines the specification of tip and stalk phenotype from ECs leading to the growth of sprouting [4], in this chapter we presented how we integrated enzymatic catalysed competitive ODEs model generating VEGF and Notch signals with ABM to simulate sprouting. Our model successfully demonstrates this regulatory mechanism, which has rarely been simulated in the current computational modelling of angiogenesis. Our simulation results are similar to the published biological report [4]. Thus, to a certain extent, our simulation results support the VEGF and Notch signalling theory from the computational viewpoint. In addition, our simulation results reveal that branching is just a special state of sprouting; it emerges at the point where a stalk is activated due to the change of VEGF and Dll4/Notch signals, and then turns into tip to begin a new sprouting. To conclude, the model we developed may be a useful tool to reveal the secret of angiogenesis. We will continue our research by improving the model through including an artificial intelligence method, especially a neuro network, which will positively promote the development of the model to decipher tumour-induced angiogenesis.

# Chapter 7. Conclusion

As the final chapter, it firstly provides an overview of the research. Then it outlines the research's original contribution to the computational modelling of complex biological systems. Reflections on the research and future studies are provided as well.

## 7.1 Overview of the research

Tumour-induced angiogenesis is a crucial step in the development of tumours. Endothelial cell (ECs) migration is the vital step in tumour-induced angiogenesis. EC migration is influenced by both tumour angiogenic factor (TAF) and fibronectin concentration gradient. In Chapter 4, we began by improving Anderson and Chaplain's model by introducing proliferation terms for ECs, the degradation of ECM, and fibronectin initial condition, thus establishing the mathematical model describing EC migration during angiogenesis. The simulation results clearly demonstrate the process of the migration of ECs, guided by chemotaxis and haptotaxis from the pre-existing vessel to the tumour.

Based on bio-clues that tumour invasion may promote production of fibronectin, we developed a mathematical model in partial different equations (PDEs) by altering TAF and fibronectin. The simulation result shows that the migration of ECs can be accelerated when both the TAF and fibronectin concentration gradients are in the same direction. This means angiogenesis can be synthetically promoted by both chemotaxis and haptotaxis simultaneously. Consensus theory states that angiogenesis supplies oxygen and nutrients to promote tumour development. By linking the relationship of tumour invasion and angiogenesis, we propose that there is a possible mechanism by which both invasion and angiogenesis promote each other to make the tumour develop faster, becoming more harmful for some subgroups of tumours.

In Chapter 5, based on the model developed in Chapter 4, we further developed the mathematical model to simulate the effect of tumour cytotoxic factor, including the

immune system and drugs delivered through the vessels formed during angiogenesis in the development of a tumour. The simulation results reveal that the influence of tumour cytotoxic factor can make the tumour regress or develop. We designed two kinds of tumour load, both large and small, in three situations. The first was the large tumour load regression using the immune tumour cytotoxic factor and then recurrence. The second was the large tumour load regression using the immune tumour cytotoxic factor and a tumour cytotoxic drug. The synthesis effects of both immune factor and drugs make the tumour regress significantly without recurrence in the simulation range. The third was a small tumour load clearance using the immune tumour cytotoxic factor.

In Chapter 6, we established a hybrid ODE model describing the VEGF and Notch signalling pathway in regulating vessel sprouting. Sprouting is the fundamental process of angiogenesis. During sprouting, ECs in the nascent sprout are specified into two distinct cellular phenotypes, called tip and stalk cells. Both are endowed with specialized functions. The fate of ECs is determined by VEGF and Notch signalling. The VEGF and Notch signalling regulatory mechanism engage in implicated crosstalk to balance tip and stalk cell differentiation and to regulate directed tip cell migration and stalk cell proliferation. In this way, the sprouting occurs and finally develops angiogenesis, which is the creation of new blood vessels from the parent vasculature [38]. Hence, VEGF and Notch signalling regulatory mechanism is vital in angiogenesis [4].

Over the past decade, VEGF and Notch signalling regulatory mechanisms have become a research focus in biology. Its computational modelling is still rare, leaving a wide gap between biology and computer engineering. We focus on developing a computational approach to decipher the VEGF and Notch signalling regulatory mechanism in order to

perceive the micro procedure of angiogenesis to provide direction for researchers in the field of angiogenesis.

In this thesis, we have presented a hybrid model to describe EC behaviours under the control of a VEGF/Notch signalling pathway. We first established a two dimensional spatiotemporal mathematical model describing the process of tumour-induced angiogenesis, and then developed the model further by involving the tumour cytotoxic factor to simulate the tumour regression. Based on the mathematical models, we finally developed the hybrid model exploring the VEGF/Notch signalling pathway regulatory mechanism in the endothelial cell differentiation, tip cell migration, stalk cell proliferation, nascent sprouting, and the emergence of branching. It is hoped that the results will assist researchers in both the experimental and theoretical angiogenesis communities in a better understanding of the complexity, and enable the identification of the fundamental principles of angiogenesis.

To realise methods, we used ordinary differential equations (ODEs) to describe the positive regulation and negative feedback signal transduction processes, nonlinear partial differential equations (PDEs) to describe the continuum field, and agent-based modelling (ABM) to discretise the model. Hence, the study enriches knowledge of modelling and provides a good example of integrating complicated and innovative modelling approaches for computer scientists in the relevant field.

## 7.2 Contributions

We have summarised the major contributions of the developed models in the six points

below, providing evidence for the thesis's original contribution to knowledge.

1) We developed a mathematical model in PDEs to simulate endothelial tip cell migration during angiogenesis influenced by chemotactic factor (e. g. TAF) and by haptotactic factor (e. g. fibronectin). The simulation results show that both chemotaxis and haptotaxis have an influence on the migration of tip cells, and their influence depends on the gradient and direction of both TAF and fibronectin. If both gradients are in the same direction, the migration of the tip cells can be promoted; if both gradients are in the opposite direction, the migration of tip cells can be offset. The simulation results imply a possible malignant mechanism for some subgroups of tumour as a potential research direction, and we assume the invasion of tumour and angiogenesis may promote each other.

2) Considering the phenomenon of vessel density becoming higher towards the tumour, described as "brush border" in the literature, we involved the term proliferation of tip cells in the mathematical model, which makes the model more reasonable. The ECM degradation by the endothelial tip cells and secreted MDE was also involved in the model. The simulation results show that the degradation degree of ECM is influenced by the migration velocity of the endothelial tip cells. The results indicate that the different migration velocities of tip cells can have different impacts on the ECM degradation and make the ECM vary in composition, and even in the direction of collagen fibre, according to the phenomenon of ECM reorganization. In this way, we have improved the breakthrough models of Anderson et al. in tumour-induced angiogenesis. The

results also indicate some research directions, such as how the ECM composition influences the migration of tip cells and how the tip cells influence the ECM reorganization during angiogenesis.

3) Based on the PDE model, we developed the enzymatic catalysed regulating model in the form of hybrid ODEs to simulate the sprouting regulated by VEGF/Notch signalling. In the model, sprouting was realised based on the specification of tip and stalk from ECs, which is dependent on the conditions of tip and stalk phenotype states, by comparing it with the magnitude of VEGF and Notch signalling. With the help of ABM to discretise the model, our simulation reveals that branching is just a special state of sprouting. When the VEGF and Notch inside a stalk change and satisfy the conditions of tip, the stalk is activated, obtains tip characteristics, and begins to sprout and form a new branch. In this way, this model can simulate EC differentiation, migration, proliferation, tip/stalk specification, sprouting, and branching behaviours based on the VEGF/Notch regulatory mechanism. This innovative model offers a huge leap over previous studies which have only simulated morphology visually based on stochastics. The simulation results are similar to the biological reports published, and thereby to a certain extent support VEGF and Notch signalling theory [4, 22-31] from the computational viewpoint.

4) We have integrated the ABM method using Java and MATLAB languages with the Euler method to solve the ODEs and realise the simulation of angiogenesis. The agents are dynamically endowed with more functions, including calculation,

memory, comparison, judgment, update, taking data from outside, and sending signals to the adjacent agents, compared with cellular automaton (CA) in similar research. In this way, we have successfully simulated the regulated ODEs, which are impossible to obtain by simply using mathematical tools. The successful simulation enriches the methods in the computational modelling of angiogenesis, providing a new perspective for computational modellers. Hence, we recommend that the ABM method is a desired approach in modelling cancers related to regulatory mechanisms, and MATLAB is a more contemporary software development tool for computer scientists.

## 7.3 Reflections on the research

The tumour's microenvironment plays a key role in the tumour growth model. To extend our understanding of the tumour microenvironment, the capillary network around the tumour should be modelled. The research in developing models of tumour-induced angiogenesis is rare, compared with the large number of biological experiments and hypotheses.

In this study, we enhanced and extended our understanding of the biological procedure of ECs in tumour-induced angiogenesis, including proliferation, migration, branching, and specification. We also narrowed down the focus on the modelling of VEGF/Notch signalling pathway regulatory mechanism during angiogenesis, and decided the methodological route towards the research goal and successfully established our models.

One major advantage of our innovative hybrid regulatory model is that it allows the modellers to focus on the agent and environment based on the PDEs. This is dissimilar to a very complicated agent-based domain model, such as the FLAME based NF-κB and IκBα signalling pathway model [122].

We attempted to develop the ODE-based technique in regulating the EC type selection procedure during angiogenesis. This approach takes the minimal abstraction of the VEGF/Notch cell signalling pathway and decreases the complexity of the system. The simulation results rely on the interaction reflection between different agents, which is very different from stochastic models.

Due to time and resource limitation, we have not conducted biological experiments to validate the models developed. We identified similar results *in vivo* and *in vitro* assays in the literature, demonstrating the validation to a large extent. In addition, we used some parameters for PDEs from relevant studies in the literature. Since those studies where we obtained parameters have their validations, our models may also be considered as validated models from this perspective.

## 7.4 Future research

The contributions of this thesis have identified a number of areas for future research.

- To further investigate VEGF/Notch signalling pathway during angiogenesis
- To explore how the ECM composition influences the migration of tip cells
- To explore how the tip cells influence the ECM reorganization during angiogenesis

- To improve the models through including an artificial intelligence method, especially a neuro network

- To develop computational models for personal treatment with tumours

- To examine both advantages and disadvantages of using ABM to develop models of complicated biological systems

- To explore alternative techniques for the computational modelling of tumour-induced angiogenesis, such as statistics, as a complementary approach

- To investigate the effects of modelling paradigms (e.g. ABM versus PDEs) and modelling framework (e.g. Java MASON versus FLAME) on the simulation results of complicated biological systems.

- Finally, future work in the next five years arising from this thesis could be focused on the three aspects: to extend the current VEGF/Notch signalling pathway regulation models developed in Chapter 6 by involving the artificial intelligence method, especially the neuro network, to improve the innovative models and make them more sophisticated; to extend the models developed in Chapter 4 by collaborating with biological and biomedical researchers to verify the proposed possible mechanism that invasive tumour and tumour-induced angiogenesis promote each other *in vivo* and *in vitro* for some special tumours, seeking ways of blockades to the angiogenesis and modelling the impact of blockaded vessels on the tumour, by adjusting the models with the parameters obtained from wet-lab to make the models suitable for application in personal treatments for some special tumours; to extend the models

developed in Chapter 5 by collaborating with biological and biomedical researchers on the tumour immune field to explore the tumour immunoediting process and to develop the tumour immune models in more details.

# References


1 Carmeliet, P., and Jain, R.: 'Angiogenesis in cancer and other diseases', Nature, 2000, pp. 407:249 - 457

2 Bautch, V.L.: 'VEGF-directed blood vessel patterning: from cells to organism', Cold Spring Harbor perspectives in medicine, 2012, 2, (9), pp. a006452-a006452

3 Fukumura, D., and Jain, R.K.: 'Tumour Microenvironment Abnormalities: Causes, Consequences, and Strategies to Normalize', Journal of Cellular Biochemistry, 2007, (101), pp. 937 - 949

4 Blanco, R., and Gerhardt, H.: 'VEGF and Notch in tip and stalk cell selection', Cold Spring Harbor Perspectives in Medicine, 2013, 3, (1)

5 Stephanou, A., McDougall, S.R., Anderson, A.R.A., and Chaplain, M.A.J.: 'Mathematical modelling of flow in 2D and 3D vascular networks: Applications to anti-angiogenic and chemotherapeutic drug strategies', Mathematical and Computer Modelling, 2005, 41, (10), pp. 1137-1156

6 McDougall, S.R., Anderson, A.R.A., Chaplain, M.A.J., and Sherratt, J.A.: 'Mathematical modelling of flow through vascular networks: Implications for ibmour-induced angiogenesis and chemotherapy strategies', Bulletin of Mathematical Biology, 2002, 64, (4), pp. 673-702

7 McDougall, S.R., Anderson, A.R.A., and Chaplain, M.A.J.: 'Mathematical modelling of dynamic adaptive tumour-induced angiogenesis: Clinical implications and therapeutic targeting strategies', Journal of Theoretical Biology, 2006, 241, (3), pp. 564-589

8 Anderson, A.R.A., and Chaplain, M.A.J.: 'Continuous and discrete mathematical models of tumor-induced angiogenesis', Bulletin of Mathematical Biology, 1998, 60, (5), pp. 857-899

9 Stamper, I.J., Byrne, H.M., Owen, M.R., and Maini, P.K.: 'Modelling the role of angiogenesis and vasculogenesis in solid tumour growth', Bulletin of mathematical biology, 2007, 69, (8), pp. 2737-2772

10 Scianna, M., Bell, C.G., and Preziosi, L.: 'A review of mathematical models for the formation of vascular networks', Journal of theoretical biology, 2013, 333, pp. 174-209

11 Mantzaris, N., Webb, S., and Othmer, H.: 'Mathematical Modelling of Tumor-induced Angiogenesis', Journal of mathematical biology, 2004

12 Maggelakis, S.A., and Savakis, A.E.: 'A mathematical model of growth factor induced capillary growth in the retina', Mathematical and Computer Modelling, 1996, 24, (7), pp. 33-41

13 Liu, G., Qutub, A.a., Vempati, P., Mac Gabhann, F., and Popel, A.S.: 'Module-based multiscale simulation of angiogenesis in skeletal muscle', Theoretical biology & medical modelling, 2011, 8, (1), pp. 6-6

14 Chaplain, M.A.J., and Anderson, A.R.A.: 'Mathematical modelling, simulation and prediction of tumour-induced angiogenesis', Invasion & Metastasis, 1996, 16, (4-5), pp. 222-234

15 Cai, Y., Xu, S., Wu, J., and Long, Q.: 'Coupled modelling of tumour angiogenesis, tumour growth and blood perfusion', Journal of theoretical biology, 2011, 279, (1), pp. 90-101

16 Gerhardt, H., Golding, M., Fruttiger, M., Ruhrberg, C., Lundkvist, A., Abramsson, A., Jeltsch, M., Mitchell, C., Alitalo, K., Shima, D., and Betsholtz, C.: 'VEGF guides angiogenic sprouting utilizing endothelial tip cell filopodia', The Journal of cell biology, 2003, 161, (6), pp. 1163-1177

17 Noguera-Troise, I., Daly, C., Papadopoulos, N.J., Coetzee, S., Boland, P., Gale, N.W., Lin, H.C., Yancopoulos, G.D., and Thurston, G.: 'Blockade of Dll4 inhibits tumour growth by promoting non-productive angiogenesis', Nature, 2006, 444, (7122), pp. 1032-1037

18 Phng, L.-K., Potente, M., Leslie, J.D., Babbage, J., Nyqvist, D., Lobov, I., Ondr, J.K., Rao, S., Lang, R.A.,

Thurston, G., and Gerhardt, H.: 'Nrarp coordinates endothelial Notch and Wnt signaling to control vessel density in angiogenesis', Developmental cell, 2009, 16, (1), pp. 70-82

19 Leslie, J.D., Ariza-McNaughton, L., Bermange, A.L., McAdow, R., Johnson, S.L., and Lewis, J.: 'Endothelial signalling by the Notch ligand Delta-like 4 restricts angiogenesis', Development (Cambridge, England), 2007, 134, (5), pp. 839-844

20 Siekmann, A.F., and Lawson, N.D.: 'Notch signalling limits angiogenic cell behaviour in developing zebrafish arteries', Nature, 2007, 445, (7129), pp. 781-784

21 Ridgway, J., Zhang, G., Wu, Y., Stawicki, S., Liang, W.-C., Chanthery, Y., Kowalski, J., Watts, R.J., Callahan, C., Kasman, I., Singh, M., Chien, M., Tan, C., Hongo, J.-A.S., de Sauvage, F., Plowman, G., and Yan, M.: 'Inhibition of Dll4 signalling inhibits tumour growth by deregulating angiogenesis', Nature, 2006, 444, (7122), pp. 1083-1087

22 Hellstrom, M., Phng, L.-K., Hofmann, J.J., Wallgard, E., Coultas, L., Lindblom, P., Alva, J., Nilsson, A.-K., Karlsson, L., Gaiano, N., Yoon, K., Rossant, J., Iruela-Arispe, M.L., Kalen, M., Gerhardt, H., and Betsholtz, C.: 'Dll4 signalling through Notch1 regulates formation of tip cells during angiogenesis', Nature, 2007, 445, (7129), pp. 776-780

23 Lobov, I.B., Renard, R.A., Papadopoulos, N., Gale, N.W., Thurston, G., Yancopoulos, G.D., and Wiegand, S.J.: 'Delta-like ligand 4 (Dll4) is induced by VEGF as a negative regulator of angiogenic sprouting', Proceedings of the National Academy of Sciences of the United States of America, 2007, 104, (9), pp. 3219-3224

24 Harrington, L.S., Sainson, R.C.A., Williams, C.K., Taylor, J.M., Shi, W., Li, J.-L., and Harris, A.L.: 'Regulation of multiple angiogenic pathways by Dll4 and Notch in human umbilical vein endothelial cells', Microvascular research, 2008, 75, (2), pp. 144-154

25 Guo, S., Liu, M., and Gonzalez-Perez, R.R.: 'Role of Notch and its oncogenic signaling crosstalk in breast cancer', Biochimica et biophysica acta, 2011, 1815, (2), pp. 197-213

26 Funahashi, Y., Shawber, C.J., Vorontchikhina, M., Sharma, A., Outtz, H.H., and Kitajewski, J.: 'Notch regulates the angiogenic response via induction of VEGFR-1', Journal of angiogenesis research, 2010, 2, (1), pp. 3-3

27 Eilken, H.M., and Adams, R.H.: 'Dynamics of endothelial cell behavior in sprouting angiogenesis', Current opinion in cell biology, 2010, 22, (5), pp. 617-625

28 Claxton, S., and Fruttiger, M.: 'Periodic Delta-like 4 expression in developing retinal arteries', Gene expression patterns : GEP, 2004, 5, (1), pp. 123-127

29 Bi, P., and Kuang, S.: 'Notch signaling as a novel regulator of metabolism', Trends in endocrinology and metabolism: TEM, 2015

30 Bentley, K., Gerhardt, H., and Bates, P.A.: 'Agent-based simulation of notch-mediated tip cell selection in angiogenic sprout initialisation', Journal of theoretical biology, 2008, 250, (1), pp. 25-36

31 Benedito, R., Roca, C., Sorensen, I., Adams, S., Gossler, A., Fruttiger, M., and Adams, R.H.: 'The notch ligands Dll4 and Jagged1 have opposing effects on angiogenesis', Cell, 2009, 137, (6), pp. 1124-1135

32 Hanahan, D., and Weinberg, R.A.: 'Hallmarks of cancer: the next generation', Cell, 2011, 144, (5), pp. 646-674

33 Adams, R.H., and Alitalo, K.: 'Molecular regulation of angiogenesis and lymphangiogenesis', Nature reviews. Molecular cell biology, 2007, 8, (6), pp. 464-478

34 Zhou, W., Wang, G., and Guo, S.: 'Regulation of angiogenesis via Notch signaling in breast cancer and cancer stem cells', Biochimica et biophysica acta, 2013, 1836, (2), pp. 304-320

35 Weinberg, R.: 'The Biology of Cancer, Second Edition' (Taylor & Francis Group, 2013. 2013)

36 Watson, M.G., McDougall, S.R., Chaplain, M.A.J., Devlin, A.H., and Mitchell, C.A.: 'Dynamics of

angiogenesis during murine retinal development: a coupled in vivo and in silico study', Journal of the Royal Society, Interface / the Royal Society, 2012, 9, (74), pp. 2351-2364

37 Folkman, J., and Klagsbrun, M.: 'Fundamental Aspects of Neoplasia' (SpringerVerlag, 1975. 1975)

38 Tracqui, P.: 'Biophysical models of tumour growth', Reports on Progress in Physics, 2009, 72, (5)

39 Folkman, J.: 'Tumor angiogenesis: therapeutic implications', The New England journal of medicine, 1971, 285, (21), pp. 1182-1186

40 Folkman, J.: 'Fundamental concepts of the angiogenic process', Current molecular medicine, 2003, 3, (7), pp. 643-651

41 Istvan Petak, J.A.H., and Kopper., L.: 'Molecular targeting of cell death signal transduction pathways in cancer.', Current Signal Transduction Therapy, 2006, (1), pp. 113-131

42 Aldakheel, S.A.A.: 'Mathematical Modelling of Negative Feedback Signal Transduction Processes', University of Dundee, 2014

43 Pfeifer, A.C., Timmer, J., and Klingmuller, U.: 'Systems biology of JAK/STAT signalling', Essays in biochemistry, 2008, 45, pp. 109-120

44 Williams, C., Budina, E., Stoppel, W.L., Sullivan, K.E., Emani, S., Emani, S.M., and Black, L.D.: 'Cardiac Extracellular Matrix-Fibrin Hybrid Scaffolds with Tunable Properties for Cardiovascular Tissue Engineering', Acta Biomaterialia, 2014, 14, pp. 84-95

45 Lodish, H., and Berk, A.: 'Molecular cell biology' (W.H. Freeman & Co, 2000, 4th edn. 2000)

46 Krauss, G.: 'Biochemistry of Signal Transduction and Regulation' (Wiley-VCH, 2003, 3rd edn. 2003)

47 Downward, J.: 'The ins and outs of signalling', Nature, 2001, 411, (6839), pp. 759-762

48 Takahashi, H., and Shibuya, M.: 'The vascular endothelial growth factor (VEGF)/VEGF receptor system and its role under physiological and pathological conditions', Clinical science (London, England : 1979), 2005, 109, (3), pp. 227-241

49 Gerlee, P., and Anderson, A.R.A.: 'An evolutionary hybrid cellular automaton model of solid tumour growth', Journal of theoretical biology, 2007, 246, (4), pp. 583-603

50 Freeman, M.: 'Feedback control of intercellular signalling in development', Nature, 2000, 408, (6810), pp. 313-319

51 Alberts, B., Bray, D., Lewis, J., Raff, M., Roberts, K., and Watson, J.D.: 'Molecular Biology of the Cell ( Third Edition ) Biochemistry for the Medical Sciences' (Garland Publishing, 1994), pp. 1994-1994

52 Benedito, R., Roca, C., SÃ¶rensen, I., Adams, S., Gossler, A., Fruttiger, M., and Adams, R.H.: 'The notch ligands Dll4 and Jagged1 have opposing effects on angiogenesis', Cell, 2009, 137, (6), pp. 1124-1135

53 Hancock, J.T.: 'Cell Signalling' (Prentice Hall, 1997, 1st edn. 1997)

54 Chang, C., and Werb, Z.: 'The many faces of metalloproteases: cell growth, invasion, angiogenesis and metastasis', Trends in Cell Biology, 2001, 11, pp. S37-S43

55 Dvorak, H.F.: 'Rous-Whipple Award Lecture. How tumors make bad blood vessels and stroma', in Editor (Ed.)^(Eds.): 'Book Rous-Whipple Award Lecture. How tumors make bad blood vessels and stroma' (2003, edn.), pp. 1747-1757

56 Bergers, G., and Benjamin, L.E.: 'Tumorigenesis and the angiogenic switch', Nature reviews. Cancer, 2003, 3, (6), pp. 401-410

57 Suchting, S., Freitas, C., le Noble, F., Benedito, R., Breant, C., Duarte, A., and Eichmann, A.: 'The Notch ligand Delta-like 4 negatively regulates endothelial tip cell formation and vessel branching', Proceedings of the National Academy of Sciences of the United States of America, 2007, 104, (9), pp. 3225-3230

58 Phng, L.K.: 'A study of Notch signalling in developmental angiogenesis', 2009

59 Uemura, A., Kusuhara, S., Wiegand, S.J., Yu, R.T., and Nishikawa, S.-i.: 'Tlx acts as a proangiogenic switch by regulating extracellular assembly of fibronectin matrices in retinal astrocytes', The Journal of

clinical investigation, 2006, 116, (2), pp. 369-377

60 Mitchell, C.A., Rutland, C.S., Walker, M., Nasir, M., Foss, A.J.E., Stewart, C., Gerhardt, H., Konerding, M.A., Risau, W., and Drexler, H.C.A.: 'Unique vascular phenotypes following over-expression of individual VEGFA isoforms from the developing lens', Angiogenesis, 2006, 9, (4), pp. 209-224

61 Hynes, R.O.: 'Integrins and Fibronectins and Their Role in Cellular Adhesion', Thrombosis and Haemostasis, 1991, 65, (6), pp. 662-662

62 Johansson, S., Gustafson, S., and Pertoft, H.: 'Identification of a fibronectin receptor specific for rat liver endothelial cells', Experimental cell research, 1987, 172, (2), pp. 425-431

63 Quigley, J.P.: 'The directed migration of B-16melanoma-cells in response to a haptotactic chemotactic gradient of fibronectin.', J.Cell Biol., 1983, 97, pp. 450-451

64 Carter, S.B.: 'Principles of cell motility: the direction of cell movement and cancer invasion. ', Nature, 1965, 208, pp. 1183–1187

65 Carter, S.B.: 'Haptotaxis and the mechanism of cell motility.', Nature, 1967, 213, pp. 256-260

66 Bowersox, J.C., and Sorgente, N.: 'Chemotaxis of aortic endothelial cells in response to fibronectin', Cancer research, 1982, 42, (7), pp. 2547-2551

67 Harper, S.J., and Bates, D.O.: 'VEGF-A splicing: the key to anti-angiogenic therapeutics?', Nature reviews. Cancer, 2008, 8, (11), pp. 880-887

68 Holmes, D.I.R., and Zachary, I.: 'The vascular endothelial growth factor (VEGF) family: angiogenic factors in health and disease', Genome biology, 2005, 6, (2), pp. 209-209

69 Keskitalo, S., Tammela, T., Lyytikka, J., Karpanen, T., Jeltsch, M., Markkanen, J., Yla-Herttuala, S., and Alitalo, K.: 'Enhanced capillary formation stimulated by a chimeric vascular endothelial growth factor/vascular endothelial growth factor-C silk domain fusion protein', Circulation research, 2007, 100, (10), pp. 1460-1467

70 Ferrara, N., Gerber, H.-P., and LeCouter, J.: 'The biology of VEGF and its receptors', Nature medicine, 2003, 9, (6), pp. 669-676

71 Houck, K.A., Ferrara, N., Winer, J., Cachianes, G., Li, B., and Leung, D.W.: 'The vascular endothelial growth factor family: identification of a fourth molecular species and characterization of alternative splicing of RNA', Molecular endocrinology (Baltimore, Md.), 1991, 5, (12), pp. 1806-1814

72 Tischer, E., Mitchell, R., Hartman, T., Silva, M., Gospodarowicz, D., Fiddes, J.C., and Abraham, J.A.: 'The human gene for vascular endothelial growth factor. Multiple protein forms are encoded through alternative exon splicing', The Journal of biological chemistry, 1991, 266, (18), pp. 11947-11954

73 Park, J.E., Keller, G.A., and Ferrara, N.: 'The vascular endothelial growth factor (VEGF) isoforms: differential deposition into the subepithelial extracellular matrix and bioactivity of extracellular matrix-bound VEGF', Molecular biology of the cell, 1993, 4, (12), pp. 1317-1326

74 Houck, K.A., Leung, D.W., Rowland, A.M., Winer, J., and Ferrara, N.: 'Dual regulation of vascular endothelial growth factor bioavailability by genetic and proteolytic mechanisms', The Journal of biological chemistry, 1992, 267, (36), pp. 26031-26037

75 Hamerlik, P., Lathia, J., Rasmussen, R., Wu, Q., Bartkova, J., Lee, M., Moudry, P., Bartek, J., Fischer, W., and Lukas, J.: 'Autocrine VEGF-VEGFR2-Neuropilin-1 signaling promotes glioma stem-like cell viability and tumor growth. ', J Exp Med, 2012, 209, (3), pp. 507-520

76 Stalmans, I., Ng, Y.-S., Rohan, R., Fruttiger, M., Bouche, A., Yuce, A., Fujisawa, H., Hermans, B., Shani, M., Jansen, S., Hicklin, D., Anderson, D.J., Gardiner, T., Hammes, H.-P., Moons, L., Dewerchin, M., Collen, D., Carmeliet, P., and D'Amore, P.A.: 'Arteriolar and venular patterning in retinas of mice selectively expressing VEGF isoforms', The Journal of clinical investigation, 2002, 109, (3), pp. 327-336

77 Dvorak, H.F.: 'Vascular permeability factor/vascular endothelial growth factor: a critical cytokine in

tumor angiogenesis and a potential target for diagnosis and therapy', Journal of clinical oncology : official journal of the American Society of Clinical Oncology, 2002, 20, (21), pp. 4368-4380

78 Bentley, K., Jones, M., and Cruys, B.: 'Predicting the future: towards symbiotic computational and experimental angiogenesis research', Experimental cell research, 2013, 319, (9), pp. 1240-1246

79 Takano, S., Yoshii, Y., Kondo, S., Suzuki, H., Maruno, T., Shirai, S., and Nose, T.: 'Concentration of vascular endothelial growth factor in the serum and tumor tissue of brain tumor patients', Cancer research, 1996, 56, (9), pp. 2185-2190

80 Benjamin, L.E., Golijanin, D., Itin, A., Pode, D., and Keshet, E.: 'Selective ablation of immature blood vessels in established human tumors follows vascular endothelial growth factor withdrawal', The Journal of clinical investigation, 1999, 103, (2), pp. 159-165

81 Gerber, H.P., McMurtrey, A., Kowalski, J., Yan, M., Keyt, B.A., Dixit, V., and Ferrara, N.: 'Vascular endothelial growth factor regulates endothelial cell survival through the phosphatidylinositol 3'-kinase/Akt signal transduction pathway. Requirement for Flk-1/KDR activation', The Journal of biological chemistry, 1998, 273, (46), pp. 30336-30343

82 Yuan, F., Chen, Y., Dellian, M., Safabakhsh, N., Ferrara, N., and Jain, R.K.: 'Time-dependent vascular regression and permeability changes in established human tumor xenografts induced by an anti-vascular endothelial growth factor/vascular permeability factor antibody', Proceedings of the National Academy of Sciences of the United States of America, 1996, 93, (25), pp. 14765-14770

83 Ferrara, N., Carver-Moore, K., Chen, H., Dowd, M., Lu, L., O'Shea, K.S., Powell-Braxton, L., Hillan, K.J., and Moore, M.W.: 'Heterozygous embryonic lethality induced by targeted inactivation of the VEGF gene', Nature, 1996, 380, (6573), pp. 439-442

84 Carmeliet, P., Ferreira, V., Breier, G., Pollefeyt, S., Kieckens, L., Gertsenstein, M., Fahrig, M., Vandenhoeck, A., Harpal, K., Eberhardt, C., Declercq, C., Pawling, J., Moons, L., Collen, D., Risau, W., and Nagy, A.: 'Abnormal blood vessel development and lethality in embryos lacking a single VEGF allele', Nature, 1996, 380, (6573), pp. 435-439

85 Ferrari, G., Cook, B.D., Terushkin, V., Pintucci, G., and Mignatti, P.: 'Transforming growth factor-beta 1 (TGF-beta1) induces angiogenesis through vascular endothelial growth factor (VEGF)-mediated apoptosis', Journal of cellular physiology, 2009, 219, (2), pp. 449-458

86 Ferrari, G., Pintucci, G., Seghezzi, G., Hyman, K., Galloway, A.C., and Mignatti, P.: 'VEGF, a prosurvival factor, acts in concert with TGF-beta1 to induce endothelial cell apoptosis', Proceedings of the National Academy of Sciences of the United States of America, 2006, 103, (46), pp. 17260-17265

87 Verheul, H.M., and Pinedo, H.M.: 'The role of vascular endothelial growth factor (VEGF) in tumor angiogenesis and early clinical development of VEGF-receptor kinase inhibitors', Clinical breast cancer, 2000, 1 Suppl 1, pp. S80-84

88 Shibuya, M.: 'Vascular endothelial growth factor receptor-1 (VEGFR-1/Flt-1): a dual regulator for angiogenesis.', Angiogenesis, 2006, (9(4)), pp. 225 - 230

89 Dimmeler, S., and Zeiher, A.: 'Endothelial cell apoptosis in angiogenesis and vessel regression. ', Circ Res, 2000, (87(6)), pp. 434-439

90 Nehls, V., and Drenckhahn, D.: 'The versatility of microvascular pericytes: from mesenchyme to smooth muscle?', Histochemistry, 1993, 99, (1), pp. 1-12

91 Orlidge, A., and D'Amore, P.A.: 'Inhibition of capillary endothelial cell growth by pericytes and smooth muscle cells', The Journal of cell biology, 1987, 105, (3), pp. 1455-1462

92 Rundhaug, J.E.: 'Matrix metalloproteinases, angiogenesis, and cancer: commentary re: A. C. Lockhart et al., Reduction of wound angiogenesis in patients treated with BMS-275291, a broad spectrum matrix metalloproteinase inhibitor. Clin. Cancer Res., 9: 00-00, 2003', Clinical cancer research : an official journal

of the American Association for Cancer Research, 2003, 9, (2), pp. 551-554

93 Kalluri, R.: 'Basement membranes: structure, assembly and role in tumour angiogenesis', Nature reviews. Cancer, 2003, 3, (6), pp. 422-433

94 Nicholson, D.E.: 'IUBMB-Nicholson metabolic pathways charts', in Ortiz, P. (Ed.) (2001), pp. 42-44

95 Hiratsuka, S., Nakao, K., Nakamura, K., Katsuki, M., Maru, Y., and Shibuya, M.: 'Membrane fixation of vascular endothelial growth factor receptor 1 ligand-binding domain is important for vasculogenesis and angiogenesis in mice', Molecular and cellular biology, 2005, 25, (1), pp. 346-354

96 Jakobsson, L., Franco, C.A., Bentley, K., Collins, R.T., Ponsioen, B., Aspalter, I.M., Rosewell, I., Busse, M., Thurston, G., Medvinsky, A., Schulte-Merker, S., and Gerhardt, H.: 'Endothelial cells dynamically compete for the tip cell position during angiogenic sprouting', Nature cell biology, 2010, 12, (10), pp. 943-953

97 Scehnet, J.S., Jiang, W., Kumar, S.R., Krasnoperov, V., Trindade, A., Benedito, R., Djokovic, D., Borges, C., Ley, E.J., Duarte, A., and Gill, P.S.: 'Inhibition of Dll4-mediated signaling induces proliferation of immature vessels and results in poor tissue perfusion', Blood, 2007, 109, (11), pp. 4753-4760

98 Patel, N.S., Li, J.-L., Generali, D., Poulsom, R., Cranston, D.W., and Harris, A.L.: 'Up-regulation of delta-like 4 ligand in human tumor vasculature and the role of basal expression in endothelial cell function', Cancer research, 2005, 65, (19), pp. 8690-8697

99 Mailhos, C., Modlich, U., Lewis, J., Harris, A., Bicknell, R., and Ish-Horowicz, D.: 'Delta4, an endothelial specific notch ligand expressed at sites of physiological and tumor angiogenesis', Differentiation; research in biological diversity, 2001, 69, (2-3), pp. 135-144

100 Gale, N.W., Dominguez, M.G., Noguera, I., Pan, L., Hughes, V., Valenzuela, D.M., Murphy, A.J., Adams, N.C., Lin, H.C., Holash, J., Thurston, G., and Yancopoulos, G.D.: 'Haploinsufficiency of delta-like 4 ligand results in embryonic lethality due to major defects in arterial and vascular development', Proceedings of the National Academy of Sciences of the United States of America, 2004, 101, (45), pp. 15949-15954

101 Li, J.-L., Sainson, R.C.A., Shi, W., Leek, R., Harrington, L.S., Preusser, M., Biswas, S., Turley, H., Heikamp, E., Hainfellner, J.A., and Harris, A.L.: 'Delta-like 4 Notch ligand regulates tumor angiogenesis, improves tumor vascular function, and promotes tumor growth in vivo', Cancer research, 2007, 67, (23), pp. 11244-11253

102 Hoey, T., Yen, W.-C., Axelrod, F., Basi, J., Donigian, L., Dylla, S., Fitch-Bruhns, M., Lazetic, S., Park, I.-K., Sato, A., Satyal, S., Wang, X., Clarke, M.F., Lewicki, J., and Gurney, A.: 'DLL4 blockade inhibits tumor growth and reduces tumor-initiating cell frequency', Cell stem cell, 2009, 5, (2), pp. 168-177

103 Li, H., Adachi, Y., Yamamoto, H., Min, Y., Ohashi, H., Ii, M., Arimura, Y., Endo, T., Lee, C.T., Carbone, D.P., Imai, K., and Shinomura, Y.: 'Insulin-Like Growth Factor-I Receptor Blockade Reduces Tumor Angiogenesis and Enhances the Effects of Bevacizumab for a Human Gastric Cancer Cell Line, MKN45', Cancer, 2011, 117, (14), pp. 3135-3147

104 Soker, S., Takashima, S., Miao, H.Q., Neufeld, G., and Klagsbrun, M.: 'Neuropilin-1 is expressed by endothelial and tumor cells as an isoform-specific receptor for vascular endothelial growth factor', Cell, 1998, 92, (6), pp. 735-745

105 Harrington, H.: 'Modeling tumor-induced angiogenesis in the cornea', in Editor (Ed.)^(Eds.): 'Book Modeling tumor-induced angiogenesis in the cornea' (2005, edn.), pp.

106 Phng, L.K., and Gerhardt, H.: 'Angiogenesis: a team effort coordinated by notch', Developmental cell, 2009, 16, (2), pp. 196-208

107 Isogai, S., Lawson, N.D., Torrealday, S., Horiguchi, M., and Weinstein, B.M.: 'Angiogenic network formation in the developing vertebrate trunk', Development (Cambridge, England), 2003, 130, (21), pp. 5281-5290

108 Dejana, E., Tournier-Lasserve, E., and Weinstein, B.M.: 'The control of vascular integrity by

endothelial cell junctions: molecular basis and pathological implications', Developmental cell, 2009, 16, (2), pp. 209-221

109 Iruela-Arispe, M.L., and Davis, G.E.: 'Cellular and molecular mechanisms of vascular lumen formation', Developmental cell, 2009, 16, (2), pp. 222-231

110 Tammela, T., Zarkada, G., Wallgard, E., Murtomaki, A., Suchting, S., Wirzenius, M., Waltari, M., Hellstrom, M., Schomber, T., Peltonen, R., Freitas, C., Duarte, A., Isoniemi, H., Laakkonen, P., Christofori, G., Yla-Herttuala, S., Shibuya, M., Pytowski, B., Eichmann, A., Betsholtz, C., and Alitalo, K.: 'Blocking VEGFR-3 suppresses angiogenic sprouting and vascular network formation', Nature, 2008, 454, (7204), pp. 656-660

111 Hynes, R.O.: 'Fibronectins' (Springer-Verlag: New York, 1990. 1990)

112 Greenberg, J.H., Seppa, S., Seppa, H., and Tyl Hewitt, A.: 'Role of collagen and fibronectin in neural crest cell adhesion and migration', Developmental biology, 1981, 87, (2), pp. 259-266

113 Albini, A., Allavena, G., Melchiori, A., Giancotti, F., Richter, H., Comoglio, P.M., Parodi, S., Martin, G.R., and Tarone, G.: 'Chemotaxis of 3T3 and SV3T3 cells to fibronectin is mediated through the cell-attachment site in fibronectin and a fibronectin cell surface receptor', The Journal of cell biology, 1987, 105, (4), pp. 1867-1872

114 Woodley, D.T., Bachmann, P.M., and O'Keefe, E.J.: 'Laminin inhibits human keratinocyte migration', Journal of cellular physiology, 1988, 136, (1), pp. 140-146

115 Lacovara, J., Cramer, E.B., and Quigley, J.P.: 'Fibronectin Enhancement of Directed Migration of B-16 Melanoma-Cells', Cancer Research, 1984, 44, (4), pp. 1657-1663

116 Mccarthy, J.B., and Furcht, L.T.: 'Laminin and Fibronectin Promote the Haptotactic Migration of B-16 Mouse Melanoma-Cells Invitro', Journal of Cell Biology, 1984, 98, (4), pp. 1474-1480

117 Addison-Smith, B.: 'Mathematical Modelling of Tumor-induced Angiogenesis', 2010

118 Greenspan, H.P.: 'On the growth and stability of cell cultures and solid tumors', Journal of theoretical biology, 1976, 56, (1), pp. 229-242

119 Goodwin, B.C.: 'Oscillatory behavior in enzymatic control processes', Advances in enzyme regulation, 1965, 3, pp. 425-438

120 Hoffmann, A., Levchenko, A., Scott, M.L., and Baltimore, D.: 'The IkappaB-NF-kappaB signaling module: temporal control and selective gene activation', Science (New York, N.Y.), 2002, 298, (5596), pp. 1241-1245

121 Williams, J.H., Carter, S.M., and Rychetnik, L.: ''Organised' cervical screening 45 years on: How consistent are organised screening practices?', European journal of cancer (Oxford, England : 1990), 2014, 50, (17), pp. 3029-3038

122 Krishna, S., Jensen, M.H., and Sneppen, K.: 'Minimal model of spiky oscillations in NF-kappaB signaling', Proceedings of the National Academy of Sciences of the United States of America, 2006, 103, (29), pp. 10840-10845

123 Carlotti, F., Dower, S.K., and Qwarnstrom, E.E.: 'Dynamic shuttling of nuclear factor kappa B between the nucleus and cytoplasm as a consequence of inhibitor dissociation', The Journal of biological chemistry, 2000, 275, (52), pp. 41028-41034

124 Balding, D., and McElwain, D.L.S.: 'A mathematical model of tumour-induced capillary growth', Journal of Theoretical Biology, 1985, 114, (1), pp. 53-73

125 Mantzaris, N.V., Webb, S., and Othmer, H.G.: 'Mathematical modeling of tumor-induced angiogenesis', Journal of Mathematical Biology, 2004, 49, (2), pp. 111-187

126 Horie, M., Saito, A., Yamaguchi, Y., Ohshima, M., and Nagase, T.: 'Three-dimensional Co-culture Model for Tumor-stromal Interaction', 2015, (96), pp. e52469

127 Masoudi-Nejad, A., Bidkhori, G., Hosseini Ashtiani, S., Najafi, A., Bozorgmehr, J.H., and Wang, E.:

'Cancer systems biology and modeling: Microscopic scale and multiscale approaches', Seminars in cancer biology, 2015, 30C, pp. 60-69

128 Rohani, M.G., and Parks, W.C.: 'Matrix Remodeling by MMPs during Wound Repair', Matrix biology : journal of the International Society for Matrix Biology, 2015

129 Paweletz, N., and Knierim, M.: 'Tumor-Related Angiogenesis', Critical Reviews in Oncology/Hematology, 1989, 9, (3), pp. 197-242

130 Lundberg, I.: 'Fibroblasts and ECM in colorectal cancer.', Umeå University, 2012

131 Kumar, S., Das, A., and Sen, S.: 'Extracellular matrix density promotes EMT by weakening cell-cell adhesions', Molecular BioSystems, 2014, 10, (4), pp. 838-850

132 Cao, Y., Liu, X., Lu, W., Chen, Y., Wu, X., Li, M., Wang, X.-A., Zhang, F., Jiang, L., Zhang, Y., Hu, Y., Xiang, S., Shu, Y., Bao, R., Li, H., Wu, W., Weng, H., Yen, Y., and Liu, Y.: 'Fibronectin promotes cell proliferation and invasion through mTOR signaling pathway activation in gallbladder cancer', Cancer letters, 2015, 360, (2), pp. 141-150

133 Elenbaas, B., and Weinberg, R.A.: 'Heterotypic signaling between epithelial tumor cells and fibroblasts in carcinoma formation.', Experimental cell research, 2001, (264), pp. 169-184

134 Liu, M., Xu, J., and Deng, H.: 'Tangled fibroblasts in tumor-stroma interactions.', International journal of cardiology, 2011, (129), pp. 1795-1805

135 Mueller, M.M., and Fusenig, N.E.: 'Friends or foes - bipolar effects of the tumour stroma in cancer.', Nat Rev Cancer, 2004, (4), pp. 839-849

136 Lee, H.O., Mullins, S.R., Franco-Barraza, J., Valianou, M., Cukierman, E., and Cheng, J.D.: 'FAP-overexpressing fibroblasts produce an extracellular matrix that enhances invasive velocity and directionality of pancreatic cancer cells.', BMC Cancer, 2011, (11), pp. 245

137 Cervantes-Arias, A., Pang, L.Y., and Argyle, D.J.: 'Epithelial-mesenchymal transition as a fundamental mechanism underlying the cancer phenotype.', Vet Comp Oncol, 2012

138 Jia, D., Yan, M., Wang, X., Hao, X., Liang, L., Liu, L., Kong, H., He, X., Li, J., and Yao, M.: 'Development of a highly metastatic model that reveals a crucial role of fibronectin in lung cancer cell migration and invasion.', BMC Cancer, 2010, (10), pp. 364

139 Wei, P.L., Kuo, L.J., Huang, M.T., Ting, W.C., Ho, Y.S., Wang, W., An, J., and Chang, Y.J.: 'Nicotine enhances colon cancer cell migration by induction of fibronectin.', Ann Surg Oncol, 2011, (18), pp. 1782-1790

140 Meng, X.N., Jin, Y., Yu, Y. , Bai, J., Liu, G.Y., Zhu, J., Zhao, Y.Z., Wang, Z., Chen, F., and Lee, K.Y.: 'Characterisation of fibronectin-mediated FAK signalling pathways in lung cancer cell migration and invasion. ', Br J Cancer, 2009, (101), pp. 327-334

141 Derya, M., Yılmaz, I., and Aytekin, M.: 'The Role of Extracellular Matrix in Lung Diseases.', Biol Med, 2014, 6, (200)

142 Macal, C.M., and North, M.J.: 'Tutorial on agent-based modelling and simulation', in Editor (Ed.)^(Eds.): 'Book Tutorial on agent-based modelling and simulation' (2010, edn.), pp. 151-162

143 Olsen, M.M., and Siegelmann, H.T.: 'Multiscale Agent-based Model of Tumor Angiogenesis', Procedia Computer Science, 2013, 18, pp. 1016-1025

144 Railsback, S.F., Lytinen, S.L., and Jackson, S.K.: 'Agent-based Simulation Platforms: Review and Development Recommendations', SIMULATION, 2006, 82, (9), pp. 609-623

145 de Pillis, L.G., Radunskaya, A.E., and Wiseman, C.L.: 'A validated mathematical model of cell-mediated immune response to tumor growth', Cancer research, 2005, 65, (17), pp. 7950-7958

146 Mallet, D.G., and De Pillis, L.G.: 'A cellular automata model of tumor-immune system interactions', Journal of theoretical biology, 2006, 239, (3), pp. 334-350

147 Byrne, H.M., Alarcon, T., Owen, M.R., Webb, S.D., and Maini, P.K.: 'Modelling aspects of cancer dynamics: a review', Philosophical transactions. Series A, Mathematical, physical, and engineering sciences, 2006, 364, (1843), pp. 1563-1578

148 Byrne, H.M., and Chaplain, M.A.: 'Mathematical models for tumour angiogenesis: numerical simulations and nonlinear wave solutions', Bulletin of mathematical biology, 1995, 57, (3), pp. 461-486

149 Eikenberry, S., Thalhauser, C., and Kuang, Y.: 'Tumor-immune interaction, surgical treatment, and cancer recurrence in a mathematical model of melanoma', PLoS computational biology, 2009, 5, (4), pp. e1000362-e1000362

150 Rejniak, K.A., and McCawley, L.J.: 'Current trends in mathematical modeling of tumor-microenvironment interactions: a survey of tools and applications', Experimental biology and medicine (Maywood, N.J.), 2010, 235, (4), pp. 411-423

151 Byrne, H.M., and Chaplin, M.A.: 'Growth of necrotic tumors in the presence and absence of inhibitors', Mathematical biosciences, 1996, 135, (2), pp. 187-216

152 Chaplain, M.A.J., McDougall, S.R., and Anderson, A.R.A.: 'Mathematical modeling of tumor-induced angiogenesis', Annual Review of Biomedical Engineering, 2006, 8, pp. 233-257

153 Orme, M.E., and Chaplain, M.A.: 'Two-dimensional models of tumour angiogenesis and anti-angiogenesis strategies', IMA journal of mathematics applied in medicine and biology, 1997, 14, (3), pp. 189-205

154 Stokes, C.L., and Lauffenburger, D.A.: 'Analysis of the roles of microvessel endothelial cell random motility and chemotaxis in angiogenesis', Journal of theoretical biology, 1991, 152, (3), pp. 377-403

155 Welter, M., Bartha, K., and Rieger, H.: 'Vascular remodelling of an arterio-venous blood vessel network during solid tumour growth', Journal of theoretical biology, 2009, 259, (3), pp. 405-422

156 Macklin, P., McDougall, S., Anderson, A.R.A., Chaplain, M.A.J., Cristini, V., and Lowengrub, J.: 'Multiscale modelling and nonlinear simulation of vascular tumour growth', Journal of mathematical biology, 2009, 58, (4-5), pp. 765-798

157 Stephanou, A., McDougall, S.R., Anderson, A.R.A., and Chaplain, M.A.J.: 'Mathematical modelling of the influence of blood rheological properties upon adaptative tumour-induced angiogenesis', Mathematical and Computer Modelling, 2006, 44, (1-2), pp. 96-123

158 Alarcon, T., Byrne, H.M., and Maini, P.K.: 'A cellular automaton model for tumour growth in inhomogeneous environment', Journal of theoretical biology, 2003, 225, (2), pp. 257-274

159 Maggelakis, S.A., and Savakis, A.E.: 'A mathematical model of retinal neovascularization', Mathematical and Computer Modelling, 1999, 29, (2), pp. 91-97

160 Deno, D.C., Saba, T.M., and Lewis, E.P.: 'Kinetics of Endogenously Labeled Plasma Fibronectin - Incorporation into Tissues', American Journal of Physiology, 1983, 245, (4), pp. R564-R575

161 Hynes, R.O.: 'Fibronectins', Scientific American, 1986, 254, (6), pp. 42-51

162 Oh, E., Pierschbacher, M., and Ruoslahti, E.: 'Deposition of Plasma Fibronectin in Tissues', Proceedings of the National Academy of Sciences of the United States of America-Biological Sciences, 1981, 78, (5), pp. 3218-3221

163 Kalluri, R., and Zeisberg, M.: 'Fibroblasts in cancer', Nat Rev Cancer, 2006, 6, (5), pp. 392-401

164 Kostourou, V., and Papalazarou, V.: 'Non-collagenous ECM proteins in blood vessel morphogenesis and cancer', Biochimica et biophysica acta, 2014, 1840, (8), pp. 2403-2413

165 Terranova, V.P., Diflorio, R., Lyall, R.M., Hic, S., Friesel, R., and Maciag, T.: 'Human-Endothelial Cells Are Chemotactic to Endothelial-Cell Growth-Factor and Heparin', Journal of Cell Biology, 1985, 101, (6), pp. 2330-2334

166 Preis, I., Langer, R., Brem, H., Folkman, J., and Patz, A.: 'Inhibition of Neovascularization by an Extract

Derived from Vitreous', American Journal of Ophthalmology, 1977, 84, (3), pp. 323-328
167 Hanahan, D.: 'Signaling vascular morphogenesis and maintenance', Science, 1997, 277, (5322), pp. 48-50
168 Ausprunk, D.H., and Folkman, J.: 'Migration and Proliferation of Endothelial Cells in Preformed and Newly Formed Blood-Vessels during Tumor Angiogenesis', Microvascular Research, 1977, 14, (1), pp. 53-65
169 Birdwell, C.R., Gospodarowicz, D., and Nicolson, G.L.: 'Identification, Localization, and Role of Fibronectin in Cultured Bovine Endothelial Cells', Proceedings of the National Academy of Sciences of the United States of America, 1978, 75, (7), pp. 3273-3277
170 Macarak, E.J., Kirby, E., Kirk, T., and Kefalides, N.A.: 'Synthesis of Cold-Insoluble Globulin by Cultured Calf Endothelial Cells', Proceedings of the National Academy of Sciences of the United States of America, 1978, 75, (6), pp. 2621-2625
171 Monaghan, P., Warburton, M.J., Perusinghe, N., and Rudland, P.S.: 'Topographical Arrangement of Basement-Membrane Proteins in Lactating Rat Mammary-Gland - Comparison of the Distribution of Type-Iv Collagen, Laminin, Fibronectin, and Thy-1 at the Ultrastructural Level', Proceedings of the National Academy of Sciences of the United States of America-Biological Sciences, 1983, 80, (11), pp. 3344-3348
172 Adams, J.C.: 'An MBoC Favorite: Fibronectin/integrin interaction induces tyrosine phosphorylation of a 120-kDa protein', Molecular Biology of the Cell, 2012, 23, (15), pp. 2821-2821
173 Clark, R.A.F., Dvorak, H.F., and Colvin, R.B.: 'Fibronectin in Delayed-Type Hypersensitivity Skin Reactions - Associations with Vessel Permeability and Endothelial-Cell Activation', Journal of Immunology, 1981, 126, (2), pp. 787-793
174 Clark, R.A.F., Dellapelle, P., Manseau, E., Lanigan, J.M., Dvorak, H.F., and Colvin, R.B.: 'Blood-Vessel Fibronectin Increases in Conjunction with Endothelial Cell-Proliferation and Capillary Ingrowth during Wound-Healing', Journal of Investigative Dermatology, 1982, 79, (5), pp. 269-276
175 Paku, S., and Paweletz, N.: '1st Steps of Tumor-Related Angiogenesis', Laboratory Investigation, 1991, 65, (3), pp. 334-346
176 Daub, J.T., and Merks, R.M.H.: 'A Cell-Based Model of Extracellular-Matrix-Guided Endothelial Cell Migration During Angiogenesis', Bulletin of Mathematical Biology, 2013, 75, (8), pp. 1377-1399
177 Gimbrone, M.A., Jr., Cotran, R.S., Leapman, S.B., and Folkman, J.: 'Tumor growth and neovascularization: an experimental model using the rabbit cornea', Journal of the National Cancer Institute, 1974, 52, (2), pp. 413-427
178 Muthukkaruppan, V.R., Kubai, L., and Auerbach, R.: 'Tumor-induced neovascularization in the mouse eye', Journal of the National Cancer Institute, 1982, 69, (3), pp. 699-708
179 Stokes, C.L., Rupnick, M.A., Williams, S.K., and Lauffenburger, D.A.: 'Chemotaxis of human microvessel endothelial cells in response to acidic fibroblast growth factor', Laboratory investigation; a journal of technical methods and pathology, 1990, 63, (5), pp. 657-668
180 Sherratt, J.A., and Murray, J.D.: 'Models of epidermal wound healing', Proceedings. Biological sciences / The Royal Society, 1990, 241, (1300), pp. 29-36
181 Bray, D.: 'Cell Movements' (New York: Garland Publishing, 1992. 1992)
182 Rupnick, M.A., Stokes, C.L., Williams, S.K., and Lauffenburger, D.A.: 'Quantitative analysis of random motility of human microvessel endothelial cells using a linear under-agarose assay', Laboratory investigation; a journal of technical methods and pathology, 1988, 59, (3), pp. 363-372
183 Lu, P., Takai, K., Weaver, V.M., and Werb, Z.: 'Extracellular Matrix Degradation and Remodeling in Development and Disease', Cold Spring Harbor perspectives in biology, 2011, 3, (12), pp. 10.1101/cshperspect.a005058 a005058
184 Lopez, J.I., Mouw, J.K., and Weaver, V.M.: 'Biomechanical regulation of cell orientation and fate',

Oncogene, 2008, 27, (55), pp. 6981-6993
185 Senger, D.R., and Davis, G.E.: 'Angiogenesis', Cold Spring Harbor perspectives in biology, 2011, 3, (8), pp. a005090-a005090
186 Nikitovic, D., Corsini, E., Kouretas, D., Tsatsakis, A., and Tzanakakis, G.: 'ROS-major mediators of extracellular matrix remodeling during tumor progression', Food and chemical toxicology : an international journal published for the British Industrial Biological Research Association, 2013, 61, pp. 178-186
187 Pankov, R., and Yamada, K.M.: 'Fibronectin at a glance.', J Cell Sci, 2002, (115), pp. 3861-3863
188 Kamoshida, G., Matsuda, A., Miura, R., Takashima, Y., Katsura, A., and Tsuji, T.: 'Potentiation of tumor cell invasion by co-culture with monocytes accompanying enhanced production of matrix metalloproteinase and fibronectin', Clinical & experimental metastasis, 2013, 30, (3), pp. 289-297
189 Chaplain, M.A.J., and Lolas, G.: 'Mathematical modelling of cancer cell invasion of tissue: The role of the urokinase plasminogen activation system', Mathematical Models & Methods in Applied Sciences, 2005, 15, (11), pp. 1685-1734
190 Folkman, J.: 'Tumor Angiogenesis Factor', Cancer Research, 1974, 34, (8), pp. 2109-2113
191 Dzivenu, O.K., and O'Donnell-Tormey, J.: 'Cancer and the immune system: The vital connection', in Editor (Ed.)^(Eds.): 'Book Cancer and the immune system: The vital connection' (Cancer research institute, 2003, edn.), pp.
192 Dunn, G.P., Old, L.J., and Schreiber, R.D.: 'The three Es of cancer immunoediting.', Annual review of immunology, 2004, 22, pp. 329-360
193 Dunn, G.P., Bruce, A.T., Ikeda, H., Old, L.J., and Schreiber, R.D.: 'Cancer immunoediting: from immunosurveillance to tumor escape.', Nat. Immunol., 2002, 3, pp. 991 - 998
194 Dunn, G.P., Old, L.J., and Schreiber, R.D.: 'The immunobiology of cancer immunosurveillance and immunoediting.', Immunity, 2004, 21, pp. 137-148
195 Teng, M.W.L., Swann, J.B., Koebel, C.M., Schreiber, R.D., and Smyth, M.J.: 'Immune-mediated dormancy: an equilibrium with cancer.', Journal of leukocyte biology, 2008, 84, pp. 988-993
196 O'Sullivan, T.: 'Cancer immunoediting by the innate immune system in the absence of adaptive immunity. ', The Journal of Experimental Medicine., 2012
197 Swann, J.B., and Smyth, M.J.: 'Immune surveillance of tumors.', The Journal of clinical investigation, 2007, 117, pp. 1137-1146
198 Muller, A.J., and Scherle, P.A.: 'Targeting the mechanisms of tumoral immune tolerance with small-molecule inhibitors.', Nature reviews. Cancer, 2006, 6, pp. 613-625
199 Maes, P.: 'The agent network architecture (ANA)', SIGART Bulletin, 1991, 2, (4), pp. 115-120
200 Müller, J.: 'The right agent (architecture) to do the right thing', Intelligent Agents V: Agents Theories, Architectures, and Languages, 1999, pp. 211-225
201 Luke, S., Cioffi-Revilla, C., Panait, L., Sullivan, K., and Balan, G.: 'MASON: A multiagent simulation environment.', SIMULATION, 2005, 81, (7), pp. 517-527
202 StÃ¤hli, C., James-Bhasin, M., and Nazhat, S.N.: 'Three-dimensional endothelial cell morphogenesis under controlled ion release from copper-doped phosphate glass', Journal of controlled release : official journal of the Controlled Release Society, 2015, 200, pp. 222-232
203 Wang, Z., Butner, J.D., Kerketta, R., Cristini, V., and Deisboeck, T.S.: 'Simulating cancer growth with multiscale agent-based modeling', Seminars in cancer biology, 2015, 30, pp. 70-78
204 An, G., and Kulkarni, S.: 'An agent-based modeling framework linking inflammation and cancer using evolutionary principles: Description of a generative hierarchy for the hallmarks of cancer and developing a bridge between mechanism and epidemiological data', Mathematical biosciences, 2014, 260, pp. 16-24
205 Brown, B.N., Price, L.M., Toapanta, F.R., DeAlmeida, D.R., Wiley, C.A., Ross, T.M., Oury, T.D., and

Vodovotz, Y.: ‘An Agent-Based Model of Inflammation and Fibrosis Following Particulate Exposure in the Lung’, Mathematical biosciences, 2012, 231, (2), pp. 186-196

206 Stern, J.R., Olivas, A.D., Valuckaite, V., Zaborina, O., Alverdy, J.C., and An, G.: ‘Agent-based model of epithelial host-pathogen interactions in anastomotic leak’, The Journal of surgical research, 2013, 184, (2), pp. 730-738

# Appendix A - Solution of the nonlinear partial differential equations

In the equations Eq.(1), Eq.(2), Eq.(3), Eq.(4) and Eq.(5), the symbols n, c, f, m and M are variables, representing ECs, VEGF, fibronectin, matrix degradation enzyme (MDE) and extra cellular matrix (ECM) respectively. The coefficients $D$, $\chi$, $\rho$, $\mu$, $\eta$, $\beta$, $\gamma$, $a$, $\varepsilon$, $\nu$ and $\omega$ are positive constants in the equations to represent different rate. $n_O$ is also a constant. $\nabla$ is the symbol of difference operator.

To solute the partial differential equations we should derivate them into difference quotient equations in order to use finite difference scheme.

$$\frac{\partial n}{\partial t} = D\nabla^2 n - \nabla \cdot (\chi(c) n \nabla c) - \rho \nabla \cdot (n \nabla f) + \mu M n (1 - \frac{n}{n_0}) \qquad (1)$$

$$\frac{\partial c}{\partial t} = -\eta n c \qquad (2)$$

$$\frac{\partial f}{\partial t} = \beta n - \gamma m f \qquad (3)$$

$$\frac{\partial m}{\partial t} = an + \varepsilon \nabla^2 m - \nu m \qquad (4)$$

$$\frac{\partial M}{\partial t} = -\omega m M \qquad (5)$$

$\chi(c)$ is the function of c. Here c represents the concentration of VEGF. This function means that at high concentration of VEGF the chemotaxis is not as sensitive as that at low concentration of VEGF to

$$\chi(c) = \frac{\chi}{1 + \delta c} \qquad (6)$$

The partial difference of $\chi(c)$ is derivative as follows：

$$[\chi(c)]_x = \frac{-\chi\delta}{(1+\delta c_x)^2} \tag{7}$$

And $$[\chi(c)]_y = \frac{-\chi\delta}{(1+\delta c_y)^2} \tag{8}$$

Such the Eq. (6) is derivative into its partial difference forms as in Eq. (7) and Eq. (8).

Eq. (1), Eq. (2), Eq. (3), Eq. (4) and Eq. (5) form a nonlinear PDEs which can be solved numerically with finite difference method. In a 2D domain $\Omega(x, y)$.

We treat Eq. (1) as follows. In the right of the Eq. (1), the first term is defined as random motility and expanded as:

$$random = D\nabla^2 n = D(\frac{\partial^2 n}{\partial x^2} + \frac{\partial^2 n}{\partial y^2}) \tag{9}$$

In the right of Eq. (1), the second term is defined as chemotaxis and expanded as：

$$\begin{aligned}
&chemotaxis = \nabla\cdot(\chi(c)n\nabla c)\\
&=\nabla\cdot[\chi(c)n(c_x+c_y)]\\
&=\nabla[\chi(c)n]\cdot(c_x+c_y)+[\chi(c)n]\cdot\nabla[(c_x+c_y)]\\
&=\{[\chi(c)_x+\chi(c)_y]n+[\chi(c)]\cdot(n_x+n_y)\}\cdot(c_x+c_y)+[\chi(c)n]\cdot[(c_{xx}+c_{yy})]\\
&=\{[\chi(c)_x+\chi(c)_y]n+[\chi(c)]\cdot(n_x+n_y)\}\cdot c_x\\
&+\{[\chi(c)_x+\chi(c)_y]n+[\chi(c)]\cdot(n_x+n_y)\}\cdot c_y+[\chi(c)n]\cdot[(c_{xx}+c_{yy})]\\
&=[\chi(c)n]\cdot(c_{xx}+c_{yy})+\{[\chi(c)_x n+\chi(c)_y n]+\chi(c)\cdot n_x\\
&+\chi(c)\cdot n_y)\}\cdot c_x+\{\chi(c)_x n+\chi(c)_y n+\chi(c)n_x+\chi(c)n_y\}\cdot c_y\\
&=[\chi(c)n]\cdot(c_{xx}+c_{yy})+\chi(c)_x n\cdot c_x+\chi(c)_y n\cdot c_x+\chi(c)\cdot n_x\cdot c_x+\chi(c)\cdot n_y\cdot c_x\\
&+\chi(c)_x n\cdot c_y+\chi(c)_y n\cdot c_y+\chi(c)n_x\cdot c_y+\chi(c)n_y\cdot c_y\\
&=\chi(c)n\cdot(c_{xx}+c_{yy})+\chi(c)_x[n\cdot c_x+n\cdot c_y]+\chi(c)_y[n\cdot c_x+n\cdot c_y]+\chi(c)[n_x\cdot c_x+n_y\cdot c_x+n_x\cdot c_y+n_y\cdot c_y]\\
&=\chi(c)n\cdot(c_{xx}+c_{yy})+\chi(c)(n_x\cdot c_x+n_y\cdot c_x+n_x\cdot c_y+n_y\cdot c_y)+\chi(c)_x(n\cdot c_x+n\cdot c_y)+\chi(c)_y(n\cdot c_x+n\cdot c_y)\\
&=\frac{\chi n}{1+\delta c}(c_{xx}+c_{yy})+\frac{\chi}{1+\delta c}(n_x\cdot c_x+n_y\cdot c_x+n_x\cdot c_y+n_y\cdot c_y)-\frac{\delta\chi n}{(1+\delta c_x)^2}(c_x+c_y)-\frac{\delta\chi n}{(1+\delta c_y)^2}(c_x+c_y)
\end{aligned}$$

Finally, the chemotaxis is expanded and difference as follows:

$$chemotaxis = \nabla \cdot (\chi(c) n \nabla c)$$
$$= \frac{\chi n}{1+\delta c} \cdot (\frac{\partial^2 c}{\partial x^2} + \frac{\partial^2 c}{\partial y^2}) + \frac{\chi}{1+\delta c} (\frac{\partial n}{\partial x} \cdot \frac{\partial c}{\partial x} + \frac{\partial n}{\partial y} \cdot \frac{\partial c}{\partial y} + \frac{\partial n}{\partial y} \cdot \frac{\partial c}{\partial x} + \frac{\partial n}{\partial x} \cdot \frac{\partial c}{\partial y}) \quad (10)$$
$$- \frac{\delta \chi n}{(1+\delta \frac{\partial c}{\partial x})^2} (\frac{\partial c}{\partial x} + \frac{\partial c}{\partial y}) - \frac{\delta \chi n}{(1+\delta \frac{\partial c}{\partial y})^2} (\frac{\partial c}{\partial x} + \frac{\partial c}{\partial y})$$

In the right of Eq. (1), the third term is defined as haptotaxis and expanded as

$$haptotaxis = \rho \nabla \cdot (n \nabla f)$$
$$= \rho \nabla \cdot [n(f_x + f_y)]$$
$$= \rho \{ [n f_x]_x + [n f_y]_y \} \quad (11)$$
$$= \rho \{ [n_x f_x + n f_{xx}] + [n_y f_y + n f_{yy}] \}$$
$$= \rho [n(f_{xx} + f_{yy}) + n_x f_x + n_y f_y]$$

Finally, the haptotaxis is expanded and difference as follows:

$$haptotaxis = \rho \nabla \cdot (n \nabla f)$$
$$= \rho [(\frac{\partial n}{\partial x} \frac{\partial f}{\partial x} + \frac{\partial n}{\partial y} \frac{\partial f}{\partial y}) + n(\frac{\partial^2 f}{\partial x^2} + \frac{\partial^2 f}{\partial y^2})] \quad (12)$$

In the right of Eq. (1), the fourth term is defined as proliferation and described as

$$prolif = \mu M n (1 - \frac{n}{n_0}) \quad (13)$$

Hence, the whole Eq. (1) can be expressed in the derivative form as:

$$\frac{\partial n}{\partial t} = D(\frac{\partial^2 n}{\partial x^2} + \frac{\partial^2 n}{\partial y^2})$$
$$- \frac{\chi n}{1+\delta c} \cdot (\frac{\partial^2 c}{\partial x^2} + \frac{\partial^2 c}{\partial y^2}) - \frac{\chi}{1+\delta c} (\frac{\partial n}{\partial x} \cdot \frac{\partial c}{\partial x} + \frac{\partial n}{\partial y} \cdot \frac{\partial c}{\partial x} + \frac{\partial n}{\partial x} \cdot \frac{\partial c}{\partial y} + \frac{\partial n}{\partial y} \cdot \frac{\partial c}{\partial y})$$
$$+ \frac{\delta \chi n}{(1+\delta \frac{\partial c}{\partial x})^2} (\frac{\partial c}{\partial x} + \frac{\partial c}{\partial y}) + \frac{\delta \chi n}{(1+\delta \frac{\partial c}{\partial y})^2} (\frac{\partial c}{\partial x} + \frac{\partial c}{\partial y}) \quad - \quad (14)$$
$$- \rho [(\frac{\partial n}{\partial x} \frac{\partial f}{\partial x} + \frac{\partial n}{\partial y} \frac{\partial f}{\partial y}) + n(\frac{\partial^2 f}{\partial x^2} + \frac{\partial^2 f}{\partial y^2})] + \mu M n (1 - \frac{n}{n_0})$$

Finite difference scheme:

To solve the equations with numerical method, we should derivate Eq. (1) from derivative form into difference quotients form. The difference quotients form is described as follows:

$$\frac{\partial n}{\partial t} = \frac{n_{i,j}^{k+1} - n_{i,j}^{k}}{\Delta t} \quad (15)$$

We set the grids in Cardial Coordinate is in the same span, and the space spans $\Delta x$ and $\Delta y$ in both x and y coordinates are same in magnitude, so

$$\Delta x = \Delta y = h \tag{16}$$

The first order difference quotient is as follows:

$$\frac{\partial c}{\partial x} = \frac{1}{2h}(c_{i+1,j} - c_{i-1,j}) \tag{17}$$

$$\frac{\partial c}{\partial y} = \frac{1}{2h}(c_{i,j+1} - c_{i,j-1}) \tag{18}$$

In the same way the second order difference quotient is as follows:

$$\frac{\partial^2 c}{\partial x^2} = \frac{c_{i+1,j} - 2c_{i,j} + c_{i-1,j}}{\Delta x^2} \tag{19}$$

$$\frac{\partial^2 c}{\partial y^2} = \frac{c_{i,j+1} - 2c_{i,j} + c_{i,j-1}}{\Delta y^2} \tag{20}$$

$$\frac{\partial^2 c}{\partial x^2} + \frac{\partial^2 c}{\partial y^2} = \frac{c_{i+1,j} + c_{i-1,j} + c_{i,j+1} + c_{i,j-1} - 4c_{i,j}}{h^2} \tag{21}$$

$$\frac{\partial n}{\partial x}\frac{\partial c}{\partial x} + \frac{\partial n}{\partial y}\frac{\partial c}{\partial y} = \frac{1}{4h^2}[(n_{i+1,j} - n_{i-1,j})(c_{i+1,j} - c_{i-1,j}) + (n_{i,j+1} - n_{i,j-1})(c_{i,j+1} - c_{i,j-1})] \tag{22}$$

$$\frac{\partial n}{\partial y}\frac{\partial c}{\partial x} + \frac{\partial n}{\partial x}\frac{\partial c}{\partial y} = \frac{1}{4h^2}[(n_{i+1,j} - n_{i-1,j})(c_{i+1,j} - c_{i-1,j}) + (n_{i,j+1} - n_{i,j-1})(c_{i,j+1} - c_{i,j-1})] \tag{23}$$

$$\begin{aligned} random &= D\nabla^2 n \\ &= D\left(\frac{n_{i+1,j} + n_{i-1,j} + n_{i,j+1} + n_{i,j-1} - 4n_{i,j}}{h^2}\right) \end{aligned} \tag{24}$$

$$
\begin{aligned}
&chemotaxis = \nabla \cdot (\chi(c) n \nabla c) \\
&= \frac{\chi n_{i,j}}{(1+\delta c_{i,j})} \cdot (\frac{c_{i+1,j} + c_{i-1,j} + c_{i,j+1} + c_{i,j-1} - 4c_{i,j}}{h^2}) \\
&+ \frac{\chi}{(1+\delta c_{i,j})} \frac{1}{4h^2} [(n_{i+1,j} - n_{i-1,j})(c_{i+1,j} - c_{i-1,j}) + (n_{i,j+1} - n_{i,j-1})(c_{i,j+1} - c_{i,j-1}) \\
&+ (n_{i+1,j} - n_{i-1,j})(c_{i+1,j} - c_{i-1,j}) + (n_{i,j+1} - n_{i,j-1})(c_{i,j+1} - c_{i,j-1})] \\
&- \frac{\delta \chi n_{i,j}}{[2h + \delta(c_{i+1,j} - c_{i-1,j})]^2} (c_{i+1,j} - c_{i-1,j} + c_{i,j+1} - c_{i,j-1}) \\
&- \frac{\delta \chi n_{i,j}}{[2h + \delta(c_{i,j+1} - c_{i,j-1})]^2} (c_{i+1,j} - c_{i-1,j} + c_{i,j+1} - c_{i,j-1})
\end{aligned}
\tag{25}
$$

$$
\begin{aligned}
&haptotaxis = \rho \nabla \cdot (n \nabla f) \\
&= \rho [\frac{1}{4h^2} [(n_{i+1,j} - n_{i-1,j})(f_{i+1,j} - f_{i-1,j}) + (n_{i,j+1} - n_{i,j-1})(f_{i,j+1} - f_{i,j-1})] \\
&+ n_{i,j} (\frac{f_{i+1,j} + f_{i-1,j} + f_{i,j+1} + f_{i,j-1} - 4f_{i,j}}{h^2})]
\end{aligned}
\tag{26}
$$

$$
prolif = \mu M_{i,j} n_{i,j} (1 - \frac{n_{i,j}}{n_O}) \tag{27}
$$

Finally, we obtained Eq. (1) in difference quotients equation which is described as follows:

$$
\begin{aligned}
&\frac{n_{i,j}^{k+1} - n_{i,j}^{k}}{\Delta t} = D(\frac{n_{i+1,j} + n_{i-1,j} + n_{i,j+1} + n_{i,j-1} - 4n_{i,j}}{h^2}) \\
&- \frac{\chi n_{i,j}}{(1+\delta c_{i,j})} \cdot (\frac{c_{i+1,j} + c_{i-1,j} + c_{i,j+1} + c_{i,j-1} - 4c_{i,j}}{h^2}) \\
&- \frac{\chi}{(1+\delta c_{i,j})} \frac{1}{4h^2} [(n_{i+1,j} - n_{i-1,j})(c_{i+1,j} - c_{i-1,j}) + (n_{i,j+1} - n_{i,j-1})(c_{i,j+1} - c_{i,j-1}) \\
&+ (n_{i+1,j} - n_{i-1,j})(c_{i+1,j} - c_{i-1,j}) + (n_{i,j+1} - n_{i,j-1})(c_{i,j+1} - c_{i,j-1})] \\
&+ \frac{\delta \chi n_{i,j}}{[2h + \delta(c_{i+1,j} - c_{i-1,j})]^2} (c_{i+1,j} - c_{i-1,j} + c_{i,j+1} - c_{i,j-1}) \\
&+ \frac{\delta \chi n_{i,j}}{[2h + \delta(c_{i,j+1} - c_{i,j-1})]^2} (c_{i+1,j} - c_{i-1,j} + c_{i,j+1} - c_{i,j-1}) \\
&- \rho [\frac{1}{4h^2} (n_{i+1,j} - n_{i-1,j})(f_{i+1,j} - f_{i-1,j}) + \frac{1}{4h^2} (n_{i,j+1} - n_{i,j-1})(f_{i,j+1} - f_{i,j-1}) \\
&+ n(\frac{f_{i+1,j} + f_{i-1,j} + f_{i,j+1} + f_{i,j-1} - 4f_{i,j}}{h^2})] + \mu M_{i,j} n_{i,j} (1 - \frac{n_{i,j}}{n_O})
\end{aligned}
\tag{28}
$$

To make it readable we may rewrite it as this:

$$\frac{n_{i,j}^{k+1} - n_{i,j}^{k}}{\Delta t} = random - chemotaxis - haptotaxis + prolif \tag{29}$$

$$n_{i,j}^{k+1} = \Delta t(random - chemotaxis - haptotaxis + prolif) + n_{i,j}^{k} \tag{30}$$

In the same way for Eq. (2) the difference quotient equation is described as follows:

$$\frac{\partial c}{\partial t} = -\eta nc$$

$$\frac{c_{i,j}^{k+1} - c_{i,j}^{k}}{\Delta t} - \eta nc_{i,j}^{k} \tag{31}$$

We obtained this as follows:

$$c_{i,j}^{k+1} = -\Delta t \eta nc_{i,j}^{k} + c_{i,j}^{k} \tag{32}$$

For Eq. (3) the difference quotient equation is described as follows:

$$\frac{\partial f}{\partial t} = \beta n - \gamma mf$$

$$\frac{f_{i,j}^{k+1} - f_{i,j}^{k}}{\Delta t} = \beta n_{i,j} - \gamma m_{i,j} f_{i,j}^{k} \tag{33}$$

We obtained this as follows:

$$f_{i,j}^{k+1} = \Delta t(\beta n_{i,j} - \gamma m_{i,j} f_{i,j}^{k}) + f_{i,j}^{k} \tag{34}$$

For Eq. (4) the difference quotient equation is described as follows:

$$\frac{\partial m}{\partial t} = an + \varepsilon \nabla^2 m - \nu m$$

$$\frac{m_{i,j}^{k+1} - m_{i,j}^{k}}{\Delta t} = \alpha n_{i,j} + \varepsilon\left(\frac{m_{i+1,j} + m_{i-1,j} + m_{i,j+1} + m_{i,j-1} - 4m_{i,j}}{h^2}\right) - \upsilon m_{i,j}^{k} \tag{35}$$

We obtained this as follows:

$$m_{i,j}^{k+1} = \Delta t\left\{\alpha n_{i,j} + \varepsilon\left(\frac{m_{i+1,j} + m_{i-1,j} + m_{i,j+1} + m_{i,j-1} - 4m_{i,j}}{h^2}\right) - \upsilon m_{i,j}^{k}\right\} + m_{i,j}^{k}$$

(36)

For Eq. (5) the difference quotient equation is described as follows:

$$\frac{\partial M}{\partial t} = -\varpi Mm$$

$$\frac{M_{i,j}^{k+1} - M_{i,j}^{k}}{\Delta t} = --\varpi M_{i,j} m_{i,j} \tag{37}$$

$$M_{i,j}^{k+1} = -\Delta t \varpi M_{i,j}^{k} \cdot m_{i,j} + M_{i,j}^{k} \tag{38}$$

We finish the derivation of Eq. (1), Eq. (2), Eq. (3), Eq. (4) and Eq. (5) from partial differential equations to difference quotient equations. The Eq. (24), Eq. (25), Eq. (26), Eq. (27) and Eq. (30) form the difference quotient equations representing partial differential equation Eq. (1); the difference quotient equations Eq. (32), Eq. (34), Eq. (36), and (38) represent the difference equations of Eq. (2), Eq. (3), Eq. () and Eq. (5) respectively. We rewrite these difference quotient equations by using the codes in Java language and run in computer.